



**Calhoun: The NPS Institutional Archive**  
**DSpace Repository**

---

Theses and Dissertations

1. Thesis and Dissertation Collection, all items

---

1984

# Application of modern guidance control theory to a back-to-turn missile.

Shin, Bohyun

Monterey, California. Naval Postgraduate School

---

<http://hdl.handle.net/10945/19161>

---

*Downloaded from NPS Archive: Calhoun*



Calhoun is the Naval Postgraduate School's public access digital repository for research materials and institutional publications created by the NPS community. Calhoun is named for Professor of Mathematics Guy K. Calhoun, NPS's first appointed -- and published -- scholarly author.

**Dudley Knox Library / Naval Postgraduate School**  
**411 Dyer Road / 1 University Circle**  
**Monterey, California USA 93943**

<http://www.nps.edu/library>







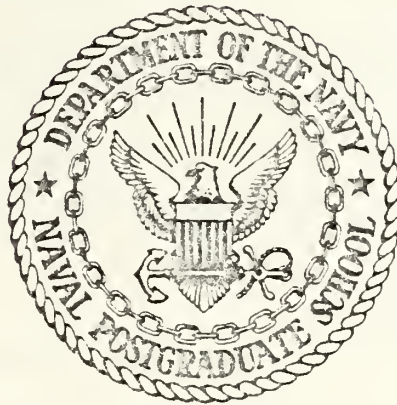




T218334

# NAVAL POSTGRADUATE SCHOOL

Monterey, California



## THESIS

APPLICATION OF MODERN GUIDANCE CONTROL THEORY  
TO A  
BANK-TO-TURN MISSILE

by

Bohyun Shin

March 1984

Thesis Advisor:

Daniel J. Collins

Approved for public release; distribution unlimited.



UNCLASSIFIED

SECURITY CLASSIFICATION OF THIS PAGE (When Data Entered)

| REPORT DOCUMENTATION PAGE   |                       | READ INSTRUCTIONS<br>BEFORE COMPLETING FORM                            |
|---|-----------------------|--|
| 1. REPORT NUMBER  | 2. GOVT ACCESSION NO. | 3. RECIPIENT'S CATALOG NUMBER  |
| 4. TITLE (and Subtitle)<br>Application of Modern Guidance Control Theory to a Back-To-Turn Missile  |                       | 5. TYPE OF REPORT & PERIOD COVERED<br>Engineer's Thesis;<br>March 1984 |
|   |                       | 6. PERFORMING ORG. REPORT NUMBER                                       |
| 7. AUTHOR(s)<br>Bohyun Shin   |                       | 8. CONTRACT OR GRANT NUMBER(s)   |
| 9. PERFORMING ORGANIZATION NAME AND ADDRESS<br>Naval Postgraduate School<br>Monterey, California 93943  |                       | 10. PROGRAM ELEMENT, PROJECT, TASK AREA & WORK UNIT NUMBERS            |
| 11. CONTROLLING OFFICE NAME AND ADDRESS<br>Naval Postgraduate School<br>Monterey, California 93943  |                       | 12. REPORT DATE<br>March 1984  |
|   |                       | 13. NUMBER OF PAGES<br>170   |
| 14. MONITORING AGENCY NAME & ADDRESS (if different from Controlling Office)   |                       | 15. SECURITY CLASS. (of this report)<br><br>Unclassified               |
|   |                       | 15a. DECLASSIFICATION DOWNGRADING SCHEDULE                             |
| 16. DISTRIBUTION STATEMENT (of this Report)<br><br>Approved for public release; distribution unlimited.   |                       |  |
| 17. DISTRIBUTION STATEMENT (of the abstract entered in Block 20, if different from Report)  |                       |  |
| 18. SUPPLEMENTARY NOTES   |                       |  |
| 19. KEY WORDS (Continue on reverse side if necessary and identify by block number)<br><br>Optimal control, missile guidance, bank-to-turn missile   |                       |  |
| 20. ABSTRACT (Continue on reverse side if necessary and identify by block number)<br><br>In this work, the control laws of a bank-to-turn missile using an optimal estimator in the terminal guidance phase were designed, and the effect of increasing the number of measurement sensors in the missile to generate more information on the state was investigated. In the design of the control law the modern optimal control theory with the a quadratic performance index was used. Implementation of this control law required the use of a |                       |  |

DD FORM 1 JAN 73 1473

EDITION OF 1 NOV 65 IS OBSOLETE  
S/N 0102-LF-014-6601UNCLASSIFIED  
1 SECURITY CLASSIFICATION OF THIS PAGE (When Data Entered)





Kalman filter as the optimal estimator. The extended Kalman filter algorithm was utilized in the present study since the measurement states were non-linear functions of the state vectors (relative distance, velocity and target acceleration). In order to test the effects of the implementation of the increased measurement sensors, two-, four- and six-measurement sensors were assumed to be implemented in the optimal estimator. By computer analysis, the designed guidance laws were evaluated and the effect of the implementation of increased measurement sensors was tested. Miss distance was chosen as a performance standard during the simulation.

The results of the simulation revealed that the designed guidance law was successful within the specified scenarios, the effect of the implementation of increased measurement sensors for the estimator was favorable only in that increased measurement sensors generated more information about the state vectors, but as the Kalman filter algorithm became more complex, the estimator performance was not enhanced to the degree expected with increased measurement sensors.



Approved for public release; distribution unlimited.

Application of Modern Guidance Control Theory  
to a  
Bank-To-Turn Missile

Bohyun Shin  
Major, Republic of Korea Air Force  
B.S., Republic of Korea Air Force Academy, 1973

Submitted in partial fulfillment of the  
requirements for the degree of

AERONAUTICAL ENGINEER

from the

NAVAL POSTGRADUATE SCHOOL  
March 1984





## ABSTRACT

In this work, the control laws of a bank-to-turn missile using an optimal estimator in the terminal guidance phase were designed, and the effect of increasing the number of measurement sensors in the missile to generate more information on the state was investigated. In the design of the control law the modern optimal control theory with the quadratic performance index was used. Implementation of this control law required the use of a Kalman filter as the optimal estimator. The extended Kalman filter algorithm was utilized in the present study since the measurement states were non-linear functions of the state vectors. In order to test the effects of the implementation of the increased measurement sensors, two-, four-, and six-measurement sensors were assumed to be implemented in the optimal estimator. By computer analysis, the designed guidance laws were evaluated and the effect of the implementation of increased measurement sensors was tested.

The results of the simulation revealed that the designed guidance law was successful within the specified scenarios, the effect of the implementation of increased measurement sensors for the estimator was favorable only in that increased measurement sensors generated more information about the state vectors.



# TABLE OF CONTENTS

|      |   |    |
|------|---|----|
| I.   | INTRODUCTION . . . . .  | 13 |
| II.  | KINEMATICS OF A BANK-TO-TURN MISSILE . . . . .                          | 15 |
|      | A. ASSUMPTIONS . . . . .  | 15 |
|      | B. MISSILE CONTROL METHOD . . . . .                                     | 16 |
|      | C. GEOMETRY OF MOTION IN SPACE . . . . .                                | 17 |
|      | D. KINEMATICS OF CONTROL VECTOR . . . . .                               | 21 |
|      | E. CO-ORDINATE TRANSFORMATION . . . . .                                 | 27 |
| III. | AN OPTIMAL CONTROLLER . . . . .   | 30 |
|      | A. GEOMETRY . . . . .   | 30 |
|      | B. SUMMARIZED DESCRIPTION OF AN OPTIMAL<br>CONTROLLER . . . . .         | 32 |
|      | C. APPROXIMATING TIME-TO-GO . . . . .                                   | 35 |
|      | D. PROJECTED-ZERO-CONTROL MISS (PZC MISS)<br>DISTANCE . . . . .         | 36 |
|      | E. SIMULATION RESULTS . . . . .   | 39 |
| IV.  | OPTIMAL ESTIMATOR . . . . .   | 54 |
|      | A. DESCRIPTION . . . . .  | 54 |
|      | B. STATE EQUATIONS . . . . .  | 55 |
|      | C. MEASUREMENT EQUATION . . . . .                                       | 62 |
|      | D. THE EXTENDED KALMAN FILTER . . . . .                                 | 69 |
|      | E. INITIALIZATION OF THE KALMAN FILTER . . . . .                        | 76 |
|      | 1. Initializing The Error Covariance<br>Matrix, $P$ . . . . .           | 77 |
|      | 2. Initializing The Measurement Noise<br>Variance Matrix, $R$ . . . . . | 79 |





|   |     |
|---|-----|
| F. EVALUATION OF THE OPTIMAL ESTIMATOR<br>PERFORMANCE . . . . . | 80  |
| V. PERFORMANCE EVALUATION OF THE CONTROL SYSTEM . . .           | 120 |
| VI. CONCLUSIONS . . . . .                                       | 150 |
| APPENDIX A: PROGRAM LISTING . . . . .                           | 152 |
| LIST OF REFERENCES . . . . .                                    | 169 |
| INITIAL DISTRIBUTION LIST . . . . .                             | 170 |



## LIST OF FIGURES

|      |  |    |
|------|--|----|
| 2.1  | MISSILE CONTROL SYSTEMS IN POLAR CO-ORD . . . . .                      | 17 |
| 2.2  | GEOMETRY OF RELATIVE MOTION . . . . .                                  | 18 |
| 2.3  | RELATIVE VELOCITY COMPONENTS IN POLAR<br>CO-ORD . . . . .              | 22 |
| 2.4  | KINEMATICS OF CONTROL VECTORS VIEWED FROM<br>REAR OF MISSILE . . . . . | 23 |
| 2.5  | KINEMATICS OF CONTROL VECTORS VIEWED FROM<br>SIDE OF MISSILE . . . . . | 23 |
| 3.1  | COMPONENTS OF PZC, MISS DISTANCE . . . . .                             | 31 |
| 3.2  | SCENARIO-1 TAIL-CHASE ENGAGEMENT . . . . .                             | 42 |
| 3.3  | SCENARIO-2 HEAD-ON ENGAGEMENT . . . . .                                | 43 |
| 3.4  | SCENARIO-3 SIDE-APPROACH ENGAGEMENT . . . . .                          | 44 |
| 3.5  | NORMAL ACCELERATION COMMAND VS TIME . . . . .                          | 45 |
| 3.6  | ROLL RATE COMMAND VS TIME . . . . .                                    | 46 |
| 3.7  | MISSILE BANK ANGLE VS TIME . . . . .                                   | 47 |
| 3.8  | NORMAL ACCELERATION COMMAND VS TIME . . . . .                          | 51 |
| 3.9  | ROLL RATE COMMAND VS TIME . . . . .                                    | 52 |
| 3.10 | MISSILE BANK ANGLE VS TIME . . . . .                                   | 53 |
| 4.1  | DISCRETE EXTENDED KALMAN FILTER TIMING<br>DIAGRAM . . . . .            | 71 |
| 4.2  | SYSTEM MODEL AND DISCRETE KALMAN FILTER . . . . .                      | 73 |
| 4.3  | DISCRETE KALMAN FILTER INFORMATION FLOW<br>DIAGRAM . . . . .           | 75 |
| 4.4  | ERROR COVARIANCE COMPONENT (P11) VS TIME . . . . .                     | 84 |
| 4.5  | ERROR COVARIANCE COMPONENT (P22) VS TIME . . . . .                     | 85 |





|      |  |     |
|------|--|-----|
| 4.6  | ERROR COVARIANCE COMPONENT (P33) VS TIME . . . . . | 86  |
| 4.7  | ERROR COVARIANCE COMPONENT (P44) VS TIME . . . . . | 87  |
| 4.8  | ERROR COVARIANCE COMPONENT (P55) VS TIME . . . . . | 88  |
| 4.9  | ERROR COVARIANCE COMPONENT (P66) VS TIME . . . . . | 89  |
| 4.10 | ERROR COVARIANCE COMPONENT (P77) VS TIME . . . . . | 90  |
| 4.11 | ERROR COVARIANCE COMPONENT (P88) VS TIME . . . . . | 91  |
| 4.12 | ERROR COVARIANCE COMPONENT (P99) VS TIME . . . . . | 92  |
| 4.13 | KALMAN GAIN COMPONENT (G11) VS TIME . . . . .      | 93  |
| 4.14 | KALMAN GAIN COMPONENT (G21) VS TIME . . . . .      | 94  |
| 4.15 | KALMAN GAIN COMPONENT (G31) VS TIME . . . . .      | 95  |
| 4.16 | KALMAN GAIN COMPONENT (G41) VS TIME . . . . .      | 96  |
| 4.17 | KALMAN GAIN COMPONENT (G51) VS TIME . . . . .      | 97  |
| 4.18 | KALMAN GAIN COMPONENT (G61) VS TIME . . . . .      | 98  |
| 4.19 | KALMAN GAIN COMPONENT (G71) VS TIME . . . . .      | 99  |
| 4.20 | KALMAN GAIN COMPONENT (G81) VS TIME . . . . .      | 100 |
| 4.21 | KALMAN GAIN COMPONENT (G91) VS TIME . . . . .      | 101 |
| 4.22 | STATE ESTIMATE: Rx VS TIME . . . . .               | 103 |
| 4.23 | STATE ESTIMATE: Ry VS TIME . . . . .               | 104 |
| 4.24 | STATE ESTIMATE: Rz VS TIME . . . . .               | 105 |
| 4.25 | STATE ESTIMATE: Vrx VS TIME . . . . .              | 106 |
| 4.26 | STATE ESTIMATE: Vry VS TIME . . . . .              | 107 |
| 4.27 | STATE ESTIMATE: Vrz VS TIME . . . . .              | 108 |
| 4.28 | STATE ESTIMATE: AT x VS TIME . . . . .             | 109 |
| 4.29 | STATE ESTIMATE: AT y VS TIME . . . . .             | 110 |
| 4.30 | STATE ESTIMATE: AT z VS TIME . . . . .             | 111 |



|      |   |     |
|------|---|-----|
| 4.31 | ESTIMATED TIME-TO-GO VS TIME . . . . .                          | 112 |
| 4.32 | NORMAL ACCELERATION COMMAND VS TIME . . . . .                   | 113 |
| 4.33 | MISSILE NORMAL LOADING VS TIME . . . . .                        | 114 |
| 4.34 | ROLL RATE COMMAND VS TIME . . . . .                             | 115 |
| 4.35 | MISSILE ROLL RATE VS TIME . . . . .                             | 116 |
| 4.36 | MISSILE BANK ANGLE VS TIME . . . . .                            | 117 |
| 5.1  | MISSILE MAXIMUM ACCELERATION VS MEAN MISS<br>DISTANCE . . . . . | 121 |
| 5.2  | MISSILE MAXIMUM ACCELERATION VS MEAN MISS<br>DISTANCE . . . . . | 122 |
| 5.3  | MISSILE MAXIMUM ROLL RATE VS MEAN MISS<br>DISTANCE . . . . .    | 125 |
| 5.4  | MISSILE MAXIMUM ROLL RATE VS MEAN MISS<br>DISTANCE . . . . .    | 126 |
| 5.5  | MISSILE TIME CONSTANT VS MEAN MISS DISTANCE . .                 | 128 |
| 5.6  | MISSILE TIME CONSTANT VS MEAN MISS DISTANCE . .                 | 129 |
| 5.7  | ONE SIGMA ANGLE ERROR VS MEAN MISS DISTANCE . .                 | 130 |
| 5.8  | ONE SIGMA ANGLE ERROR VS MEAN MISS DISTANCE . .                 | 131 |
| 5.9  | MISSILE VELOCITY VS MEAN MISS DISTANCE . . . . .                | 133 |
| 5.10 | MISSILE VELOCITY VS MEAN MISS DISTANCE . . . . .                | 134 |
| 5.11 | ENGAGEMENT TIME VS MEAN MISS DISTANCE . . . . .                 | 136 |
| 5.12 | ENGAGEMENT TIME VS MEAN MISS DISTANCE . . . . .                 | 137 |
| 5.13 | MISSILE MAXIMUM ACCELERATION VS MEAN MISS<br>DISTANCE . . . . . | 140 |
| 5.14 | MISSILE MAXIMUM ROLL RATE VS MEAN MISS<br>DISTANCE . . . . .    | 141 |
| 5.15 | MISSILE TIME CONSTANT VS MEAN MISS<br>DISTANCE . . . . .        | 142 |



|      |  |     |
|------|--|-----|
| 5.16 | ONE SIGMA ANGLE ERROR VS MEAN MISS<br>DISTANCE . . . . . | 143 |
| 5.17 | MISSILE VELOCITY VS MEAN MISS DISTANCE . . . . .         | 144 |
| 5.18 | ENGAGEMENT TIME VS MEAN MISS DISTANCE . . . . .          | 145 |
| 5.19 | ONE SIGMA ANGLE RATE ERROR VS MEAN MISS DISTANCE         | 146 |





## LIST OF TABLES

|     |                              |    |
|-----|------------------------------|----|
| 4.1 | NOMINAL PARAMETERS . . . . . | 81 |
|-----|------------------------------|----|



## ACKNOWLEDGEMENT

The author wishes to express his sincere appreciation to Professor Daniel J. Collins, whose assistance and encouragement contributed immeasurably to this research.

The author also wishes to dedicate this thesis to his wife, Eunsook. Without her constant support and understanding this work would not have been possible.



## I. INTRODUCTION

The bank-to-turn missile has high lift acceleration in a direction perpendicular to its wings. For airbreathing missiles which are required for large stand-off ranges it also offers the advantage of lower inlet angles of attack than that of skid-to-turn missiles.

Although the control laws using the modern guidance control theory are more complex than the normally used proportional navigation air-to-ground method, they have great potential for maneuvering targets in air-to-air engagement situations. The application of optimal control and estimation theory to bank-to-turn missile configurations has been tried in order to obtain increased performance. In the application of the optimal control theory to the bank-to-turn missile, it is necessary to have information on all states or an estimate of the state variables that have not been measured. Since the state information available from the typical missile sensors is limited, it is necessary to employ an estimator. The estimator used in this study was a first order extended Kalman filter.

The present work addressed the design and evaluation of the optimal state estimator and optimal control laws for application to a bank-to-turn missile. In the development of this work, Chapter 2 will describe the kinematics of the



missile and formulate the equations of the motion. All major assumptions are listed. The optimal controller is described in Chapter 3. The simulation results of the controller on three scenarios described later are used to check the suitability of the optimal controller. The optimal estimator is covered in Chapter 4, the formulation of the state equation, measurement equations and the derivations of the elements of Jacobean matrix are covered. The extended Kalman filter algorithm for non-linear system is then reviewed. Before the final computer simulation a discussion is given on the nominal parameters needed in initializing the Kalman filter. The results of the simulation of estimators with two-, four-, and six-measurement vectors on a typical scenario are then presented. In Chapter 5, the simulation results of the control laws implemented the estimator with two-, four- and six-measurement sensors on three scenarios is described. The detail analysis of the results is developed in order to investigate the effect of the key variables of the control system on a bank-to-turn missile. The mean miss distance determined from 50 Monti Carlo runs as a performance standard was used in the analysis of the results of the control laws as a function of the key variables. Finally, the conclusion are summarized in the last Chapter.





## II. KINEMATICS OF A BANK-TO-TURN MISSILE

### A. ASSUMPTIONS

The geometry and the equations of motion of the missile will be developed, representing the positions in space, under the following assumptions:

1. The local geographic coordinate system will be used as the inertial reference.
2. To simplify the equation of motion the stability axes are adopted for the missile body.
3. The missile velocity due to thrust is constant.  
There is no missile acceleration in velocity due to thrust.
4. Each control surface or surfaces is rigid.
5. Relative to the body axes, each control system has only one degree of freedom. The missile's control acceleration vector acts normal to the velocity vector, that is, the dot product of acceleration vector and velocity vector is zero, also the acceleration acts through the missile center of gravity.
6. The Euler angles  $\phi_v$ ,  $\theta_v$  and  $\phi$  will be used to describe the orientation of the missile with respect to inertial space, where  $\phi_v$  and  $\theta_v$  are horizontal and vertical flight path angles, and  $\phi$  is the roll or bank angle.



7. The first order lags with time constants  $\tau_p$  and  $\tau_o$  to a roll rate command  $P_c$  and a normal acceleration command  $a_c$  will be considered for the dynamic response of the missile.

## B. MISSILE CONTROL METHOD

Before going into the mathematical detail concerning the motion of a missile in space as a result of a guidance command, it is helpful to review with the control law for a bank-to-turn missile. The guidance system detects whether the missile is flying too much or too high to the left, right or vertical. The guidance system measures these deviations or errors and sends signals to the control system to reduce these errors to zero. The task of the control system therefore is to maneuver the missile quickly and efficiently as a result of these signals. In a bank-to-turn missile system, the guidance angular error detector produces two signals  $R$  and  $\phi$  in terms of polar coordinate expression, showed in Figure 2.1. The same signals can be expressed in another way, that is, in cartesian coordinate. The usual method is to regard the  $\phi$  signal as a command to roll through an angle  $\sigma$  measured from the vertical and then to maneuver outwards by means of the missile's elevators. The method of maneuvering the missile is as follows. The  $\phi$  command goes as a positive command to one control surface and a negative command to the other, this



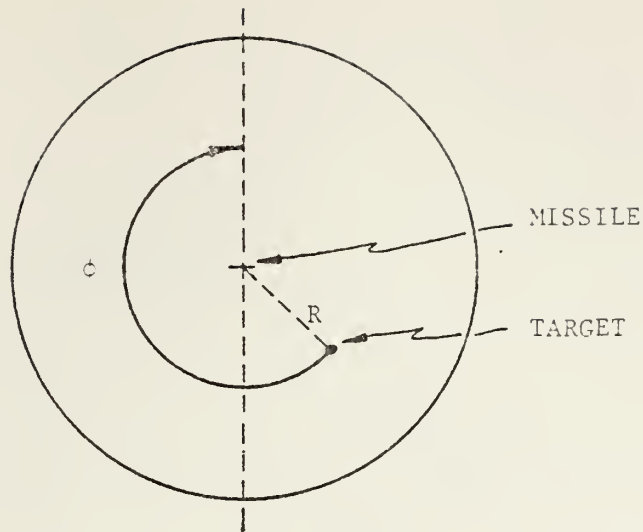


FIGURE 2.1. MISSILE CONTROL SYSTEM IN POLAR CO-ORD.

causes the missile to roll. The  $R$  command goes to surfaces always as a positive demand, this causes the missile to accelerate normal to the velocity vector. The intention is to make the response in roll fast so that the commands can be applied simultaneously which makes for simplicity, only a pair of control surfaces are used as ailerons and elevators at the same time, control is obtained by means of the separated servos.

#### C. GEOMETRY OF MOTION IN SPACE

The motion of a missile as a particle may be described by using coordinate measured with moving axes (relative-motion analysis). The analysis of motion can be simplified by using measurements made with respect to a moving coordinate system. In present work, the equations of motion will



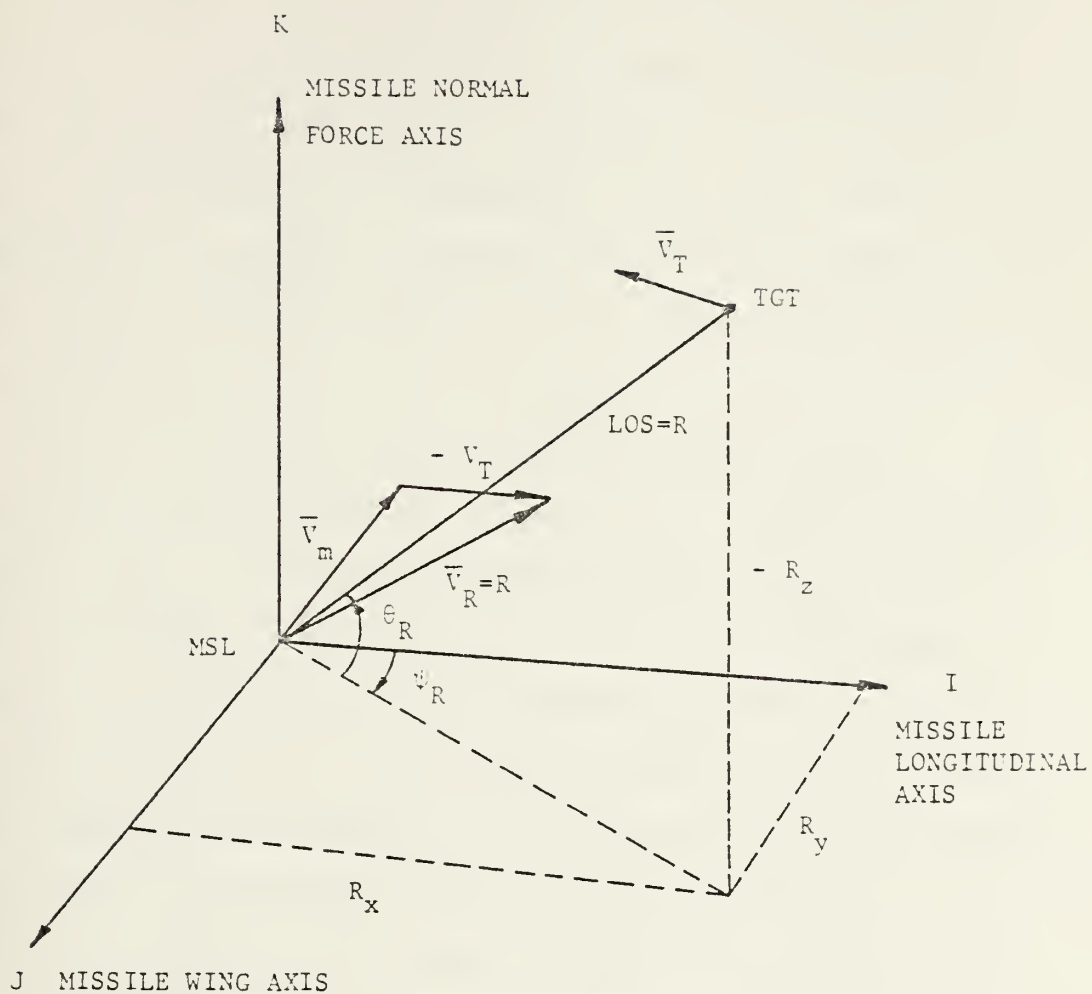


FIGURE 2.2 GEOMETRY OF RELATIVE MOTION.





be described with respect to the initial missile body axes taken as the inertial axes. After launching, the missile body axes changes position, but the relative position, velocity and acceleration are still computed in inertial axes, that is, in the initial body axes. The current zero effort miss distance is calculated. This will then be transformed to values in missile body axes to compute the amount of the control inputs to the missile using Euler's transformation.

Figure 2.2 shows the missile and target as points with respective vector velocity  $V_m$  and  $V_t$ . In this analysis, because  $|V_m|$  is assumed to be at least  $2|V_t|$ , and the angle of attack is assumed to be small, the lead angle  $\phi$  between  $V_R$  and the missile longitudinal axis is small. Let the vector denote the relative position of the target with respect to the missile. The orientation of the sight line vector in inertial space can be represented by the angle  $\psi_R$  and  $\theta_R$ , as shown in Figure 2.2. The sight line vector is resolved into three components in inertial axes as follows:

$$R_x = R \cos(\theta_R) \cos(\psi_R) = X_t - X_m \quad (2.1)$$

$$R_y = R \cos(\theta_R) \sin(\psi_R) = Y_t - Y_m \quad (2.2)$$

$$R_z = - R \sin(\phi_R) = Z_t - Z_m \quad (2.3)$$

Where  $R$  is the magnitude of the sight line vector.



Define the relative velocity vector:

$$\underline{V}_r = \underline{V}_t - \underline{V}_m \quad (2.4)$$

Where  $V_t$  and  $V_m$  are target and missile velocities.

The rate of change of the sight line vector's magnitude is equal to the component of  $V_R$  along  $R$ . It can be expressed as following:

$$\dot{R} = \frac{|\underline{V}_t \cdot \underline{R}|}{R} \quad (2.5)$$

$$\dot{R} = \frac{V_{rx} * R_x + V_{ry} * R_y + V_{rz} * R_z}{(R_x^2 + R_y^2 + R_z^2)^{1/2}} \quad (2.6)$$

Where  $V_{rx} = V_{tx} - V_{mx}$

$V_{ry} = V_{ty} - V_{my}$

$V_{rz} = V_{tz} - V_{mz}$

are the relative velocity components in the inertial frame.

In the geometry, the relative angles  $\psi_R$  and  $\theta_R$  also will be expressed by the relative vectors:

$$\theta_R = - \tan^{-1} \left[ \frac{R_z}{(R_x^2 + R_y^2)^{1/2}} \right] \quad (2.6)$$



$$\psi_R = -\tan^{-1} \left[ \frac{R_y}{R_z} \right] \quad (2.7)$$

Where  $\theta_R$  and  $\psi_R$  are the elevation and the azimuth angles of the relative sight line vector in the inertial frame.

Then the rate of change of both angles are

$$\begin{aligned} \dot{\theta}_R &= \frac{V_{r\theta}}{R} \\ &= \frac{-\sin\theta_v \cos\psi_v V_{rx} - \sin\theta_v \sin\psi_v V_{ry} + \cos\theta_v V_{rz}}{(R_x^2 + R_y^2 + R_z^2)^{1/2}} \end{aligned} \quad (2.8)$$

$$\dot{\psi}_R = \frac{V_{r\psi}}{R \cos\theta_v} = \frac{-\sin\psi_v V_{rx} + \cos\psi_v V_{ry}}{(R_x^2 + R_y^2 + R_z^2)^{1/2} \cos\theta_v} \quad (2.9)$$

Where  $V_{R\theta}$  and  $V_{R\psi}$  are the rates of change in  $\theta_v$  and  $\psi_v$  components, is shown in Figure 2.3. These quantities will be used later in developing the estimator state equations and will also be used to represent the variables for the missile seeker. The quantities  $\theta_R$ ,  $\dot{\theta}_R$ ,  $\psi_R$ ,  $\dot{\psi}_R$ ,  $R$  and  $\dot{R}$  (corrupted by noise) are the set of measurements assumed available from the missile seeker.

#### D. KINEMATICS OF CONTROL VECTOR

Figures 2.4 and 2.5 are views from near and side of missile.  $a_m$  and  $\phi$  represent the magnitudes of the



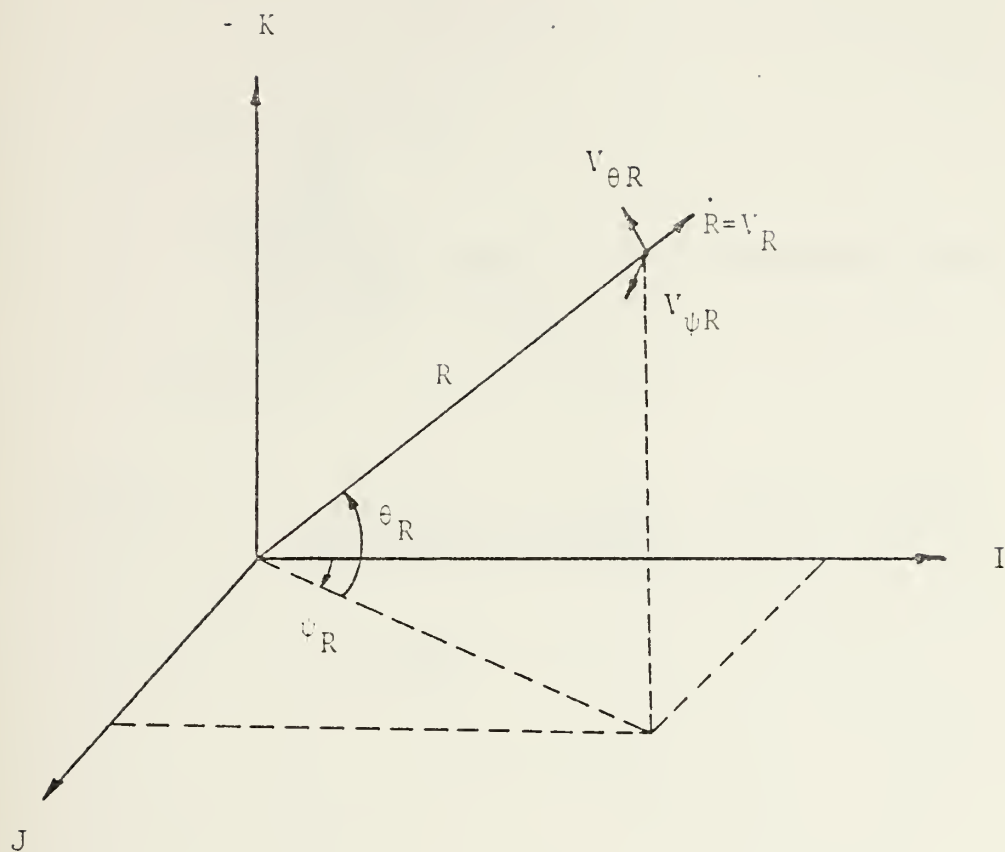


FIGURE 2.3 RELATIVE VELOCITY COMPONENTS IN POLAR CO-ORD.





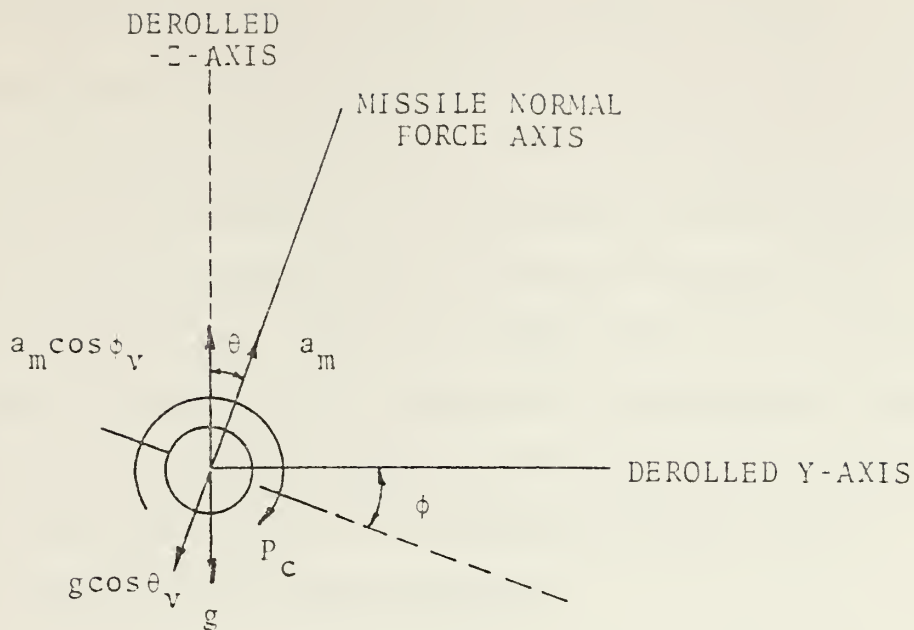


FIGURE 2.4 KINEMATICS OF CONTROL VECTORS VIEWED FROM REAR OF MISSILE.

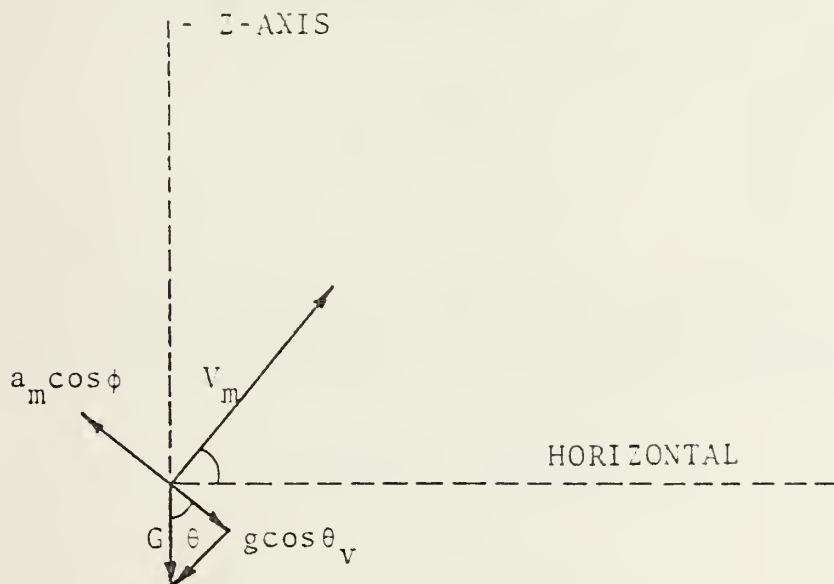


FIGURE 2.5 KINEMATICS OF CONTROL VECTORS VIEWED FROM SIDE OF MISSILE.



missile acceleration due to the acceleration command ( $a_c$ ) and the bank angle due to the roll rate command ( $P_c$ ) each other.  $g$  represents the gravitational effect at the center of gravity of the missile. As mentioned in control method, the sign of  $a$  is such that it is positive upward with respect to the wings. Figure 2.5 shows that the acceleration normal to the velocity vector has the components due to the elevator control input and the effect of the gravity. The total magnitude of the acceleration normal to the velocity vector can be represented as

$$a_m \cos \phi - g \sin \theta_v .$$

The velocity and acceleration components for simple circular motion can be represented as

$$a_n = V^2 / \rho$$

See Reference 1.

Using this definition, the differential equations describing the rate of change of the flight path angles are

$$\dot{\phi}_v = \frac{a_m \cos \phi - g \cos \theta_v}{V_m} \quad (2.10)$$



$$\psi_v = \frac{a_m \sin \phi}{V_m \cos \theta_v} \quad (2.11)$$

Note  $a_m \cos \phi - g \cos \theta_v$  is the magnitude of the normal acceleration component to the velocity vector in missile side plane and  $a_m \sin \phi$  is the magnitude of the normal acceleration component to the velocity vector in the x-y plane. The acceleration component of the missile velocity  $V_m$  has only the component of the effect of gravity in the missile side plane under the assumption that the missile velocity is constant. The differential equation is:

$$\dot{V}_m = -g \sin \theta_v \quad (2.12)$$

The rates of change of the missile position components ( $X_m, Y_m, Z_m$ ) can be obtained by integrating the components of missile velocity. From Figure 2.2, the components of missile velocity ( $V_{mx}, V_{my}, V_{mz}$ ) in inertial frame are given by

$$\dot{X}_m = V_{mx} = V_m \cos \theta_v \cos \psi_v \quad (2.13)$$

$$\dot{Y}_m = V_{my} = V_m \cos \theta_v \sin \psi_v \quad (2.14)$$

$$\dot{Z}_m = V_{mz} = -V_m \sin \theta_v \quad (2.15)$$

Let the response of the missile to input command in normal acceleration and roll rate be considered. If a demand is made on a missile for a transverse acceleration,



it is initiated by sending a signal to the appropriate control surface. The missile acceleration  $a_m$  follows the demanded acceleration  $a_d$  in a manner which may be characterized by a frequency  $\omega_m$  (weather cock frequency) and a damping factor  $P$ . For simplicity, in present work, only the first order lags with time constant  $\tau_p$  and  $\tau_o$  are assumed, the equation of the first-order system can be represented as follows:

$$\dot{X}(t) + 1./\tau * X(t) = f(t)$$

Taking the Laplace transformation on has

$$X(S) = F(S)/(S+1./T)$$

with zero initial condition. Applying these to the BTT missile control system.

$$\tau_a * \dot{a}_m + a_m = a_c \quad (2.16)$$

$$\tau_p * \dot{P} + P = P_c \quad (2.17)$$

Rearranging the differential equation.

$$\dot{a}_m = (a_c - a_m)/\tau_a \quad (2.18)$$

$$\dot{P} = (P_c - P)/\tau_p \quad (2.19)$$

$$\dot{\phi} = P \quad (2.20)$$





Where  $a_c$  and  $P_c$  are the acceleration and roll rate commands. Equation (2.20) is by definition. From the above differential equations the control ratios are transformed as follows:

$$\frac{a_m(S)}{a_c(S)} = \frac{1}{\tau_a S + 1} \quad (2.21)$$

$$\frac{P(S)}{P_c(S)} = \frac{1}{\tau_p S + 1} \quad (2.22)$$

Equations (2.10) through (2.22) constitutes the dynamic equations describing missile motion in response to the command inputs  $a_c$  and  $P_c$ . The solution of these equations provide missile position  $(X_m, Y_m, Z_m)$ , orientation and magnitude of velocity  $(\psi_v, \theta_v, V_m)$  and orientation and magnitude of control acceleration  $(\phi, a_m)$ .

#### E. CO-ORDINATE TRANSFORMATION

Given that the missile is on guided flight to compute the magnitudes of the control inputs at any moment, it is necessary to transform the instantaneous values from the sensors in the inertial frame to the instantaneous values in body frame. The transformation from one frame to another can be accomplished through a transformation matrix. The transformation matrix will be developed.

Define an inertial coordinate system with unit vectors  $I, J, K$ . Also, define a missile body axis coordinate system



with unit vectors  $i, j, k$ . It is desired to find the transformation between the  $I, J, K$  system and the  $i, j, k$  system.

The  $I, J, K$  system can be thought to be oriented so that  $I$  points north,  $J$  east, and  $K$  down. Similarly, the  $i, j, k$  system has  $i$  along the longitudinal axis of the missile (which by assumption is along the velocity vector  $V_m$ ),  $j$  out the right wing, and  $k$  down.

Consider three successive rotations  $\psi_v$ ,  $\theta_v$  and  $\phi$ . The  $\psi_v$  rotation is about the inertial  $z$  axis, and transforms to an intermediate axis systems  $i_1, j_1, k_1$ . The  $\theta_v$  rotation is about the  $j_1$  axis and transforms to an axis system  $i_2, j_2, k_2$ . The last rotation  $\phi$  about the  $i_2$  axis transforms from flight path axes to missile body axes. As a result, the total transformation from inertial to body axes is given by

$$\begin{bmatrix} i \\ j \\ k \end{bmatrix} = [\phi][\theta_v][\psi_v] \begin{bmatrix} I \\ J \\ K \end{bmatrix} = [A] \begin{bmatrix} I \\ J \\ K \end{bmatrix} \quad (2.23)$$

Where  $A$  is the total transformation matrix from inertial to body frame. The elements of the  $a$  matrix from Reference 1 are:

$$a_{11} = \cos(\theta_v) * \cos(\psi_v)$$

$$a_{12} = \cos(\theta_v) * \sin(\psi_v)$$

$$a_{13} = -\sin(\theta_v)$$



$$\begin{aligned}
a_{21} &= \sin(\phi) * \sin(\theta_V) * \cos(\psi_V) - \cos(\phi) * \sin(\psi_V) \\
a_{22} &= \sin(\phi) * \sin(\theta_V) * \sin(\psi_V) + \cos(\phi) * \cos(\psi_V) \\
a_{23} &= \sin(\phi) * \cos(\theta_V) \\
a_{31} &= \cos(\phi) * \sin(\theta_V) * \cos(\psi_V) + \sin(\phi) * \sin(\psi_V) \\
a_{32} &= \cos(\phi) * \sin(\theta_V) * \sin(\psi_V) - \sin(\phi) * \cos(\psi_V) \\
a_{33} &= \cos(\phi) * \cos(\theta_V)
\end{aligned}$$



### III. AN OPTIMAL CONTROLLER

Although this work is primarily concerned with the effect of an optimal estimator on the performance of a bank-to-turn missile, we will first outline the theory of an optimal controller in this section. The guidance laws considered here were first developed by Stallard [Ref. 10]. The following is a brief outline of his work.

#### A. GEOMETRY

Figure 3.1 shows the applicable geometry representing the Projected-Zero-Control miss (PZC miss) distance in the terminal state. The problem is considered to be three-dimensional and two major axes system are used:

1. A seeker-oriented axis system for estimation or measurement, and
2. The three principal axes of the missile for the control problem,

$X_b$ ,  $Y_b$ ,  $Z_b$  denote the target coordinates relative to the missile along its principal axes. The body system is represented a time  $T = 0$  by a set of Eulian angles which relate it to an earth fixed system. The angle  $\Delta\phi$  is the incremental roll angle from the present missile axes to any future orientation at time  $T$ , shown dashed in Figure 3.1. The PZC miss represents the total Projected-Zero effort - miss distance and is defined as the miss distance which





would occur if no further control was exercised on the missile at  $T = T_i$ . It is composed of a Y-components (PZCY miss) and a Z-component (PZCZ miss). Under the assumption of constant velocity the X-component (PZCX miss) is represented by the distance that the missile has to fly at any time, since it is not effected by control, it is not shown in Figure 3.1.

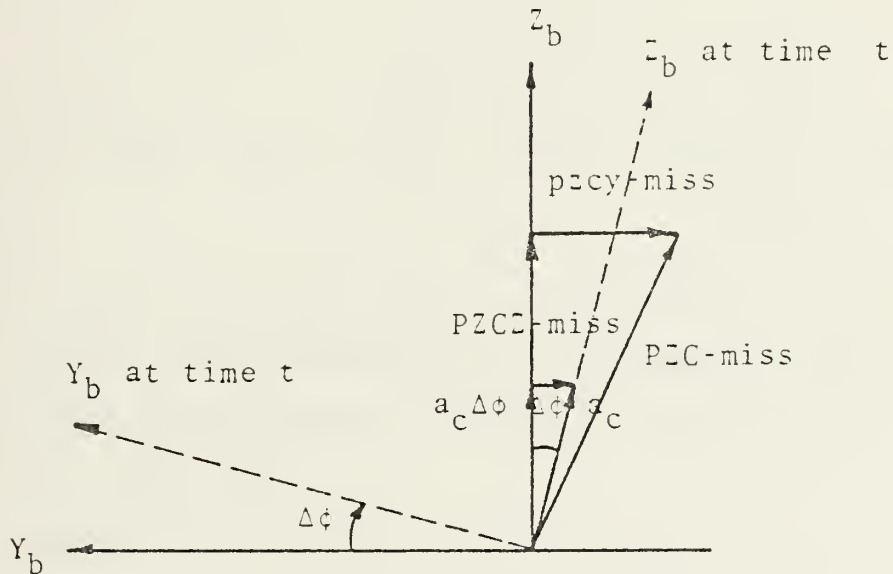


FIGURE 3.1 COMPONENTS OF PZC, MISS DISTANCE.



## B. SUMMARIZED DESCRIPTION OF AN OPTIMAL CONTROLLER

Given a time-varying linear system of the form,

$$\dot{\underline{X}} = F(t)\underline{X} + G(t)\underline{U} \quad (3.1)$$

Where  $\underline{X}$  is n-component state vector

$\underline{U}$  is m-component control vector.

An optimal control is one that minimizes a performance index made up of a quadratic form in the terminal state plus an integral form of quadratic forms in the control and the state:

$$J = \frac{1}{2} (\underline{X}^T S_f \underline{X} \big|_{T=T_i}) + \frac{1}{2} \int_{T_0}^{T_i} (\underline{X}^T A \underline{X} + \underline{U}^T B \underline{U}) dt \quad (3.2)$$

Where the  $S_f$  and  $A$  are positive semidefinite matrix and  $B$  is a positive definite matrix. An appropriate choice of these matrices must be made to obtain acceptable level of  $\underline{X}(T_i)$ ,  $\underline{X}(t)$  and  $\underline{U}(t)$ .

The guidance law determined in Reference 8 is of the form:

$$\underline{U}_c = (a_c, p_c)^T$$

With the performance index chosen (the weighting on the state vector was not considered in Reference 8.



$$J = \frac{1}{2} (X_b^2 + Y_b^2 + Z_b^2) |_{T_i} + \frac{1}{2} \int_{T_o}^{T_i} (\underline{U} - \underline{U}_b)^T B (\underline{U} - \underline{U}_b) dt \quad (3.3)$$

Where the first term is one-half the required miss distance, the second term is included in order to eliminate infinite energy solutions.  $B$  is a 2 by 2 positive definite, symmetric weighting matrix and of the form

$$B = \begin{bmatrix} B1 & 0 \\ 0 & B2 \end{bmatrix} \quad (3.4)$$

with  $1/B_{ij} = (T_i - T_o) \times$  maximum acceptable value of  $|U_i(T)|^2$ . A detailed derivative of the optimal guidance law is given in Reference 10.

The solutions of the above equation from Reference 8 give the optimal acceleration command at time  $T$  between  $T_0$  and  $T_i$  as

$$a_c = \frac{3T_{go}}{3B_1 + T_{go}^3} (-M_{bz}) \quad (3.5)$$

Where  $T_{go}$  is the remaining time to go until intercept and  $M_{bz}$  is the PZC-miss along the missile normal force axis and the negative sign is due to definition of the normal



acceleration as positive in the upward direction. The optimal roll rate command at time  $T$  between  $T_0$  and  $T_1$  from Reference 8 is given by

$$P_c = \frac{21a_c^2 T_{go}^2 (M_{by})}{a_c^2 T_{go}^5 + 63 B_2} \quad (3.6)$$

Where  $M_{by}$  is the PAC-miss along the wing axis. Defining the roll error:

$$\Delta\phi = \tan^{-1} \left| \frac{M_{by}}{M_{bz}} \right| \quad (3.7)$$

An alternate form for  $P_c$  can be obtained by dividing Equation (3.6) by Equation (3.5), then

$$P_c = \frac{7a_c^2 T_{go} (T_{go}^3 + 3 B_1)}{a_c^2 T_{go}^5 + 63 B_2} \tan(\Delta\phi) \quad (3.8)$$

Because the solution of  $P_c$  was based on an assumption of small missile roll excursions, the  $\tan\Delta\phi$  term in Equation (3.8) can be replaced by  $\Delta\phi$  to yield

$$P_c = \frac{7a_c^2 T_{go} (T_{go}^3 + 3 B_1)}{a_c^2 T_{go}^5 + 63 B_2} \Delta\phi \quad (3.9)$$





The optimal controller is implemented in the present work using Equations (3.5), (3.7), and (3.9). In computing the control input,  $T_{go}$ ,  $Y$  and  $Z$ -component of PZC-miss and the elements of the weighting matrix are needed.

### C. APPROXIMATING TIME-TO-GO

It is necessary for the Time-To-Go and the Projected-Miss-Distance in missile body axes to be specified at time  $T$  to compute the optimum control input. The Time-To-Go will be defined at first, then the state variables will be introduced as means for formulating the necessary equations. The target acceleration components of the state variables will be modeled since it is assumed that any information about the target acceleration cannot be obtained from the active seeker of the missile. Then using this target acceleration model the algorithm for computing the other state variables will be developed.

The Time-To-Go until intercept,  $T_i$ , is required for computing the control input. Let the time to intercept be defined as the time to minimum range. Under the assumption that the relative velocity vectors may be considered constant at its present value until intercept.  $T$  can be found at time,  $T$ , as:

$$T_i = - \frac{1}{|\underline{V}_r|} \left| \frac{\underline{R}_r^T \underline{V}_r}{|\underline{V}_r|} \right| \quad (3.10)$$



Where  $R$  is the present position of the target relative to the missile and the factor in brackets in the component of  $V$  along  $R$ . An alternate form of  $T$  is:

$$T_i = \frac{- |R_x V_{rx} + R_y V_{ry} + R_z V_{rz}|}{|V_{rx}^2 + V_{ry}^2 + V_{rz}^2|} \quad (3.11)$$

The negative sign comes from the sign of  $V_r$  as shown in Figure 2.2 and Equation (2.6).

#### D. PROJECTED-ZERO-CONTROL MISS (PZC MISS) DISTANCE

The Projected-Zero-Control miss distance (PZC-miss) is defined as the miss distance which would occur if there were no further control input after time  $T$ .

In this work the state vectors are defined as the following state variables

$$\dot{\underline{X}} = (R_x, R_y, R_z, V_{rx}, V_{ry}, V_{rz}, a_{tx}, a_{ty}, a_{tz})^T$$

Where  $R_r$  is the relative missile distance to target

$V_r$  is the relative missile velocity to target

$a_t$  is the target acceleration

A model for target acceleration has been assumed. This is given as follows:

$$a_t(T) = a_{t0} e^{-\alpha |T|} \quad \alpha \geq 0 \quad (3.12)$$



Where  $a$  is the initial target acceleration and  $\alpha$  is the reciprocal of the acceleration time constant. The initial target acceleration,  $4g$ 's, will be assumed for each scenario, and  $\alpha = 1/20$  for evasive maneuver as indicated in Reference 10 will be chosen. These values will be used in the simulation of the optimal controller.

With the assumption that a state estimator is available to provide estimates of the state vector at current time  $(t)$ , the values of the state variables for no control inputs at future time, can be obtained easily using the integration, i.e.,

$$V_r(t) = V_r(t_0) + \int_{t_0}^t a_t(\tau) d\tau$$

$$R(t) = R(t_0) + \int_{t_0}^t V_r(\tau) d\tau$$

The results of these integrations are

$$V_r(t) = V_r(t_0) + 1/\alpha (1 - e^{-\alpha(t - t_0)}) a_t(t_0) \quad (3.13)$$

$$R(t) = R(t_0) + (t - t_0) * V_r(t_0) \quad (3.14)$$

$$+ [1/\alpha^2 (\alpha(t - t_0) - 1 + e^{-\alpha(t - t_0)})] * a_t(t_0)$$

Where  $t_0$  and  $t$  denote current time and future time. It should be noticed that above integration is based on the



assumption of a single physical dimension. If this assumption is to be applied to three-dimensional problem, it must be concluded that there are no coupling among the X, Y, Z dimension. Let  $T_{go} = t - t_0$ , then the components of the PZC-miss in inertial axes at current time ( $t_0$ ) can be expressed as

$$\begin{aligned}
 \begin{bmatrix} M_x \\ M_y \\ M_z \end{bmatrix}_{Ti} &= \begin{bmatrix} R_x \\ R_y \\ R_z \end{bmatrix}_{T0} + T_{go} \begin{bmatrix} V_{rx} \\ V_{ry} \\ V_{rz} \end{bmatrix}_{T0} \\
 &+ \begin{bmatrix} f_x & 0 & 0 \\ 0 & f_y & 0 \\ 0 & 0 & f_z \end{bmatrix} * \begin{bmatrix} a_{tx} \\ a_{ty} \\ a_{tz} \end{bmatrix}_{T0} \quad (3.15) \\
 &- \begin{bmatrix} 0 \\ 0 \\ (1/2) * g * T_{go}^2 \end{bmatrix}
 \end{aligned}$$

Where  $f_x = f_y = f_z = 1/\alpha^2 [\alpha T_{go} - 1 + e^{-\alpha T_{go}}]$  and the last term accounts for the free fall effect of gravity in the vertical axis.

The components of the PZC-miss in missile body axes for control input calculation are obtained via the Euler transformation matrix:





$$\begin{bmatrix} M_{bx} \\ M_{by} \\ M_{bz} \end{bmatrix} = [\phi][\theta_v][\psi_v] \begin{bmatrix} M_x \\ M_y \\ M_z \end{bmatrix} = [A] \begin{bmatrix} M_x \\ M_y \\ M_z \end{bmatrix} \quad (3.16)$$

Where it is assumed that the missile has exact knowledge of its orientation angles  $\psi_v$  ,  $\theta_v$  ,  $\phi$  , from the accurate inertial measurement units.

The values of optimal control vectors ( $a_c$  and  $P_c$ ) , then, are calculated from time to go ( $T_{go}$ ) , PEC-miss in body axes and weighting matrix components ( $B1$  and  $B2$ ) which may be determined according to the desired miss distance and intercepting time. In a later section, the weighting matrix will be developed and the scenarios will be set up for computer simulation.

## E. SIMULATION RESULTS

The guidance law in this work was tested on a simple six-degree-of-freedom simulation using only plausible numbers without reference to any actual missile or design.

Before the computer simulations, the weighting matrix of the performance index selected in Reference 8 will be calculated using the initial state,  $X(0)$  , the missile operating time imposed,  $T$  (5 sec) and the constraint input vectors. It is assumed that the missile has a velocity advantage of two over that of the target, a zero- and 0.5



second-time lag auto pilots for pitch with limits of  $-3g$ 's,  $+20g$ 's and for roll rate with limits of  $+6.28$  rad/sec.

The allowable miss distance which is usually determined by sizing of the warhead was chosen as 5 meters. Which makes the first term of the performance index Equation (5.3) equal to 12.5 meters. The acceleration term and the roll-rate term in the performance index are set equal to this respectively (one-half of square mean miss distance), then

$$\frac{B_1}{2} \int_0^{T_i} (a_c - a_d)^2 dt = 12.5 \text{ m}^2 \quad (5.16)$$

$$\frac{B_2}{2} \int_0^{T_i} (p_c^2) dt = 12.5 \text{ m}^2 \quad (5.17)$$

The nominal time of flight for the terminal phase is set equal to 5 seconds. The components of the weighting matrix B were based on the following assumptions. It is assumed for  $(4g's)^2$  as a mean-square value of  $(a_c - a_d)$  and  $(2 \text{ rad/sec})^2$  as a mean-square roll rate to be acceptable. Then the components of weighting matrix are:

$$B_1 = 0.003254 \text{ sec}^3$$

$$B_2 = 1.25 \text{ m}^2 \text{ sec}$$



The commands  $a$  and  $P$  are computed every 0.05 sec and are frozen when the Time-To-Go falls below this interval.

In order to simulate the optimal controller appropriate scenarios were developed below with restriction that the Time-To-Go was 5 sec and the speed of missile is two times faster than that of target. Three scenarios; tail-chase, head-on, side-approach engagements, were chosen as possible cases in this work.

In case 1, tail-chase engagement, the target flies 100m above the missile and 2500m uprange with a horizontal eastward acceleration of 4g's. Figure 3.3 shows the case 2. In case 3, side-approach engagement, the target flies 400m above the missile and 1900m uprange with a horizontal northward acceleration of 4g's at  $t = 0$  as shown in Figure 3.4. For simplicity, when the scenarios were set up, 1000m/s was taken as a missile speed, 500m/s as a target speed in case 1 and case 2, 600m/s as a missile speed, 300m/s as a target speed in case 3, and 4g's as a target acceleration for all three cases. When simulation was executing, this first simulation assumed perfect state feedback without the use of an optimal estimator.

The simulation results are shown in Figure 3.5 through Figure 3.10. At first, the optimal controller with no time lag was tested for three scenarios, as shown in Figures 3.5 and 3.6. For scenario 1, the normal acceleration command in initial phase is very large, then decreases to zero at



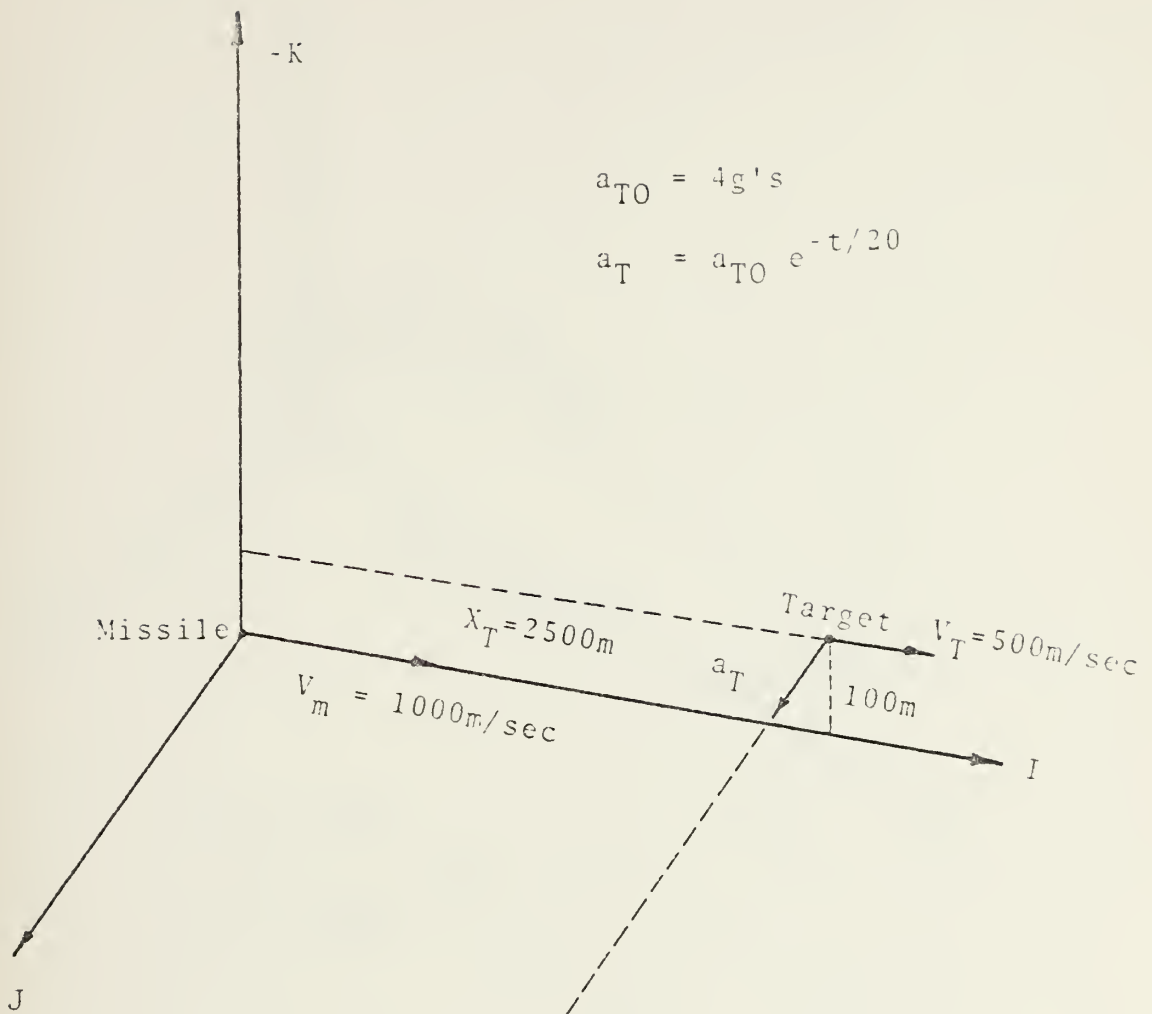


FIGURE 3.2 SCENARIO-1 TAIL-CHASE ENGAGEMENT.





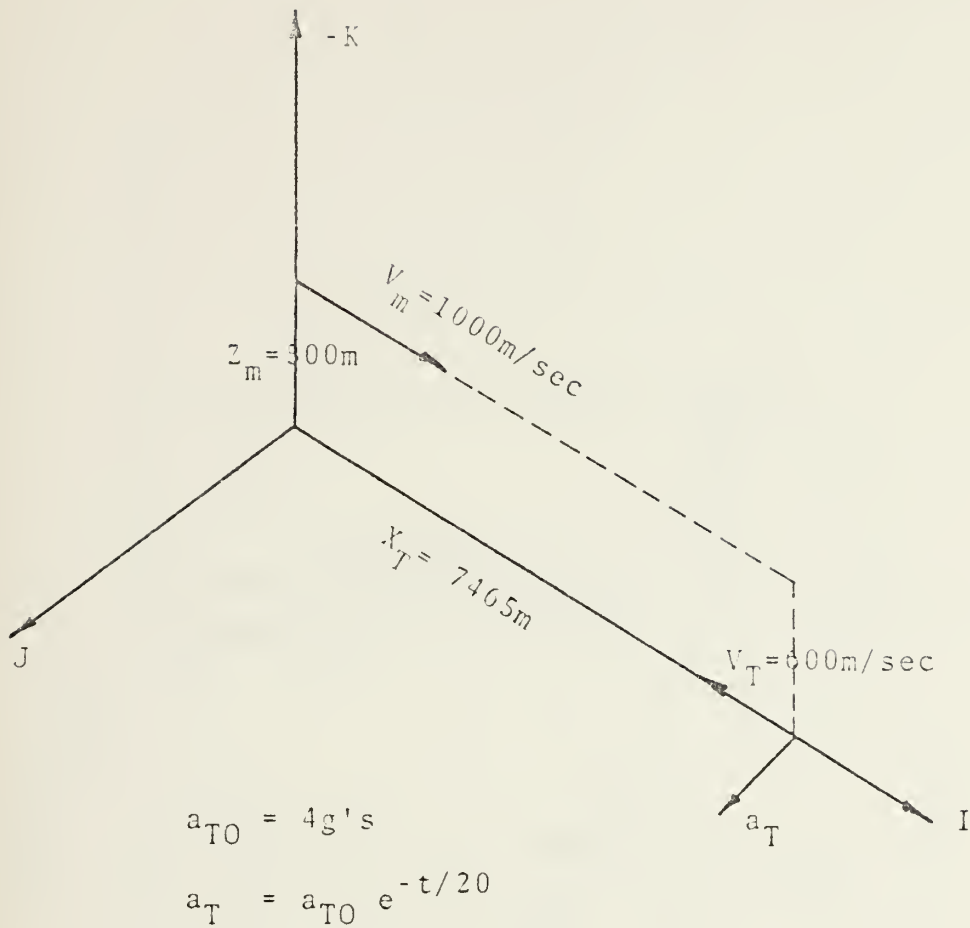


FIGURE 3.3 SCENARIO-2 HEAD-ON ENGAGEMENT.



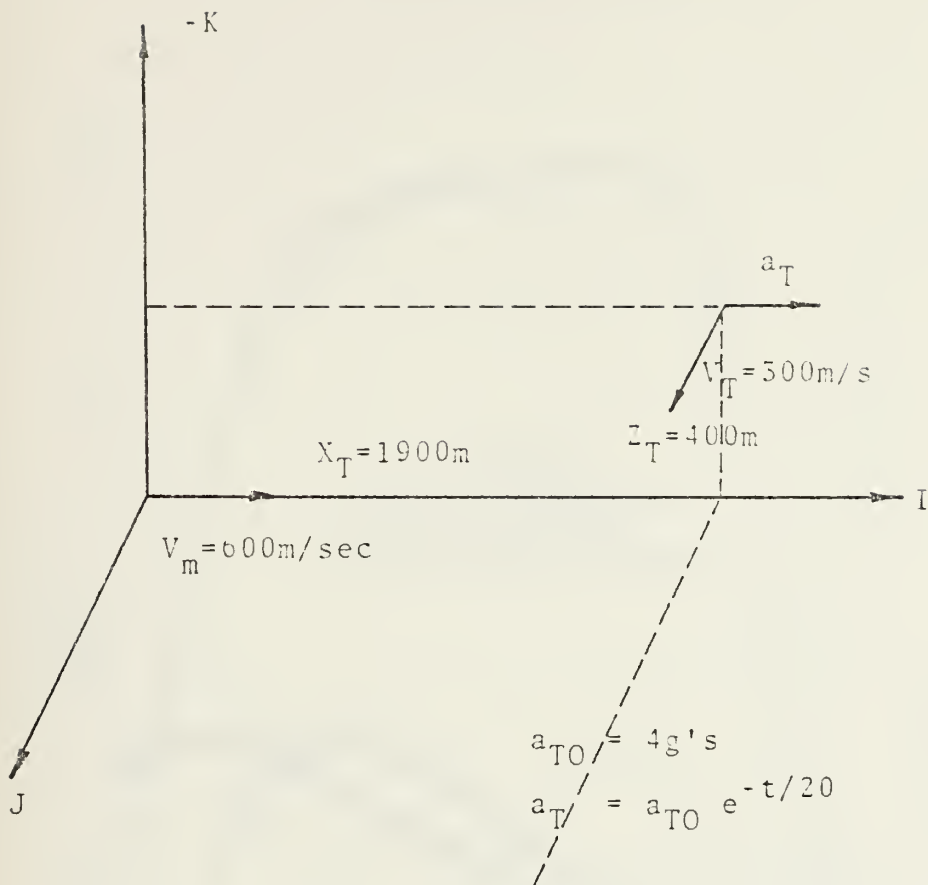


FIGURE 3.4 SCENARIO-3 SIDE-APPROACH ENGAGEMENT.



NO TIME LAG CASE

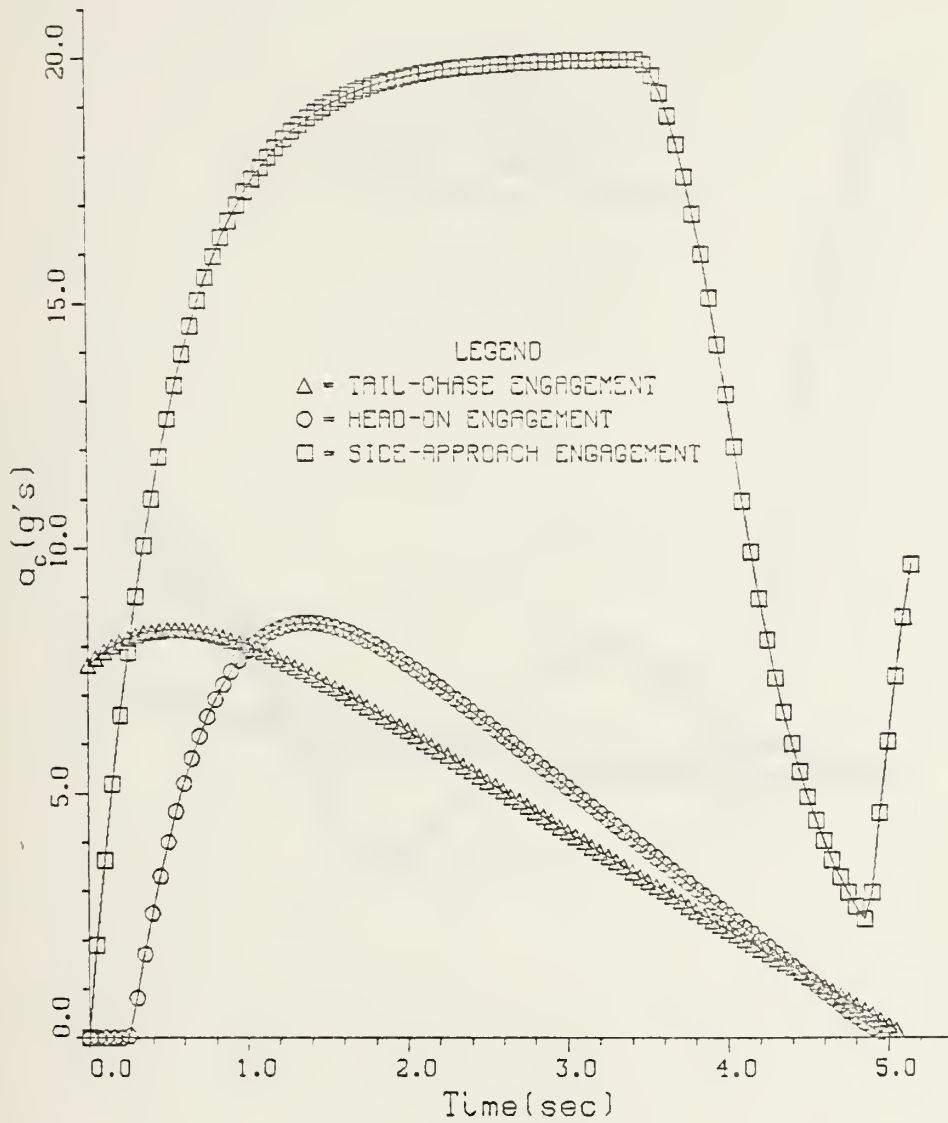


FIGURE 3-5. NORMAL ACCELERATION COMMAND VS TIME



NO TIME LAG CASE

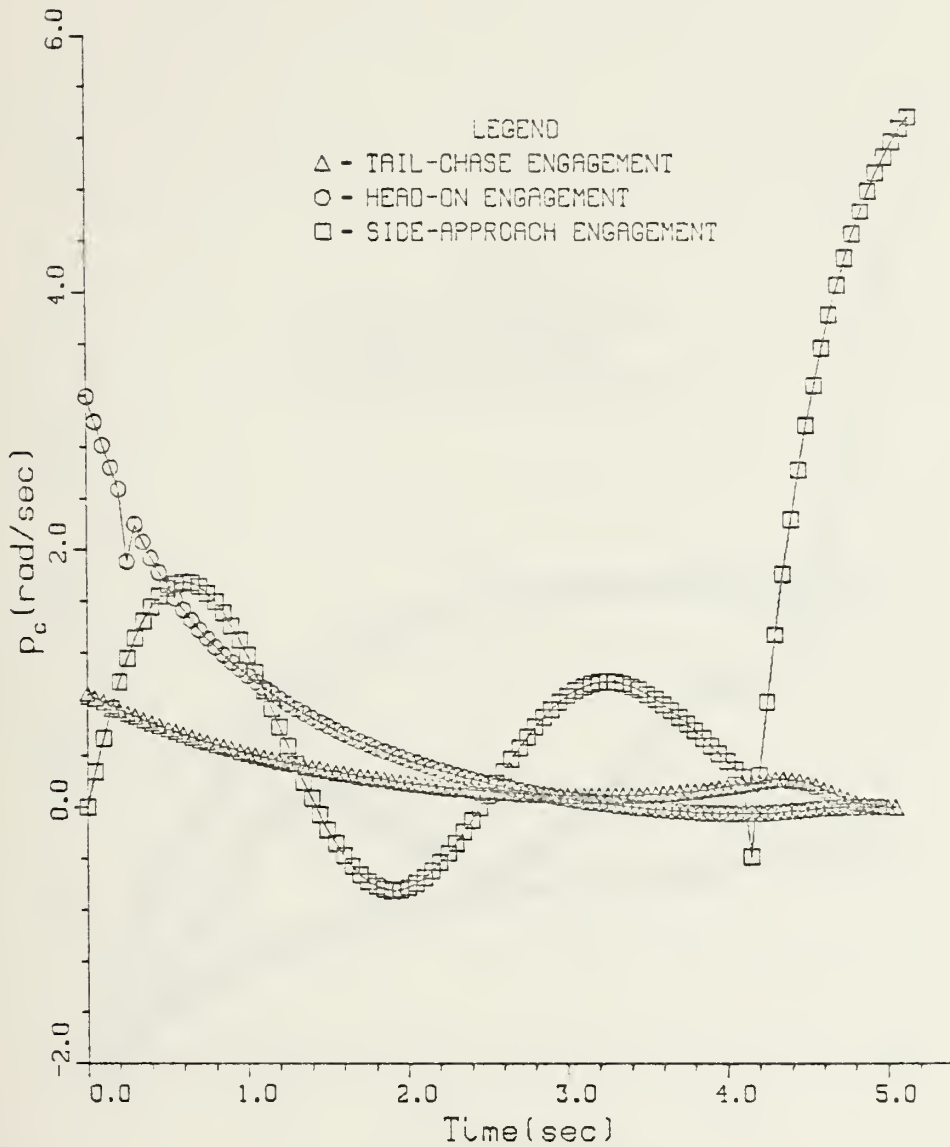


FIGURE 3-6. ROLL RATE COMMAND VS TIME





NO TIME LAG CASE

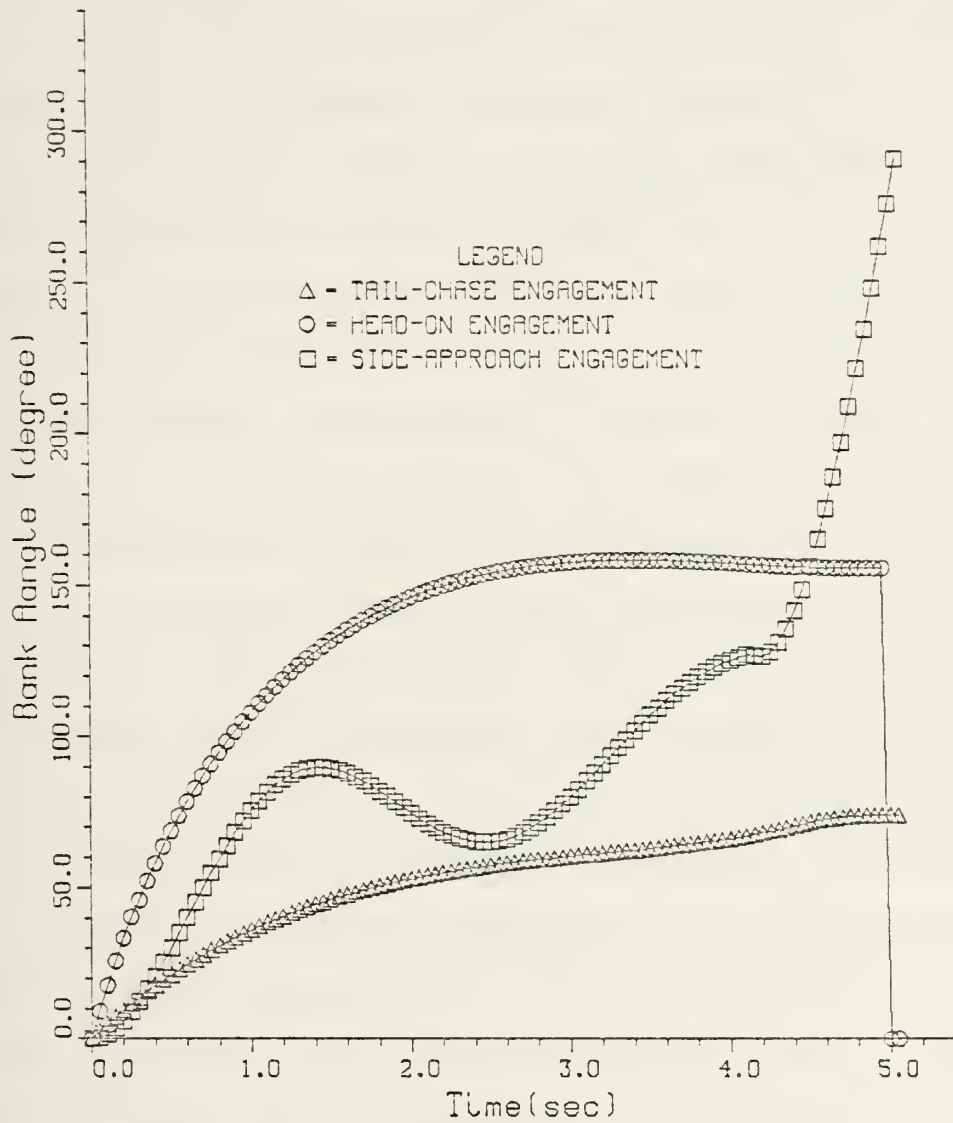


FIGURE 3-7. MISSILE BANK ANGLE VS TIME



at the final time. For scenario 2, the acceleration is zero in the initial phase, then increases and converges to zero finally. For scenario 5, the acceleration starts from zero, but, increases rapidly up to the maximum acceleration then freezes for seconds before decreasing. The acceleration does not converge to zero at the final time. Comparing these results with the variation of the roll rate command in Figure 3.6, the opposite trends are observed in the results of scenarios 1 and 2, i.e., if an acceleration command in the initial phase is large, a roll rate command is small. The acceleration command in Equation (3.5) is a linear function of PZC-miss in the z-direction of the missile coordinate system. For scenario 1, PAC-miss in the z-direction is relatively large, this causes a large acceleration command and a small roll rate command in initial phase. For scenario 2, the relative magnitude of the PZC-miss in the z-direction is small. This causes a large roll rate command in the initial phase. For scenario 5, the PZC-miss in y-direction is of the same magnitude as the relative distance as the Time-To-Go decreases. This means that a larger acceleration command than the maximum value allowable in the missile body coordinate system is required at some of instance time during the missile flying. Thus the acceleration does not converge to zero at the final time. In the derivation of the equations for control commands, a small angle approximation was assumed. However, in the



scenario 3 this assumption is questionable. The roll rate command computed as shown in Figure 3.6 shows a sine wave characteristics which is possibly due to overcorrection.

The simulation results for a 0.5 second time lag are shown in Figure 3.8 and Figure 3.9. The time lag causes much larger acceleration control commands. This includes overcorrections, so that the control commands do not converge in the final phase. The other characteristics follow the explanations given in the analysis of the cases with no time lag.

For all three scenarios the miss distances were obtained in the simulation of both cases, no- and 0.5 second-time lag. The miss distances are below 0.5m for all three scenarios in the case of no-lag. In the no lag case the control laws gave excellent results. In the lag case, the miss distances are 5.9m for tail-chase engagement, 0.8m for head-on engagement, and 32.9m for side-approach engagement. The miss distance of the side-approach engagement with a different maximum acceleration limit of 23g's results in a miss distance of less than 5m. This higher maximum acceleration limit will be used in the scenario 3 during the simulations for testing the performances of whole control system in Chapter 5.

The previous results are summarized as follows: (1) the tracking of a target is very dependent of the missile and target geometry, (2) the capabilities of the missile



(maximum acceleration and maximum roll rate limits and time constant) in maneuvering against the target is very important factors, (3) higher maximum accelerations are required in any side approach engagement, and (4) the assumption of small  $\Delta\phi$  in the optimal control law is a limitation in the general case. Nevertheless, the control laws developed from the optimal control theory for both the no lag and the 0.5 second-time lag cases yielded successful results for the specified scenarios. Since the optimal controller with 0.5 second-time lag autopilots resulted in a miss distance of approximately 5m with complete state variables feedback, it is expected that the inclusion of an optimal estimator for these particular scenarios will result in still larger miss distances.





TIME LAG (.5SEC) CASE

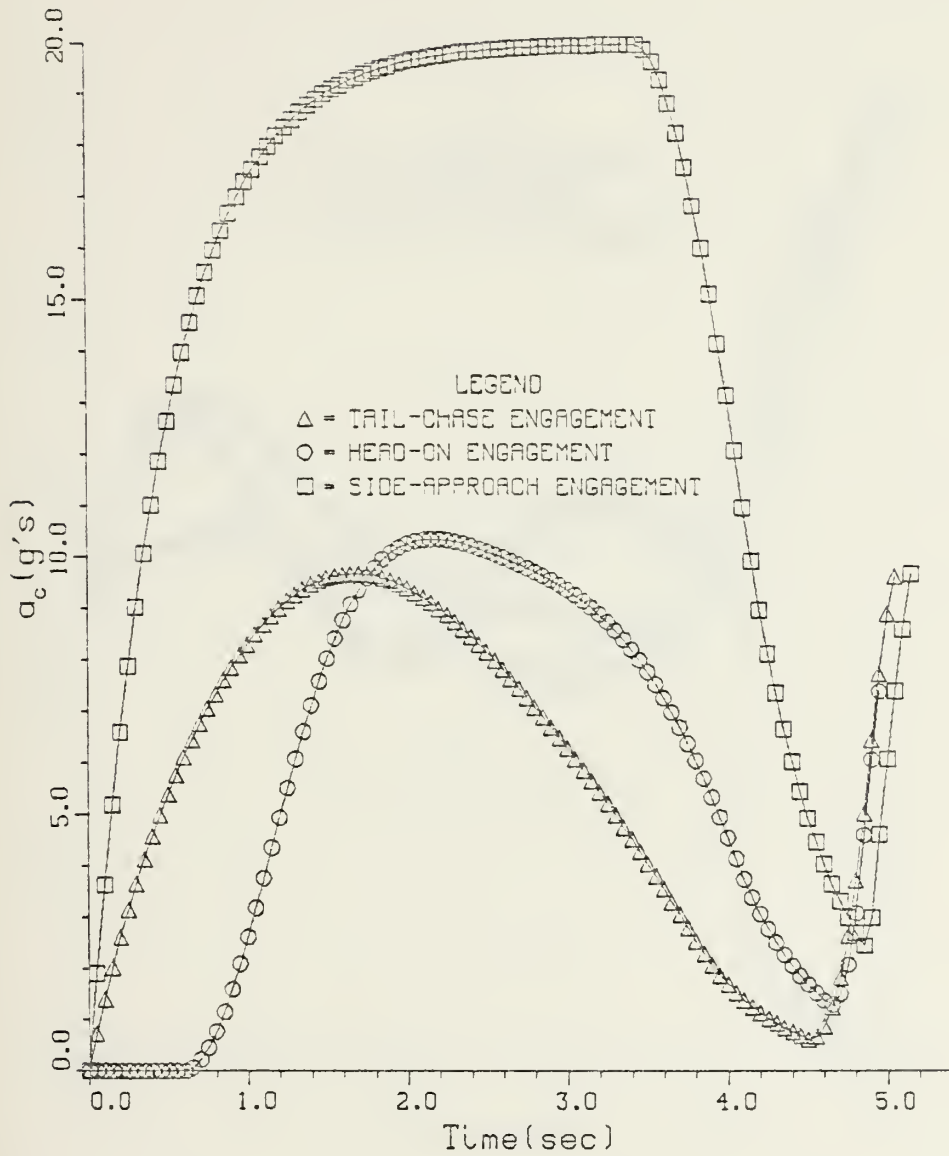


FIGURE 3-8. NORMAL ACCELERATION COMMAND VS TIME



TIME LAG (.5SEC) CASE

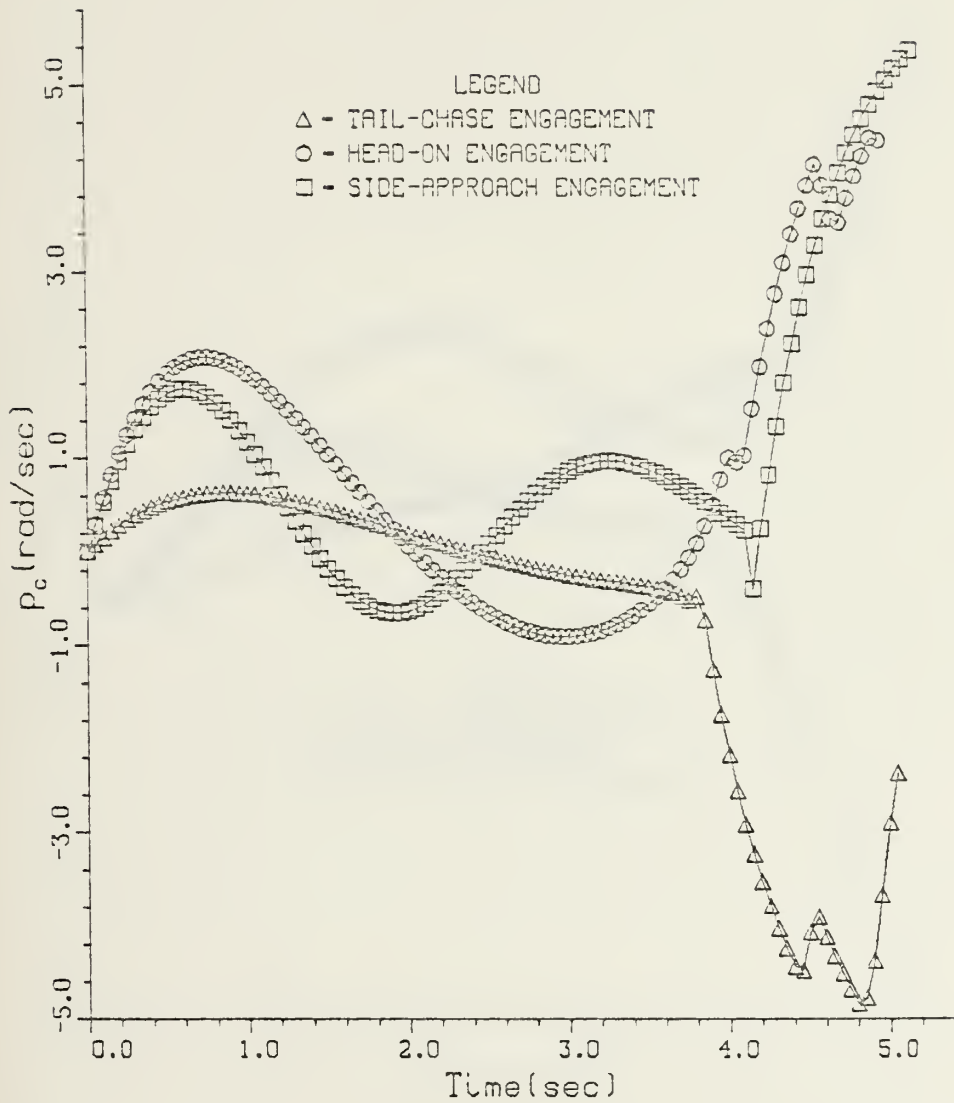


FIGURE 3-9. ROLL RATE COMMAND VS TIME



TIME LAG (.5SEC) CASE

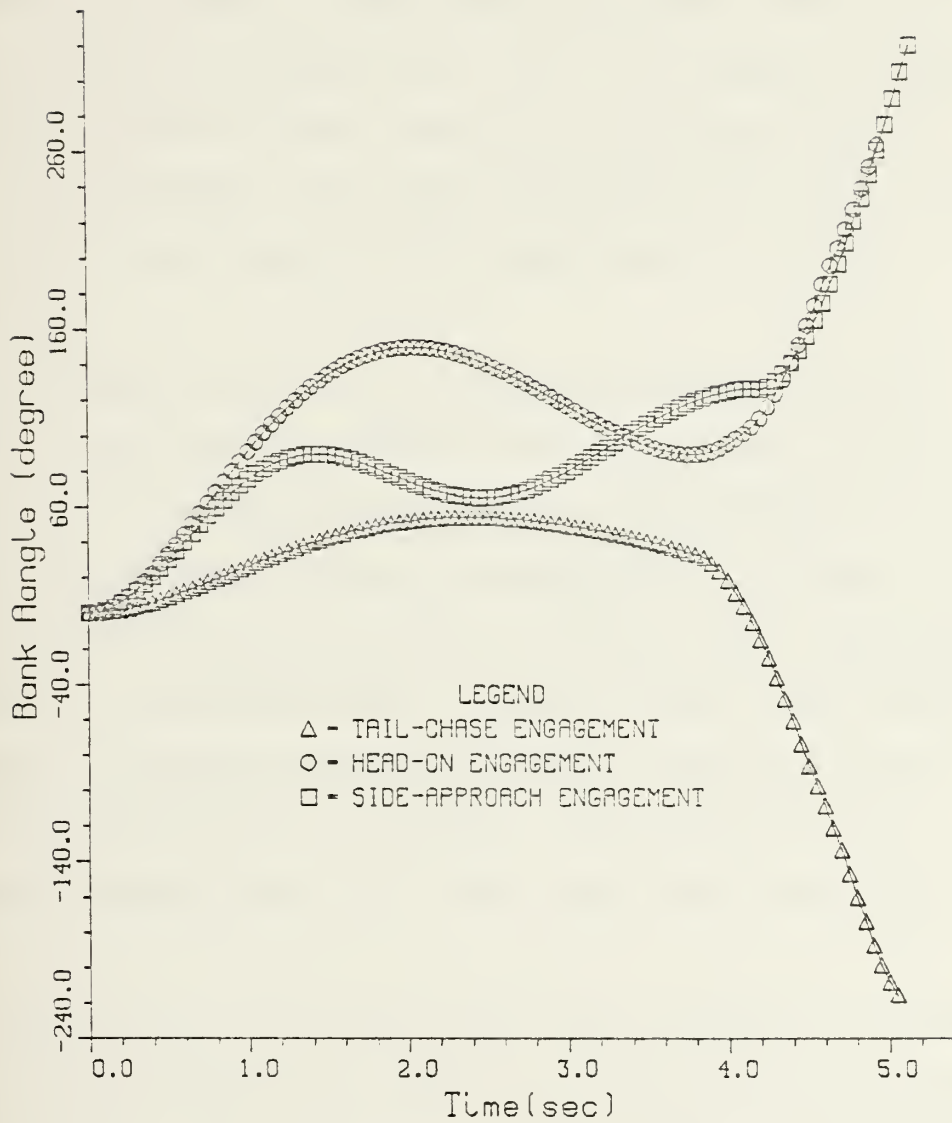


FIGURE 3-10. MISSILE BANK ANGLE VS TIME



#### IV. OPTIMAL ESTIMATOR

##### A. DESCRIPTION

Without full state variable feedback it is necessary to estimate the state variables. This chapter describes the Kalman filters used in the state estimation. These filters were designed for respectively: (a) two measured states, (b) four measured states, and (c) six measured states.

All measurements have noise superimposed on them. It is assumed that the nature of the noise source is known completely.

The Kalman filter is the optimal estimator of the states. Since the measurements are non-linear, it was necessary to use the extended Kalman filter theory. A first order extended filter was assumed in this work. In developing the filter algorithm, the non-linear measurement equation is linearized about the most recent state estimate and then the Kalman filter algorithm is applied. This is an extended Kalman filter algorithm. The results of the extended Kalman filter will yield suboptimal state estimation.

In practice, the missile will have sensors of various types that provide inputs which are related in some fashion to the states to be estimated. The main emphasis in the present work will be on active seeker which is assumed to





provide the optimal estimator with measurements of line-of-sight angles for the case of the missile having two measurement sensors. For the case of four measurements one has two of line-of-sight angles, range and time rate change of range. For the case of six-measurements one has two of line-of-sight angles, two of time rate change of the line-of-sight angles, range and its time rate change. When the measurement equations and the Jacobean matrix are developed the six-measurement case will be derived since the other cases have the same kind but less number of measurement sensors.

We will first consider the state equations and then the measurement equations. This will be followed by a discussion of the extended Kalman filter. Measurement error effects on the initialization of the Kalman filter will be analyzed. Finally, the estimator for the measurement cases will be simulated in order to test the effects of the implementation of the different measurment vectors on the extended Kalman filter.

## B. STATE EQUATIONS

The state vector is limited for convenience to the following state variables:

$$\underline{X} = (R_x, R_y, R_z, V_{rx}, V_{ry}, V_{rz}, a_{tx}, a_{ty}, a_{tz})^T \quad (4.1)$$



Where  $X_1 = R_x$ ,  $X_2 = R_y$ ,  $X_3 = R_z$  are the components of relative position,  $X_4 = V_{rx}$ ,  $X_5 = V_{ry}$ ,  $X_6 = V_{rz}$  the components of relative velocity, and  $X_7 = a_{tx}$ ,  $X_8 = a_{ty}$ ,  $X_9 = a_{tz}$  the components of target acceleration.

In order to develop the state equations, dynamic equations of target motion are needed. The target model selected for tracking applications must be sufficiently simple to permit ready implementation in weapons system for which computation time is at a premium yet sufficiently sophisticated to provide satisfactory tracking accuracy. To meet these requirements, the model described by Singer [Ref. 10] will be used in this work. The model will be presented for a single spatial dimension in order to enable accurate tracking performance estimates to be made for a variety of sensor measurement. If the targets under consideration normally move at constant velocity, the accelerations due to turns or evasive maneuvers may be viewed as perturbations upon the constant velocity trajectory. The target acceleration  $a(t)$  therefore will be termed the target maneuver variable, in a single physical dimension. The target maneuver capability can be satisfactorily specified by two quantities: the variance or magnitude of the target maneuver and the time constant, or duration, of the target maneuver. Hence the target acceleration, namely, the target maneuver is correlated



in time. A typical representative model of the target acceleration as a correlation function, can be expressed as follows:

$$a_t(\tau) = E[a_t(t)a_t(t + \tau)] = \sigma_m^2 e^{-\alpha|\tau|} \quad \alpha \geq 0 \quad (4.2)$$

Where the  $\sigma_m^2$  is the variance of the target acceleration and  $\alpha$  is the reciprocal of the maneuver time constant. The variance  $\sigma_m^2$  of the model will be approximated using the following formula which represents the acceleration probability density suggested by Singer [Ref. 10]:

$$\sigma_m^2 = \frac{a_{\max}^2}{5} [1 + 4P_{\max} - P_0] \quad (4.3)$$

where  $a_{\max}$  is a maximum acceleration rate,  $P_{\max}$  is the probability of maneuvering at  $a_{\max}$ , and  $P_0$  is the probability of no target maneuvering. And as mention in previous chapter,  $\alpha = 1/20$  for an evasive maneuver will be used in this work.

The above process can be modeled as the output of a low pass filter driven by white noise and it can be described by the equation

$$\dot{a}_t = -a_t + W \quad (4.4)$$



where  $\sigma_w^2(t)$ , the correlation function of the white noise input satisfies

$$\sigma_w^2(\tau) = 2\alpha\sigma_m^2\delta(\tau) \quad (4.5)$$

The acceleration model above will be applied to each X, Y, Z dimension with no cross coupling, the system state equations can be written then as:

$$\dot{\underline{X}} = \underline{F} \underline{X} + \underline{a} + \underline{W}$$

$$\begin{array}{c|ccc|ccc|ccc|c|ccc|c} \begin{array}{l} R_x \\ \dot{R}_y \\ R_z \\ \dot{V}_{rx} \\ \dot{V}_{ry} \\ \dot{V}_{rz} \\ \dot{a}_{tx} \\ \dot{a}_{ty} \\ \dot{a}_{tz} \end{array} & \begin{array}{cccccccc} 0 & 0 & 0 & 1 & 0 & 0 & 0 & 0 & 0 \end{array} & \begin{array}{l} R_x \\ R_y \\ R_z \\ V_{rx} \\ V_{ry} \\ V_{rz} \\ a_{tx} \\ a_{ty} \\ a_{tz} \end{array} & = & \begin{array}{cccccccc} 0 & 0 & 0 & 0 & 0 & 0 & 0 & 1 & 0 \end{array} & \begin{array}{l} R_x \\ R_y \\ R_z \\ V_{rx} \\ V_{ry} \\ V_{rz} \\ a_{tx} \\ a_{ty} \\ a_{tz} \end{array} & + & \begin{array}{ccc} 0 & -a_{mx} & -a_{ty} \\ 0 & -a_{ty} & -a_{yz} \\ 0 & -a_{yz} & 0 \end{array} & + & \begin{array}{ccc} 0 & 0 & 0 \\ W_x \\ W_y \\ W_z \end{array} \end{array} \quad (4.7)$$

The Equation (4.7) is a linear state equation with the assumption that the forcing function a vector, i.e., missile acceleration, can be precisely measured and also resolved into X, Y, Z components in the inertial frame.





Many sensors have a constant data rate, sampling the data every  $T$  seconds. If the above system equation is represented in discrete equations. The appropriate system equations of motion may be expressed by

$$\underline{X}(K + 1) = \Phi(T)\underline{X}(K) + \underline{B}(K) + \underline{U}(K) \quad (4.8)$$

where  $\Phi(T)$  is the target state transition matrix,  $\underline{B}(K)$  the deterministic forcing input vector which is composed of first and second integration and  $\underline{U}(K)$  the inhomogeneous driving input due to white noise. Since it is assumed that the missile acceleration is a known deterministic forcing function, the system equation of motion can be obtained by direct integration in each single dimension with  $E|W(t)|=0$ . The desired integration in discrete form yields

$$\begin{vmatrix} R(t_0+T) \\ V_r(t_0+T) \\ a_T(t_0+T) \end{vmatrix} = \begin{vmatrix} 1 & T & 1/\alpha^2(-1 + \alpha T + e^{-\alpha T}) \\ 0 & 1 & 1/\alpha(1 - e^{-\alpha T}) \\ 0 & 0 & e^{-\alpha T} \end{vmatrix} \begin{vmatrix} R(t_0) \\ V_r(t_0) \\ a_t(t_0) \end{vmatrix} + \begin{vmatrix} -\int\int_{t_0}^{t_0+T} a_m(t) dt dt \\ -\int_{t_0}^{t_0+T} a_m(t) dt \\ 0 \end{vmatrix}$$

$$\underline{X}(K + 1) = \Phi(t, \alpha) \underline{X}(K) + a_m(K) \quad (4-9)$$

Where  $K + 1 = (K + 1)T = t + T$ ,  $K = KT = t_0$ .



Next, if the driving input  $U(t)$  vector is considered, this input is not a sampled version of the continuous time white noise input  $W(t)$ . Since  $W(t)$  is white noise,  $U(k)$  also should be a discrete time white noise sequence, that is,  $E[U(K)U(K+i)] = 0$  for  $i \neq 0$ . Then as shown in Reference 10,  $U$  and  $W$  are related by

$$\underline{U}(k) = \int_{KT}^{(K+1)T} \Phi | [K+1]t - \tau | \underline{W}(t) dt \quad (4.10)$$

Where  $\underline{U}(K)$  is a white noise sequence with covariance matrix

$$E[\underline{U}(K)\underline{U}(K)^T] = Q \quad (4.11)$$

Following the above derivation, it can be easily expanded to the case of three independent dimensions in  $X$ ,  $Y$ ,  $Z$ . For  $\alpha_x = \alpha_y = \alpha_z = \alpha$ , and  $\sigma_x = \sigma_y = \sigma_z = \sigma$  since the model of target acceleration is for one dimension, the transition matrix is

$$\Phi = \begin{bmatrix} I & TI & f_1 I \\ 0 & I & f_2 I \\ 0 & 0 & I \end{bmatrix} \quad (4.12)$$



Where  $I$  and  $0$  are 3 by 3 identity and null matrices, and

$$f_1 = 1/\alpha^2 (\alpha T - 1 + e^{-\alpha T})$$

$$f_2 = 1/\alpha (1 - e^{-\alpha T})$$

$$f_3 = e^{-\alpha T}$$

The forcing acceleration vector is

$$\underline{B} = \begin{array}{c|c|c} B_1 & - \int \int_{KT} (K + 1) T a_{mx}(\tau) d\tau dt & \\ B_2 & - \int \int_{KT} (K + 1) T a_{my}(\tau) d\tau dt & \\ B_3 & - \int \int_{KT} (K + 1) T a_{mz}(\tau) d\tau dt & \\ B_4 & - \int_{KT} (K + 1) T a_{mx}(\tau) d\tau & \\ B_5 & - \int_{KT} (K + 1) T a_{my}(\tau) d\tau & \\ B_6 & - \int_{KT} (K + 1) T a_{mz}(\tau) d\tau & \\ B_7 & 0 & \\ B_8 & 0 & \\ B_9 & 0 & \end{array} \quad (4.15)$$



The covariance matrix of white noise  $\underline{u}(K)$  is

$$Q = \begin{bmatrix} Q_{11}^I & Q_{12}^I & Q_{13}^I \\ Q_{12}^I & Q_{22}^I & Q_{23}^I \\ Q_{13}^I & Q_{23}^I & Q_{33}^I \end{bmatrix} \quad (4.14)$$

Where

$$Q_{11} = (\sigma^2/\alpha^4) [1 - e^{-2\alpha T} + 2\alpha T + (2/3)(\alpha T)^3 - 2(\alpha T)^2 - 4\alpha T e^{-\alpha T}]$$

$$Q_{12} = (\sigma^2/\alpha^3) [e^{-2\alpha T} + 1 - 2e^{-\alpha T} + 2\alpha T e^{-\alpha T} - 2\alpha T + (\alpha T)^2]$$

$$Q_{13} = (\sigma^2/\alpha^2) [1 - e^{-2\alpha T} - 2\alpha T e^{-\alpha T}]$$

$$Q_{22} = (\sigma^2/\alpha^2) [4e^{-\alpha T} - 3 - e^{-2\alpha T} + 2\alpha T]$$

$$Q_{23} = (\sigma^2/\alpha) [e^{-2\alpha T} + 1 - 2e^{-\alpha T}]$$

$$Q_{33} = \sigma^2 [1 - e^{-2\alpha T}]$$

### C. MEASUREMENT EQUATION

In the case of the estimator with six-measurement sensors the present study assumes that the active seekers of missile give the measurements of the sightline angles





$\dot{\theta}_R$ ,  $\dot{\psi}_R$ , the time rate change of the sight line angles  
 $\dot{\theta}_R$ ,  $\dot{\psi}_R$ , the relative range  $R$ , and the time rate change  
of the relative range  $R$  contaminated by the Gaussian white  
noise. Then the equations of measurements in discrete time  
form are

$$\underline{z}(K) = \underline{h}(x,K) + \underline{v}(K) \quad (4.15)$$

where  $\underline{z}(K)$  is a sequence of measurement vector contaminated  
by white noise  $\underline{v}(K)$  and

$$h(x) = \begin{vmatrix} \text{elevation angle} \\ \text{elevation angle rate} \\ \text{azimuth angle} \\ \text{azimuth angle rate} \\ \text{range} \\ \text{range rate} \end{vmatrix} = \begin{vmatrix} \theta_r \\ \dot{\theta}_r \\ \psi_r \\ \dot{\psi}_r \\ R \\ \dot{R} \end{vmatrix}$$

The missile seekers actually measure the data about the  
seeker axes. Thus, throughout this development the assump-  
tion is made that the missile possesses an inertial measure-  
ment unit that accurately specifies the missile's orienta-  
tion in space so that a transformation from seeker to  
inertial coordinates can be made.

Referring to Figures 2.2 and 2.3, the six-measurement  
vectors can be written



$$\theta_R = \tan^{-1} \left[ \frac{R_z}{(R_x^2 + R_y^2)^{1/2}} \right]$$

$$\dot{\theta}_r = \frac{V_{r\theta}}{R} = \frac{R_x R_z V_{rx} + R_y R_z V_{ry} - (R_x^2 + R_y^2) V_{rz}}{(R_x^2 + R_y^2 + R_z^2) (R_x^2 + R_y^2)^{1/2}}$$

$$\psi_r = \tan^{-1} \left[ \frac{R_y}{R_x} \right]$$

$$\dot{\psi}_r = \frac{V_{r\psi}}{R \cos \theta_v} = \frac{-R_y V_{rx} + R_x V_{ry}}{(R_x^2 + R_y^2)}$$

$$R = (R_x^2 + R_y^2 + R_z^2)^{1/2}$$

$$\dot{R} = (\underline{V}_r \cdot \underline{R}) / R = \frac{R_x V_{rx} + R_y V_{ry} + R_z V_{rz}}{(R_x^2 + R_y^2 + R_z^2)^{1/2}}$$

$$\text{but } R_x = X_1, R_y = X_2, R_z = X_3, V_{rx} = X_4, V_{ry} = X_5,$$

$$V_{rz} = X_6$$



The measurement vector can be expressed in terms of state vector

$$\underline{h}(\underline{x}) = \begin{bmatrix} h_1 \\ h_2 \\ h_3 \\ h_4 \\ h_5 \\ h_6 \end{bmatrix} = \begin{bmatrix} \tan^{-1} \left[ \frac{X_3}{(X_1^2 + X_2^2)^{1/2}} \right] \\ \frac{X_1^2 X_3 X_4 + X_2^2 X_3 X_5 + (X_1^2 + X_2^2) X_3 X_6}{(X_1^2 + X_2^2 + X_3^2)^{3/2} (X_1^2 + X_2^2)^{1/2}} \\ \tan^{-1} \left[ \frac{X_2}{X_1} \right] \\ \frac{-X_1 X_2 X_4 + X_1 X_2 X_5}{(X_1^2 + X_2^2 + X_3^2)^{1/2} (X_1^2 + X_2^2)} \\ (X_1^2 + X_2^2 + X_3^2)^{1/2} \\ \frac{X_1 X_4 + X_2 X_5 + X_3 X_6}{(X_1^2 + X_2^2 + X_3^2)^{1/2}} \end{bmatrix} \quad (4.16)$$

The measurement noise covariance matrix for the active seeker can be written

$$E[\underline{V}(K)\underline{V}(K)^T] = R = \begin{bmatrix} \sigma_\theta^2 & 0 & 0 & 0 & 0 & 0 \\ 0 & \sigma_\theta^2 & 0 & 0 & 0 & 0 \\ 0 & 0 & \sigma_\psi^2 & 0 & 0 & 0 \\ 0 & 0 & 0 & \sigma_\psi^2 & 0 & 0 \\ 0 & 0 & 0 & 0 & \sigma_R^2 & 0 \\ 0 & 0 & 0 & 0 & 0 & \sigma_R^2 \end{bmatrix} \quad (4.17)$$



Where the diagonal elements are the variances of the individual measured quantities.

As shown in Equation (4.16), the measurement vectors are the non-linear functions of state vectors. It is impractical to implement in non-linear form because the computation of gain  $K$  and error covariance matrix  $P$  in update process in extended Kalman filter algorithm is not possible. To simplify this computation, and to implement the extended Kalman filter, the Jacobean or matrix of partial derivatives  $H$  will be determined, i.e.,

$$H_{ij} = \frac{\partial h_i}{\partial X_j} \quad (4.18)$$

The Jacobean will be a 6 by 9 matrix because  $\underline{h}$  is a vector with six elements and  $\underline{X}$  is a vector with nine elements. Performing the operation, the components of the matrix  $H$  are

$$\begin{aligned} H_{44} &= (-X_1 X_2) / (D_0 D_1^2) \\ H_{45} &= (X_1 X_2) / (D_0 D_1^2) \\ H_{46} &= 0 \quad H_{47} = 0 \quad H_{48} = 0 \quad H_{49} = 0 \\ H_{51} &= (X_1) / (D_c) \\ H_{52} &= (X_2) / (D_c) \\ H_{53} &= (X_3) / (D_c) \end{aligned}$$





$$H_{54} = 0 \quad H_{55} = 0 \quad H_{56} = 0 \quad H_{57} = 0 \quad H_{58} = 0 \quad H_{59} = 0$$

$$H_{61} = [(D_0^2 x_4) - (D_2 x_1)] / (D_0^3)$$

$$H_{62} = [(D_0^2 x_5) - (D_2 x_2)] / (D_0^3)$$

$$H_{63} = [(D_0^2 x_6) - (D_2 x_3)] / (D_0^3)$$

$$H_{64} = (X_1) / (D_0)$$

$$H_{65} = (X_2) / (D_0)$$

$$H_{66} = (X_3) / (D_0)$$

$$H_{67} = 0 \quad H_{68} = 0 \quad H_{69} = 0$$

$$D_0 = (X_1^2 + X_2^2 + X_3^2)^{1/2}$$

$$D_1 = (X_1^2 + X_2^2)^{1/2}$$

$$E_1 = X_1 X_3 [(X_4 + X_6) (2D_0^2 D_1^2 - X_1^2 - X_2^2 (X_5 + X_6))] (3D_1^2 + D_0^2)$$

$$E_2 = X_2 X_3 [(X_5 + X_6) (2D_0^2 D_1^2 - X_2^2 - X_1^2 (X_5 + X_6))] (3D_1^2 + D_0^2)$$

$$E_3 = [X_1^2 (X_4 + X_6) + X_2^2 (X_5 + X_6)] (D_1^2 + 2D_0^2)$$

$$H_{11} = (X_1 X_3) / (D_0^2 D_1)$$

$$H_{12} = (X_2 X_3) / (D_0^2 D_1)$$

$$H_{13} = (-D_1) / (D_0^2)$$

$$H_{14} = 0 \quad H_{15} = 0 \quad H_{16} = 0 \quad H_{17} = 0 \quad H_{18} = 0 \quad H_{19} = 0$$



$$F_{21} = (E_1) / (D_0^5 D_1^3)$$

$$H_{22} = (E_2) / (D_0^5 D_1^3)$$

$$F_{23} = (E_3) / (D_0^5 D_1^3)$$

$$H_{24} = (X_1^2 X_3) / (D_0^3 D_1^3)$$

$$F_{25} = (X_2^2 X_3) / (D_0^3 D_1^3)$$

$$H_{26} = (D_1 X_3) / (E_0^3)$$

$$H_{27} = 0 \quad H_{28} = 0 \quad H_{29} = 0$$

$$H_{31} = (-X_2) / (X_1^2 + X_2^2)$$

$$H_{32} = (X_1) / (X_1^2 + X_2^2)$$

$$H_{33} = 0 \quad H_{34} = 0 \quad H_{35} = 0 \quad H_{36} = 0 \quad H_{37} = 0 \quad H_{38} = 0$$

$$H_{39} = 0$$

$$H_{41} = (E_4) / (D_0^3 D_1^4)$$

$$H_{42} = (D_5) / (D_0^3 D_1^4)$$

$$H_{43} = [X_1 X_2 X_3 (X_4 - X_5)] / (D_0^3 D_1^2)$$

$$E_4 = X_2 (X_4 - X_5) [-D_0^2 D_1^2 + X_1^2 (D_1^2 + 2D_0^2)]$$

$$E_5 = X_1 (X_4 - X_5) [-D_0^2 D_1^2 + X_2^2 (D_1^2 + 2D_0^2)]$$



#### D. THE EXTENDED KALMAN FILTER

Optimal estimators that minimize the estimation error, can be divided into two processes, the one is the updating process to estimate the state vector at the current time, based upon all past measurements, the other is the extrapolating process to estimate the state at some future time. Optimal estimation procedure for linear state equations and non-linear measurement in the form of discrete time will be described referring to Reference 6. Figure 4.1, a timing diagram shows the flow of the various quantities involved in the discrete optimal filter equations.

The discrete system equation whose state at time  $kt$  is denoted by simply  $\underline{X}(K)$ , where  $\underline{U}(K)$  is a zero mean, white sequence of covariance  $\underline{Q}(K)$ , is

$$\underline{X}(K) = \Phi \underline{X}(K - 1) + \underline{B}(K - 1) + \underline{U}(K - 1) \quad (4.21)$$

where  $\Phi$  is a transition matrix

$$E[\underline{U}(K)] = 0 \quad (4.22)$$

$$E[\underline{U}(i)\underline{U}(j)^T] = \underline{Q}\delta_{ij} \quad (4.23)$$

The measurements are the non-linear function of the system state variables, corrupted by uncorrelated white noise of covariance  $R(K)$ . The measurement equation is written as



$$\underline{z}(K) = \underline{h}(\underline{x}, K) + \underline{v}(K) \quad (4.24)$$

where 
$$E[\underline{u}(K)] = 0 \quad (4.25)$$

$$E[\underline{v}(i)\underline{v}(j)^T] = R\delta_{ij} \quad (4.26)$$

The initial conditions are

$$E[\underline{x}(0)] = \underline{x}(0) \quad E[(\underline{x}(0) - \hat{\underline{x}}_0)(\underline{x}(0) - \hat{\underline{x}}_0)^T] = P_0 \quad (4.27)$$

$$E(\underline{w}_k \underline{v}_j^T) = 0 \quad \text{uncorrelated} \quad (4.28)$$

The Kalman filter algorithm is to minimize the estimation error, i.e., error covariance. If  $\hat{\underline{x}}$  denotes an estimate of state vector,  $\underline{x}$ , and  $\tilde{\underline{x}}$  is the mean value of the state vector, the error covariance matrix is defined as

$$P = E[(\tilde{\underline{x}} - \hat{\underline{x}})(\tilde{\underline{x}} - \hat{\underline{x}})^T] \quad (\text{symmetric}) \quad (4.29)$$

The development of the extended Kalman filter algorithm with a few definitions is essentially more application of the expectation operator  $E$ . We will consider the updating process then the extrapolating process. The update equations are used to incorporate the latest measurement in the estimate and in the covariance. After we obtain the updated covariance matrix we will then consider the optimum choice of Kalman gain and derive the equation for the estimation of state. Let  $\underline{x}(K-1)(-)$  denote an estimate of  $\underline{x}$





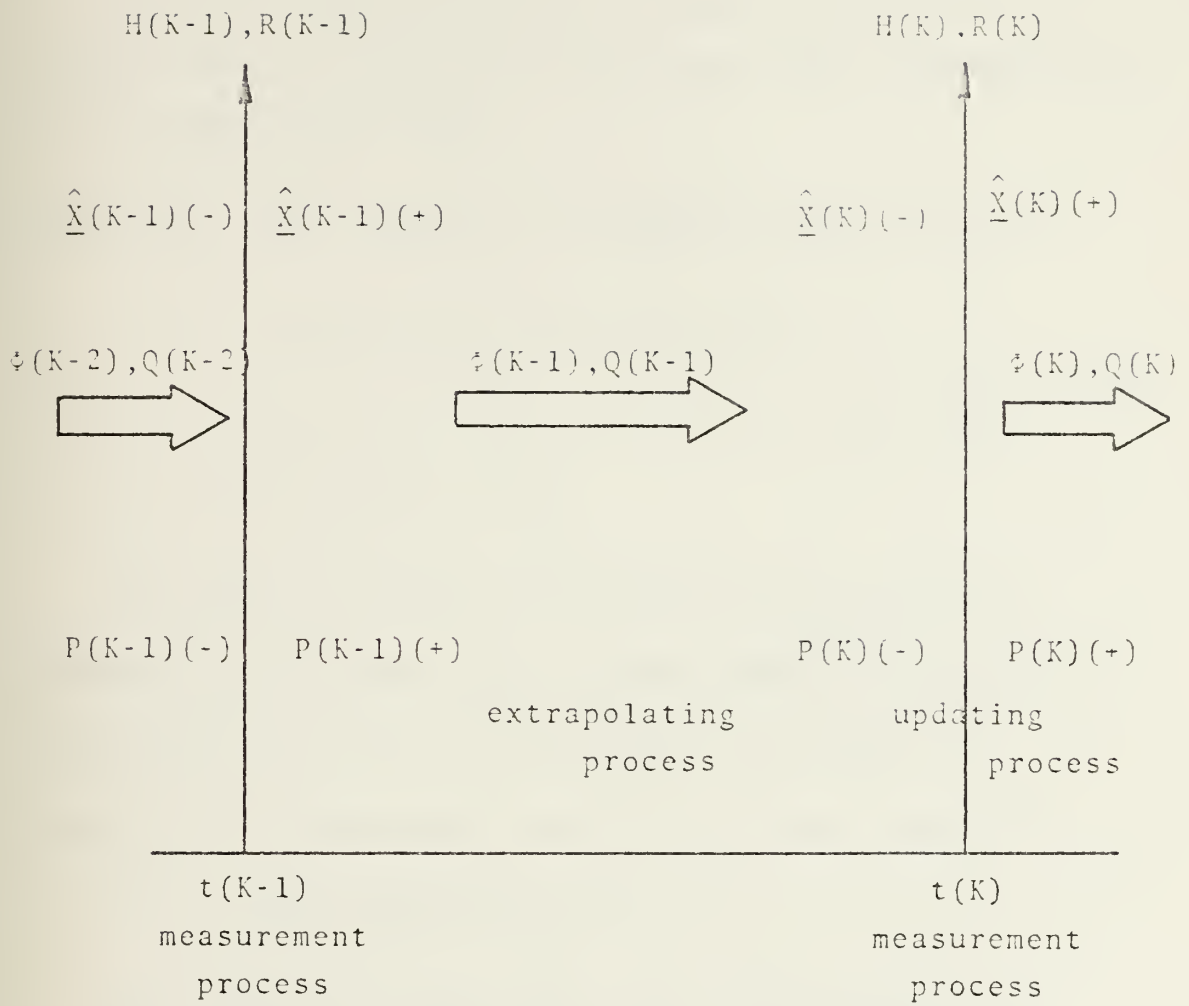


FIGURE 4.1 DISCRETE EXTENDED KALMAN FILTER TIMING DIAGRAM.



at time  $K-1$  , given measurements up to and including time  $K-2$  ,  $P(K-1)(-)$  denote the error covariance,  $K(K-1)$  denote Kalman gain and  $H(k-1)$  denote the Jaccobean matrix at time  $K-1$  . We will seek an optimal observer in the presence of the state excitation noise and in the presence of the observation noise.

$$\begin{aligned}
 P(K-1)(+) = E \{ & [I - K(K-1)H(K-1)] \tilde{X}(K-1) [X(K-1)^T(-)(I-K \\
 & (K-1)H(K-1)^T) + V(K-1)^TK(K-1)^T] \\
 & + K(K-1)V(K-1)[X(K-1)(-)^T(I-K(K-1)H(K-1)^T) \\
 & + V(K-1)^TK(K-1)^T] \} \quad (4.30)
 \end{aligned}$$

Rearranging Equation (4.30) using the definitions Equations (4.26) and (4.29) and the assumption that the measurement errors are uncorrelated, then one has

$$\begin{aligned}
 P(K-1)(+) = & [I-K(K-1)H(K-1)]P(K-1)(-)[I-K(K-1)H(K-1)^T] \\
 & + K(K-1)R(K-1)K(K-1)^T \quad (4.31)
 \end{aligned}$$

This equation updates the error covariance matrix. Then we still need an optimal gain  $K$ . We will choose to minimize the diagonal elements of the covariance matrix, i.e.,

$$J(K-1) = E[\hat{\underline{X}}(K-1)(+)^T \hat{\underline{X}}(K-1)(+)] = \text{trace} [P(K-1)(+)] \quad (4.32)$$



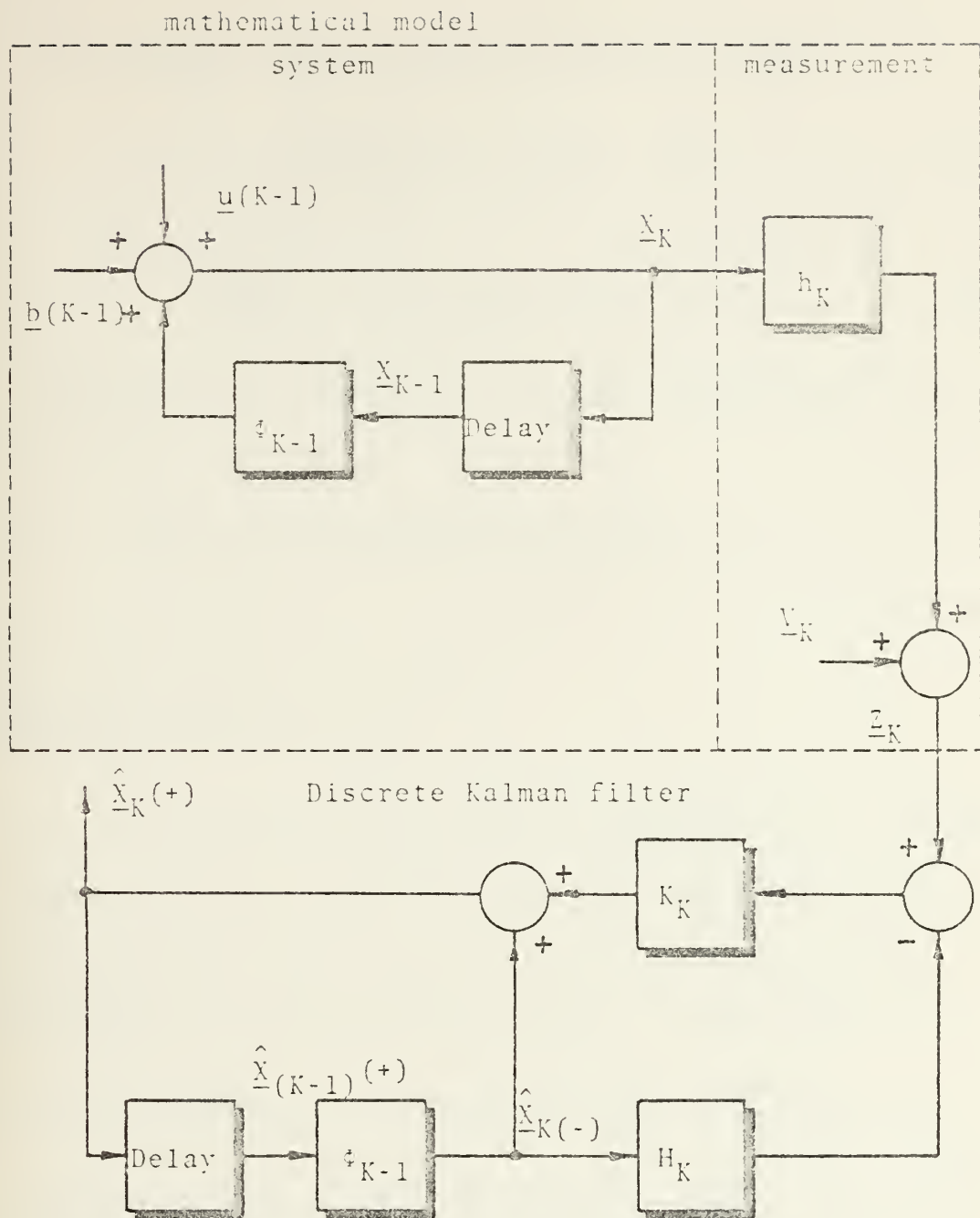


FIGURE 4.2 SYSTEM MODEL AND DISCRETE KALMAN FILTER.



Introducing a bit of matrix calculus, one has

$$\frac{a}{aA} [\text{trace } A B A^T] = 2AB \quad (4.33)$$

$$\frac{a}{aK(K-1)} [I - K(K-1)H(K-1)] = -H(K-1)^T \quad (4.34)$$

Applying these formulas to Equation (4.31) and solving for  $K(K-1)$ ,

$$K(K-1) = P(K-1)(-)H(K-1)^T [H(K-1)P(K-1)(-)H(K-1)^T + R(K-1)]^{-1} \quad (4.35)$$

This is the Kalman Gain Matrix.

Rearranging Equation (4.31)

$$P(K-1)(+) = [I - K(K-1)H(K-1)]P(K-1)(-) \quad (4.36)$$

Then the update state estimate at time  $K-1$  is equal to the extrapolated state estimate at time  $K-2$  plus a term which weights the measurement residual via gain  $K(K-1)$ .

$$\hat{\underline{X}}(K-1)(+) = \hat{\underline{X}}(K-1)(-) + K(K-1)[\underline{z}(K-1) - \underline{h}(K-1), \hat{\underline{X}}(K-1)(-)] \quad (4.37)$$

We need to consider also the propagation of the estimate  $\hat{\underline{X}}(+)$  between measurements and the propagation of the covariance matrix  $P(K-1)(+)$  between measurements. Propagation of the estimate is straight forward and involves only





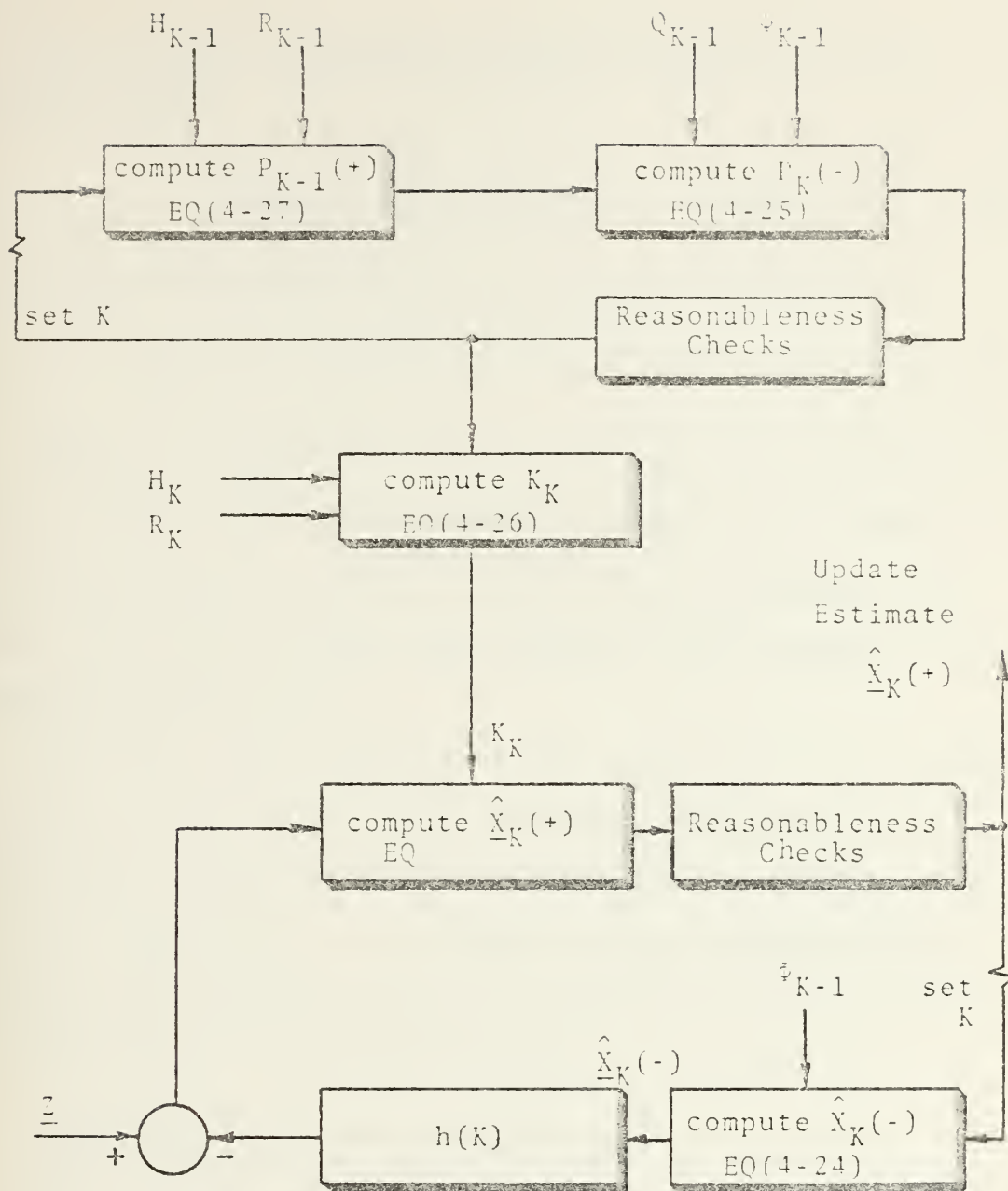


FIGURE 4.3 DISCRETE KALMAN FILTER INFORMATION FLOW DIAGRAM.



the application of the state transition matrix and the forcing terms.

$$\hat{\underline{x}}(K)(-) = \phi(K-1)\hat{\underline{x}}(K-1)(+) + \underline{u}(K-1) \quad (4.38)$$

By the definition (4.29), solving for  $P(K)(-)$

$$P(K)(-) = \phi(K-1)P(K-1)(+)\phi(K-1)^T + Q(K-1) \quad (4.39)$$

Figure 4.2 illustrates the above developed equations in block diagram form which contains a system model, measurement process and the Kalman filter to be implemented, and Figure 4.3 shows a simplified computer flow diagram of the discrete Kalman filter.

Equations (4.35) through (4.39) constitute the recursive formulas for implementing the extended Kalman filter algorithm. The process is initializing by providing values  $\hat{\underline{x}}(0)(-)$  and  $p(0)(-)$ . In order for the extended Kalman filter to be simulated, the next section will describe the initialization of the Kalman filter.

#### E. INITIALIZATION OF THE KALMAN FILTER

The one objective of this work is to test the performance of BTT missile control system having a Kalman filter as an optimal estimator as a function of different measurement vectors. All values for initialization of former worker in this work (Ref. 14) will be used for computer simulation.



## 1. Initializing the Error Covariance Matrix, P

Let  $\sigma_p$ ,  $\sigma_v$  and  $\sigma_a$  define the standard deviation of relative position estimate, of relative velocity estimate, and of target acceleration estimate. The initial values of error covariance matrix  $p$ , will be chosen as follows. The first six elements of the initial state vector are determined by

$$\hat{\underline{X}}(0) = \underline{X}(0) + \underline{V}(0)$$

Where the measurement vector  $\hat{\underline{X}}$  is the true measurement vector  $\underline{X}$  plus  $\underline{V}$  caused by measurement uncertainties. The expected mean square of initial covariance matrix components. With the assumption that the initial covariance matrix is diagonal with the diagonal elements reflecting the uncertainties associated with the initial state vector estimates, the components of the covariance matrix are

$$E[V_1^2] = E[V_2^2] = E[V_3^2] = \sigma_p$$

$$E[V_4^2] = E[V_5^2] = E[V_6^2] = \sigma_v^2$$

The last three elements of the state vector, acceleration components, are set to zeros

$$X_7 = X_8 = X_9 = 0$$



## 2. Initializing the Measurement Noise Variance Matrix R

Measurement errors for the active seeker are assumed to be due to thermal noise, gimbal angle pickoff error, environmental noise, and glint. The values of one sigma errors in each measurement will be used in present study. Because in the case of angle measurement, the environmental noise is proportional to the square of range to target and glint errors the wander of the apparent target centroid as seen by the seeker as varying inversely with range to target. The errors caused by noise are generally a highly complex function of the target geometry, target radar cross section, radar receiver, signal-to-noise ratio and etc. For simplicity, in present study, the constant one sigma errors (average values) in each measured vector are assumed to initialize the Kalman filter. Referring to Reference 13, the one sigma values of the average errors for measurement of angle, angle rate, range and range rate of the present active seeker are tabulated below.

- (1) angle measurement errors : 0.15 -0.6 deg
- (2) angle rate measurement errors : 0.5 -2.0 deg/sec
- (3) range measurement errors : 3 meters
- (4) range rate measurement errors : 6 m/sec

Before the simulation runs is undertaken, it will be briefly discussed the manner in which the Kalman filter on board the missile is initialized at the start of the





engagement based on sensor data from the launch aircraft. The launch aircraft's sensors are assumed capable of determining, within some prescribed accuracy, the relative position and relative velocity of the target with respect to the missile at the instant of launch. This information is used to initialize the first six elements of the filter's state vector. However, the launch aircraft is assumed to be able to provide no information regarding target acceleration. Thus the three elements of the initial state vector are set to zero, finally, the complete list of nominal parameters for initialization is provided in Table 4.1.

#### F. EVALUATION OF THE OPTIMAL ESTIMATOR PERFORMANCE

The performance of the state estimator with two-measurement vectors (case 1), with four-measurement vectors (case 2), and with six-measurement vectors (case 3), was simulated to evaluate the effect of the possible implementation of the more measurement sensors on the bank-to-turn missile for typical scenario (tail chase engagement case). The error covariance and the Kalman gain components selected, and the states estimated, were computed as shown in Figure 4.4 through Figure 4.30. The control laws implemented with the estimator also were tested to evaluate the performance of the control system of the BTT missile as shown in Figures 4.31 through 4.35.



TABLE 4-1  
NOMINAL PARAMETERS

| Description                              | Symbol                                   | Nominal Value            | Range      |
|--|--|--------------------------|------------|
| 1 data sampling time                     | $T$                                      | 0.5 sec                  | -----      |
| 2 one sigma angle<br>error               | $\sigma_\theta, \sigma_\psi$             | 0.15 deg                 | 0.15 - 1.0 |
| 3 one sigma angle rate<br>error          | $\dot{\sigma}_\theta, \dot{\sigma}_\psi$ | 0.5 deg/sec              | 0.5 - 2.0  |
| 4 one sigma slant<br>range error         | $\sigma_r$                               | 3.0 m                    | -----      |
| 5 one sigma slant<br>range rate error    | $\dot{\sigma}_r$                         | 6.0 m/sec                | -----      |
| 6 missile roll rate<br>time constant     | $\tau_p$                                 | 0.5 sec                  | 0.3 - 1.0  |
| 7 missile normal acc.<br>time constant   | $\tau_a$                                 | 0.5 sec                  | 0.3 - 2.0  |
| 8 missile maximum<br>normal acc.         | $a_{max}$                                | 20 g's                   | 5 - 25     |
| 9 missile maximum<br>roll rate           | $p_{max}$                                | 6.28 rad/sec             | 1 - 10     |
| 10 filter process noise<br>parameter     |  |                          |            |
| a target rms acc.                        | $\sigma$                                 | 5 g's                    | -----      |
| b target maneuver<br>bandwidth           | $\alpha$                                 | 1/20 sec                 | -----      |
| 11 controller cost<br>function parameter |  |                          |            |
| a weight on $a_c$                        | $B_1$                                    | 0.003234 sec             | -----      |
| b weight on $\dot{p}_c$                  | $B_2$                                    | 1.25 m <sup>2</sup> /sec | -----      |



Figures 4.4 to 4.12 represent the variations of the error covariances of each state variable. Figures 4.4 through 4.7 show the three covariances for the relative positions, i.e.,  $P_{11}$ ,  $P_{22}$ ,  $P_{33}$ . Only the covariance of the two measurement case varies substantially. Thus one would expect that the gain components  $G_{11}$ ,  $G_{21}$ ,  $G_{31}$  would show only variations in the two measurement case as are shown in Figures 4.13 through 4.15. The trend noted in the set of graphs (4.4, 4.5, 4.5) and in the corresponding Kalman gains is also observed in the other covariance components. Thus the covariance components for the velocity (Figures 4.7, 4.8 and 4.9) should larger variation is reflecting in the corresponding Kalman gains of 4-16, 4-17, 4-18. The covariances of the acceleration components show a similar development but there appears to be less variation in  $a_{ty}$  and  $a_{tz}$  acceleration covariances. In the case of  $a_{tz}$  the variation of the Kalman gains are restricted to a much narrower range. The error covariance and the Kalman gain components in all three cases eventually converge to very small values. Figure 4.22 through Figure 4.30 show the results of the state estimations of the three estimators. Figures 4.22, 4.23 and 4.24 show the variations of the estimated relative position ( $R_x$ ,  $R_y$ ,  $R_z$ ). Figures 4.25, 4.26 and 4.27, the variations of the estimated relative velocity ( $V_{rx}$ ,  $V_{ry}$ ,  $V_{rz}$ ). Figures 4.28, 4.29 and 4.30 the



variations of the estimated target acceleration ( $a_{tx}$ ,  $a_{ty}$ ,  $a_{tz}$ ) . The trends of the curves representing the estimated states are similar except for Figure 4.25 which shows a wide variation in the estimated  $V_{rx}$  component of the two measurement case from the true state values. Generally, the estimated states of the estimator with two- and four-measurement are close to the true states, in spite of the wide variation of error covariance components of two-measurement case. The estimator with six-measurement vectors generates the estimated states which show almost same characteristics as the estimator with four-measurement vectors, but usually underestimated the states in comparison with the generated states of the estimator with four-measurement vectors. Figure 4.32 and Figure 4.34 show the curves of the control commands computed using the estimated states. The results of the six-measurement case have a wholly different form from the curves representing the computed control commands in the other cases. The normal acceleration commands computed using the estimated states with the six-measurement vectors initially have smaller values, but finally reach maximum value as shown in Figure 4.32. Also as shown in Figure 4.34, the roll rate commands run from the minimum limit to the maximum limit. The large variations of the both control commands of case 3 during a short time interval result in





# TAIL-CHASE ENGAGEMENT CASE

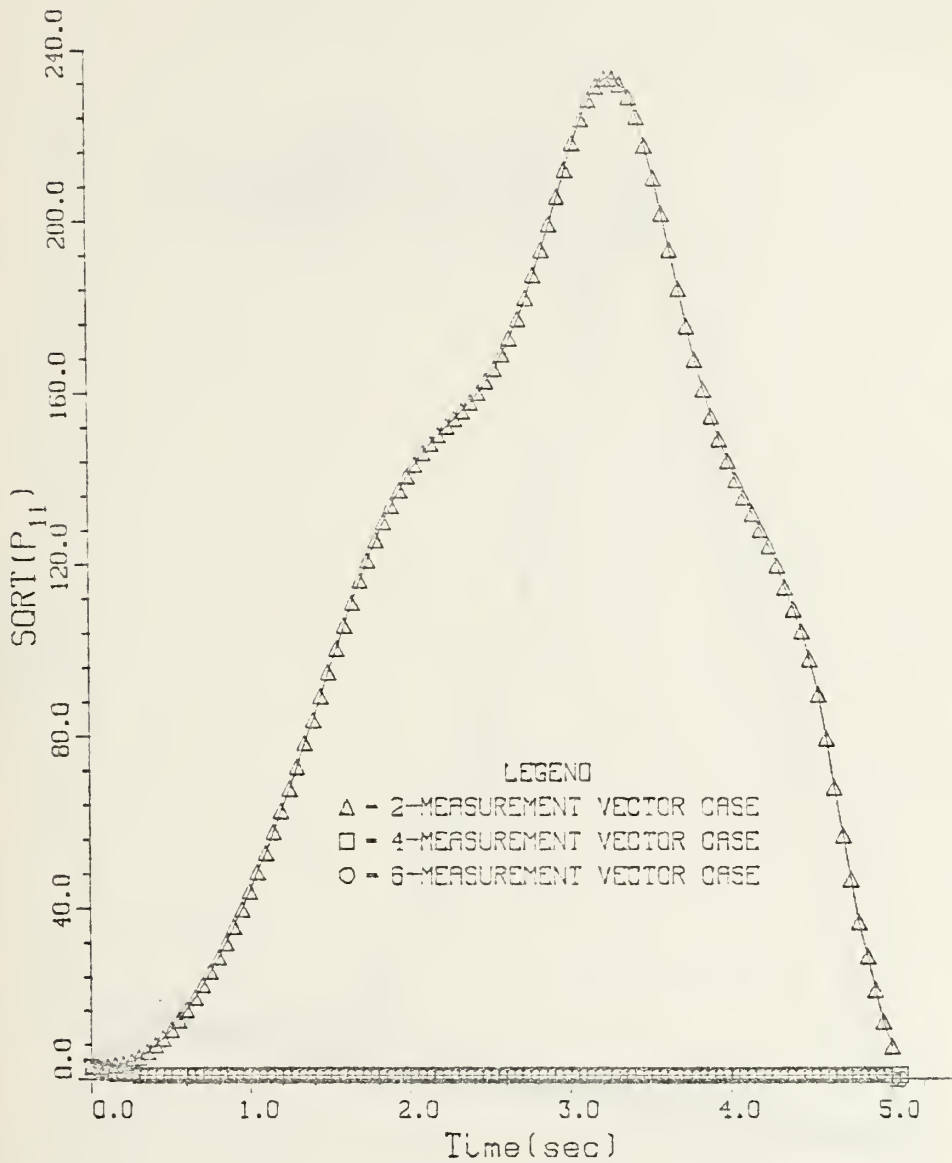


FIGURE 4-4. ERROR COVARIANCE COMPONENT( $P_{11}$ )  
VS TIME



# TAIL-CHASE ENGAGEMENT CASE

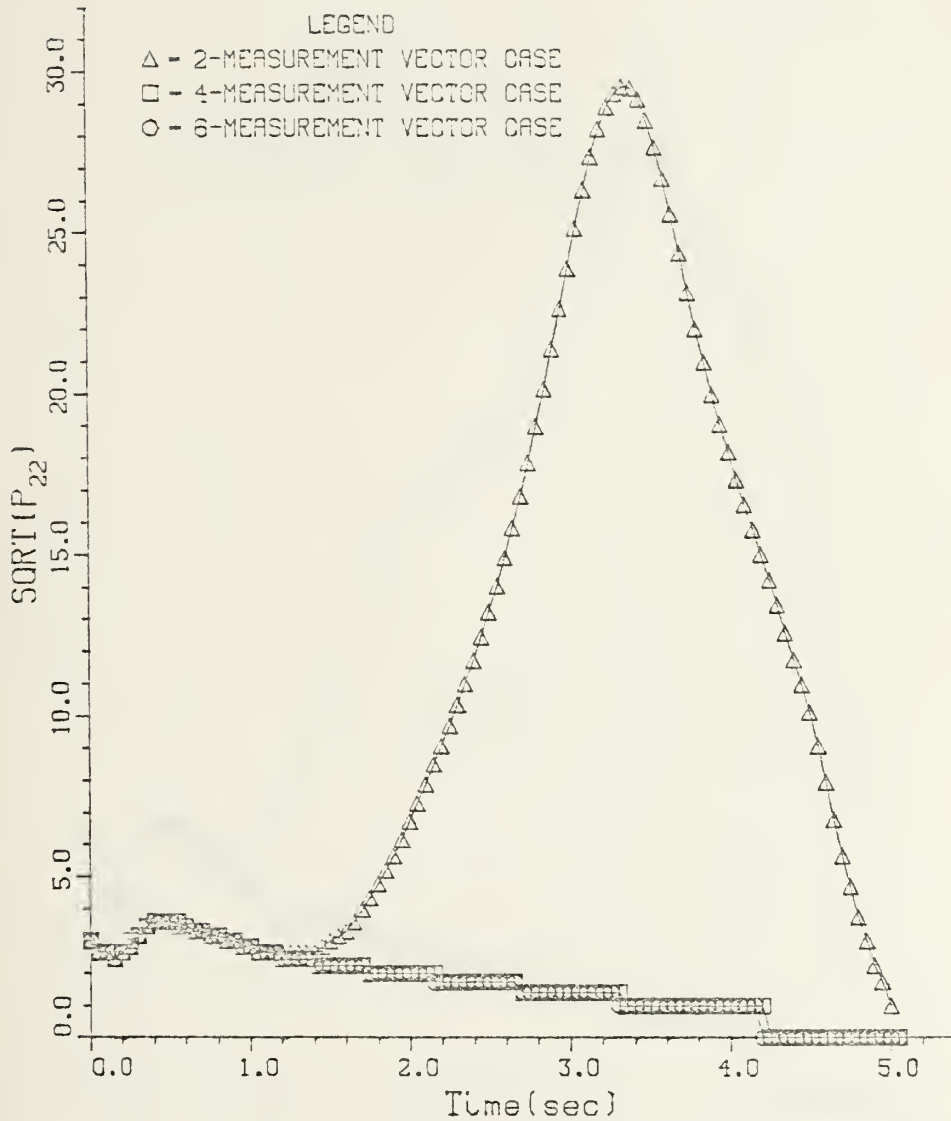


FIGURE 4-5. ERROR COVARIANCE COMPONENT( $P_{22}$ )  
VS TIME



# TAIL-CHASE ENGAGEMENT CASE

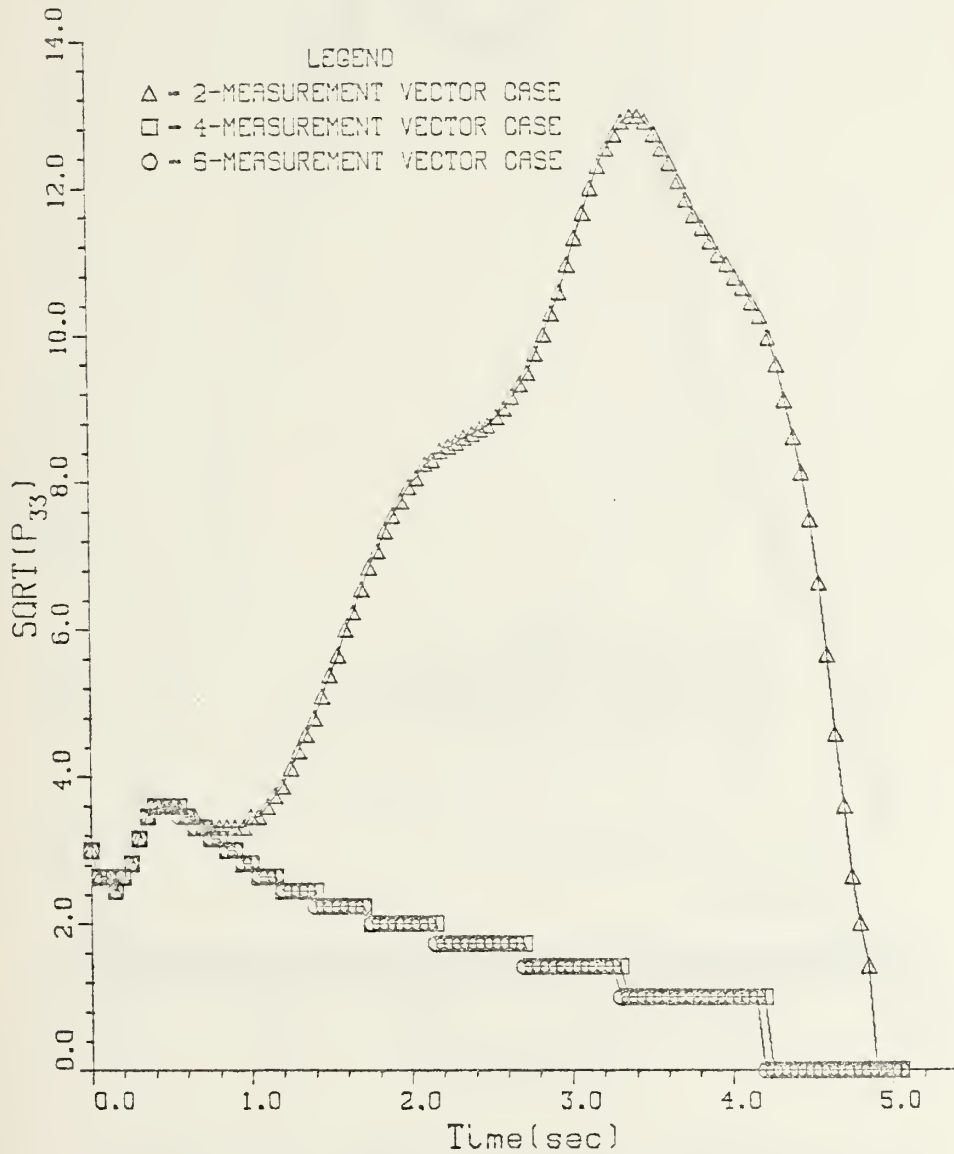


FIGURE 4-6. ERROR COVARIANCE COMPONENT ( $P_{33}$ )

VS TIME



# TAIL-CHASE ENGAGEMENT CASE

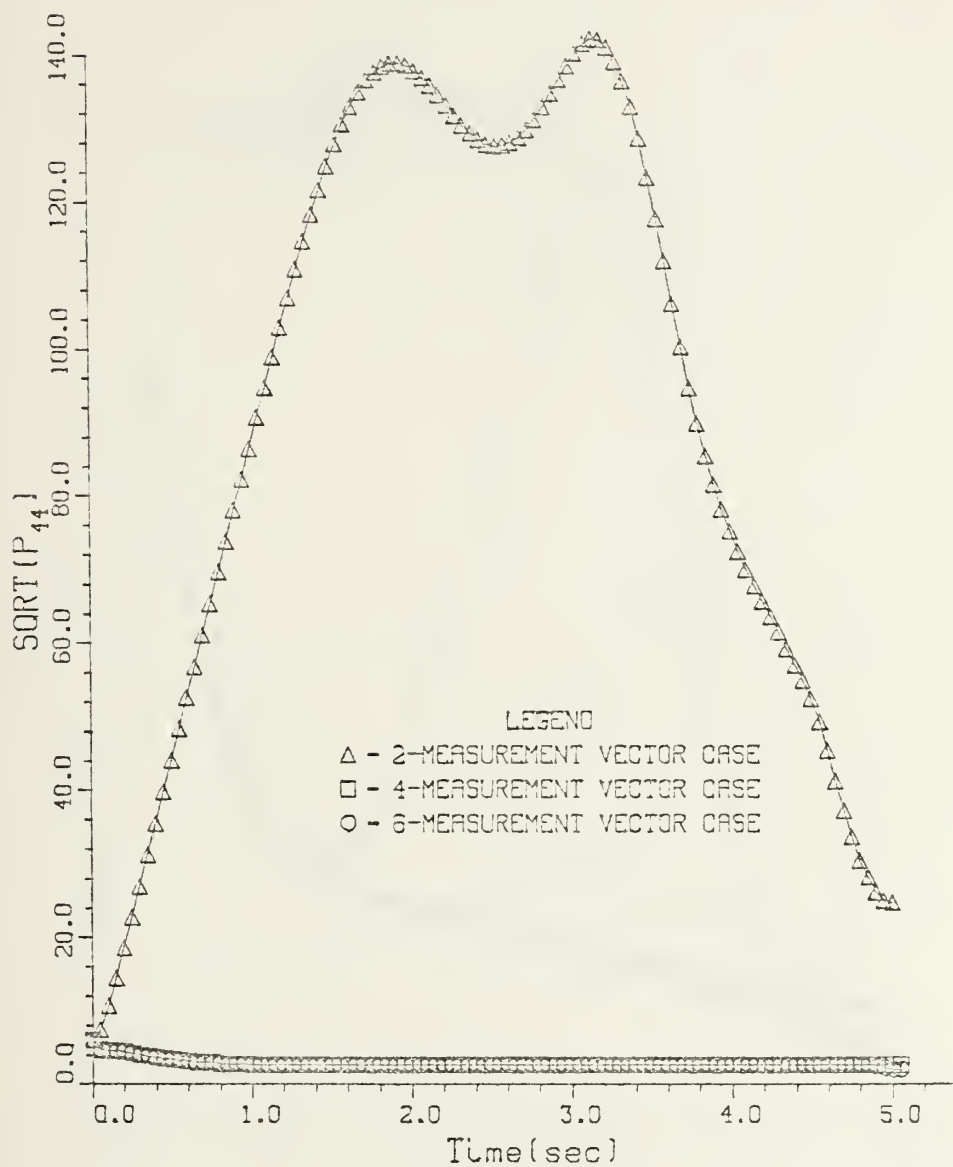


FIGURE 4-7. ERROR COVARIANCE COMPONENT(P<sub>44</sub>)  
VS TIME





# TAIL-CHASE ENGAGEMENT CASE

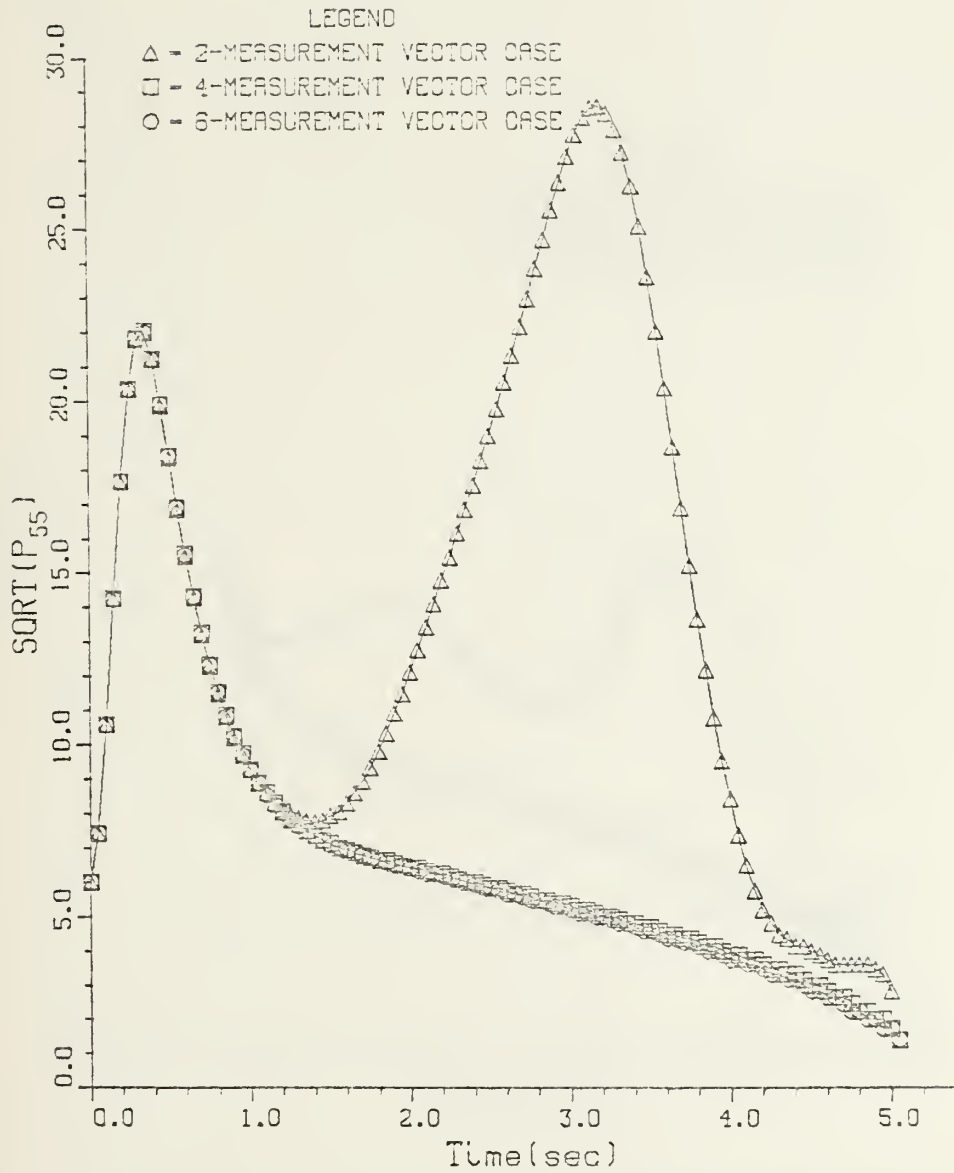


FIGURE 4-8. ERROR COVARIANCE COMPONENT( $P_{55}$ )  
VS TIME



# TAIL-CHASE ENGAGEMENT CASE

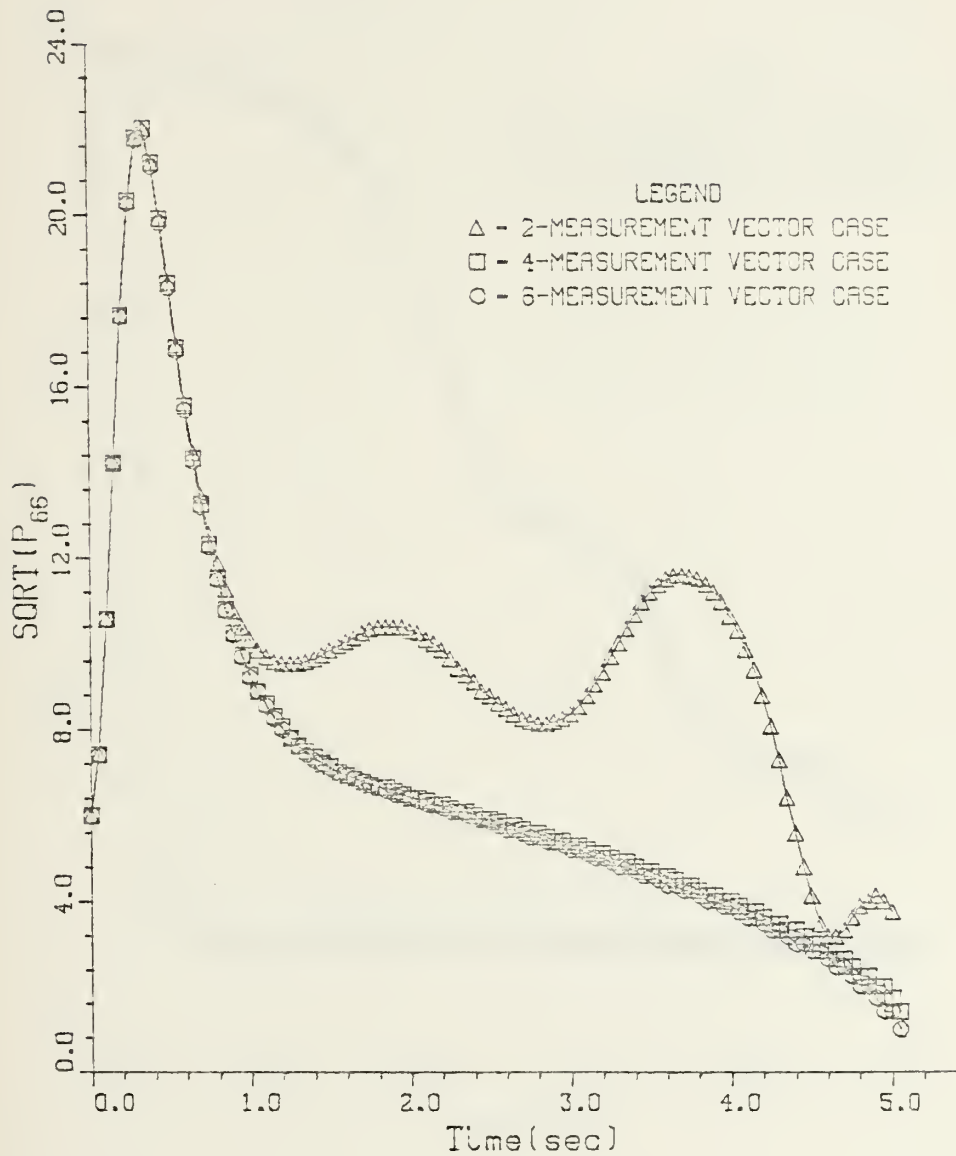


FIGURE 4-9. ERROR COVARIANCE COMPONENT( $P_{66}$ )  
VS TIME



# TAIL-CHASE ENGAGEMENT CASE

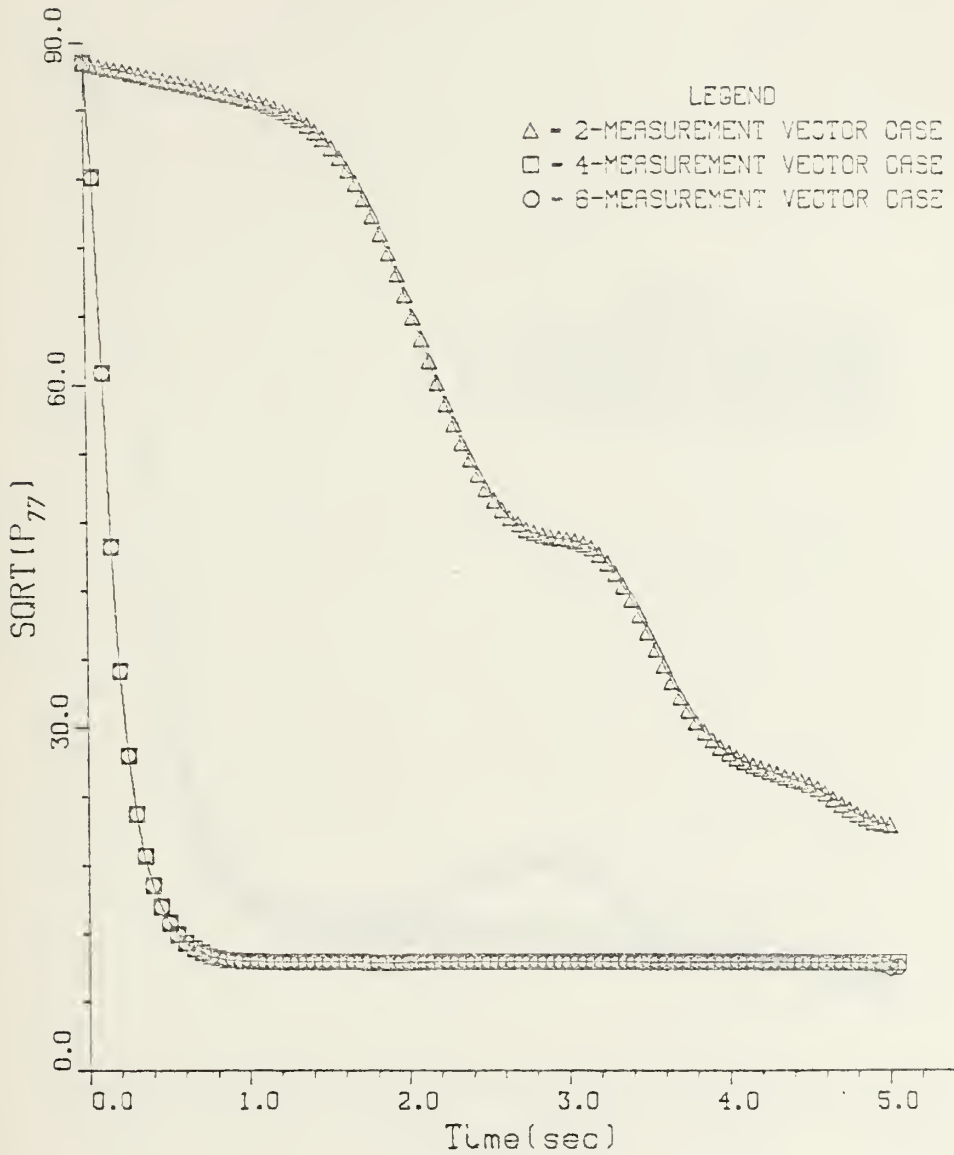


FIGURE 4-10. ERROR COVARIANCE COMPONENT( $P_{77}$ )  
VS TIME



# TRAIL-CHASE ENGAGEMENT CASE

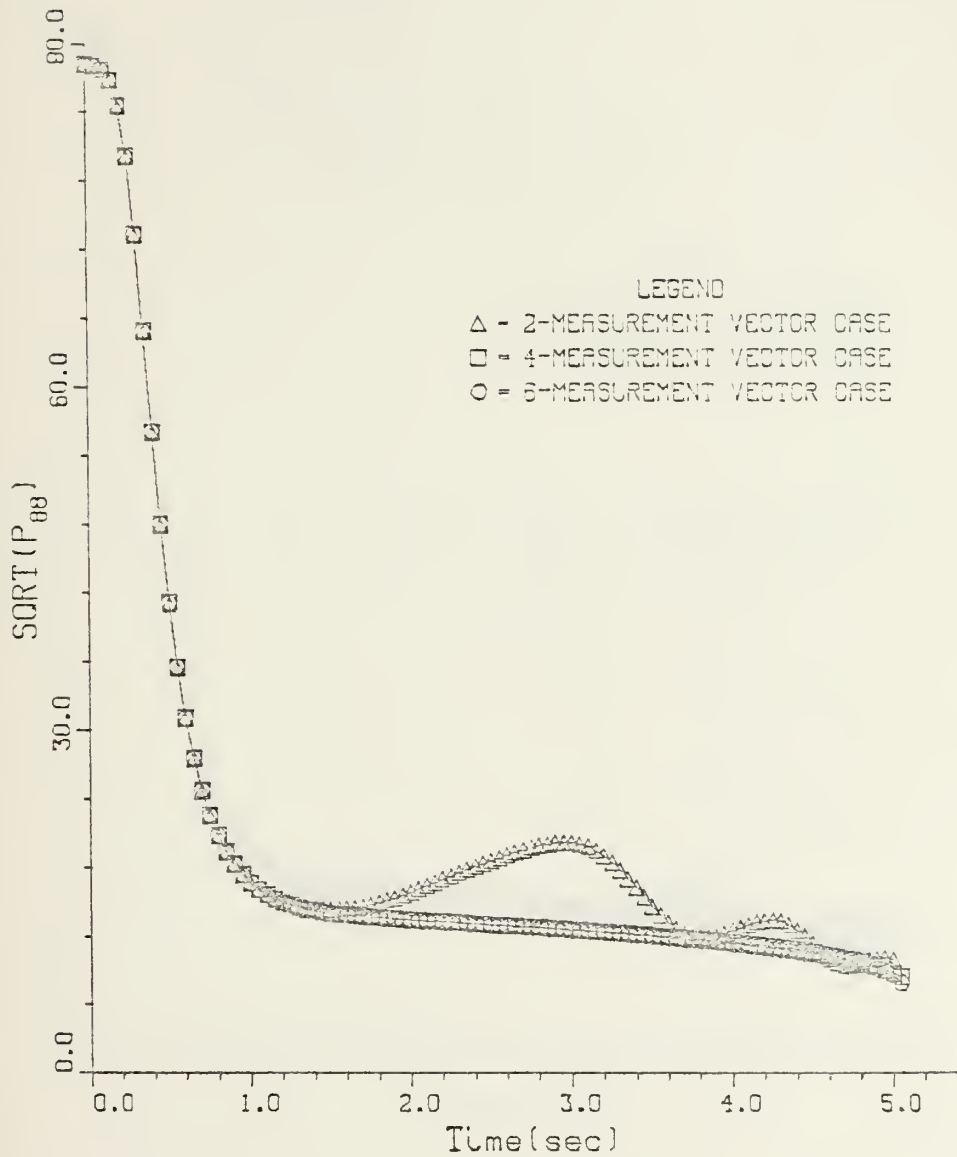


FIGURE 4-11. ERROR COVARIANCE COMPONENT( $P_{88}$ )  
VS TIME





# TAIL-CHASE ENGAGEMENT CASE

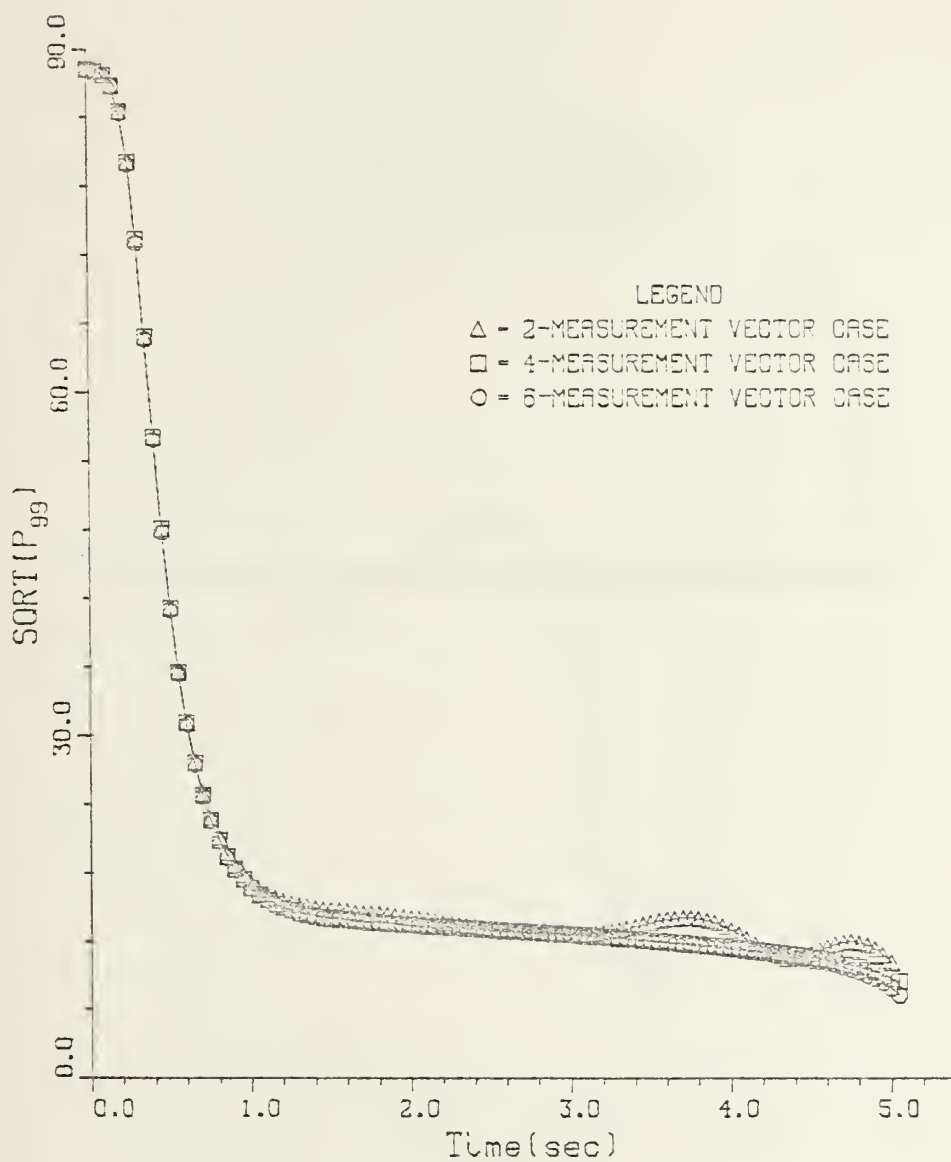


FIGURE 4-12. ERROR COVARIANCE COMPONENT( $P_{99}$ )  
VS TIME



# TAIL-CHASE ENGAGEMENT CASE

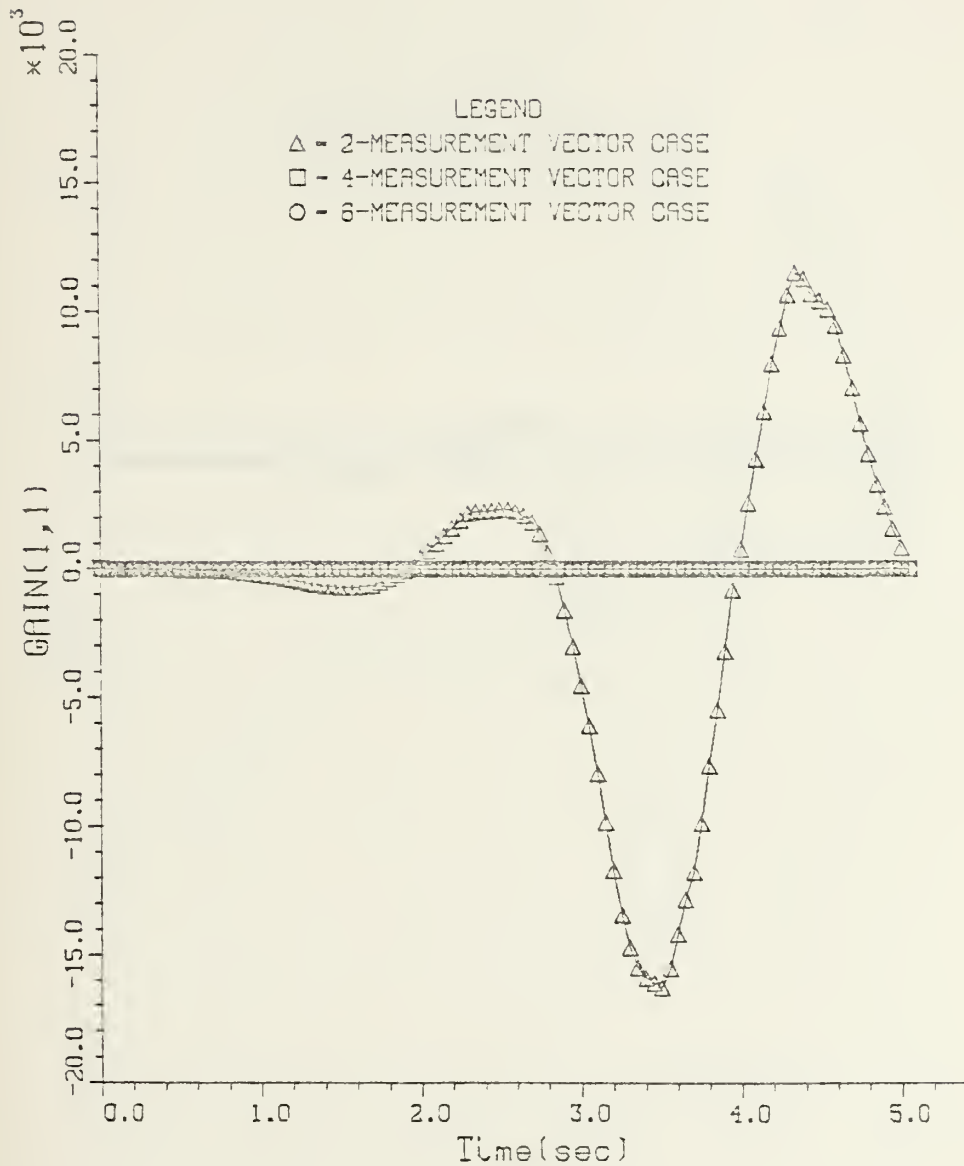


FIGURE 4-13. KALMAN GAIN COMPONENT( $G_{11}$ ) VS TIME



# TRAIL-CHASE ENGAGEMENT CASE

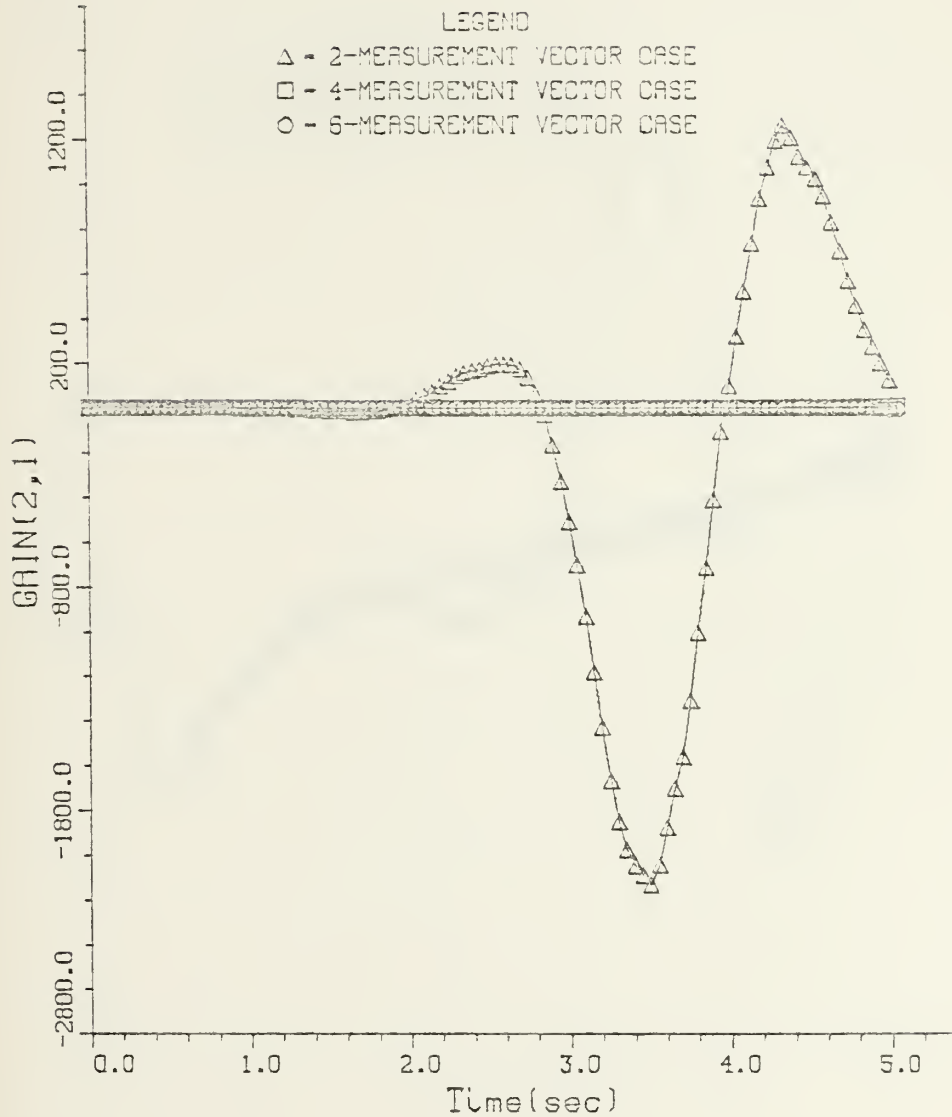


FIGURE 4-14. KALMAN GAIN COMPONENT( $G_{21}$ ) VS TIME



# TAIL-CHASE ENGAGEMENT CASE

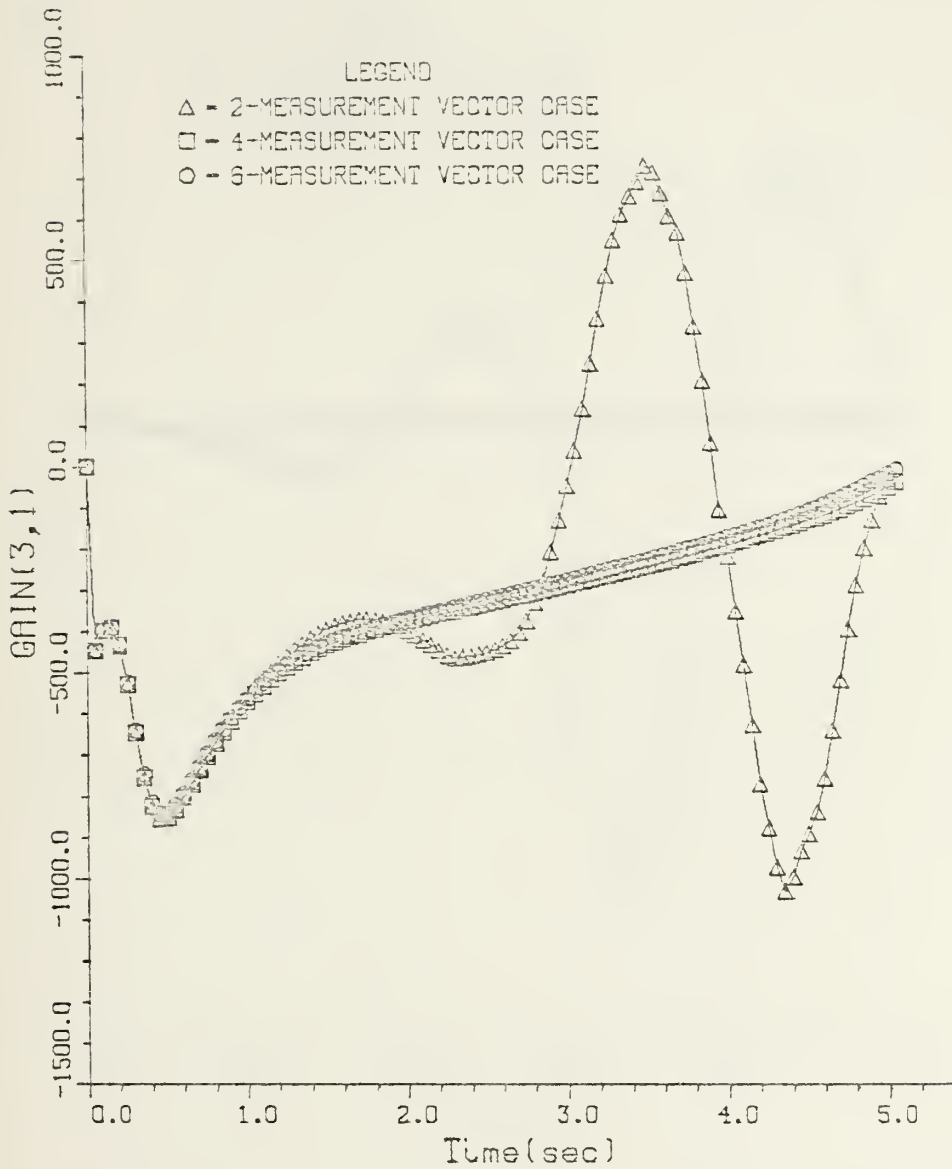


FIGURE 4-15. KALMAN GAIN COMPONENT( $G_{31}$ ) VS TIME





# TAIL-CHASE ENGAGEMENT CASE

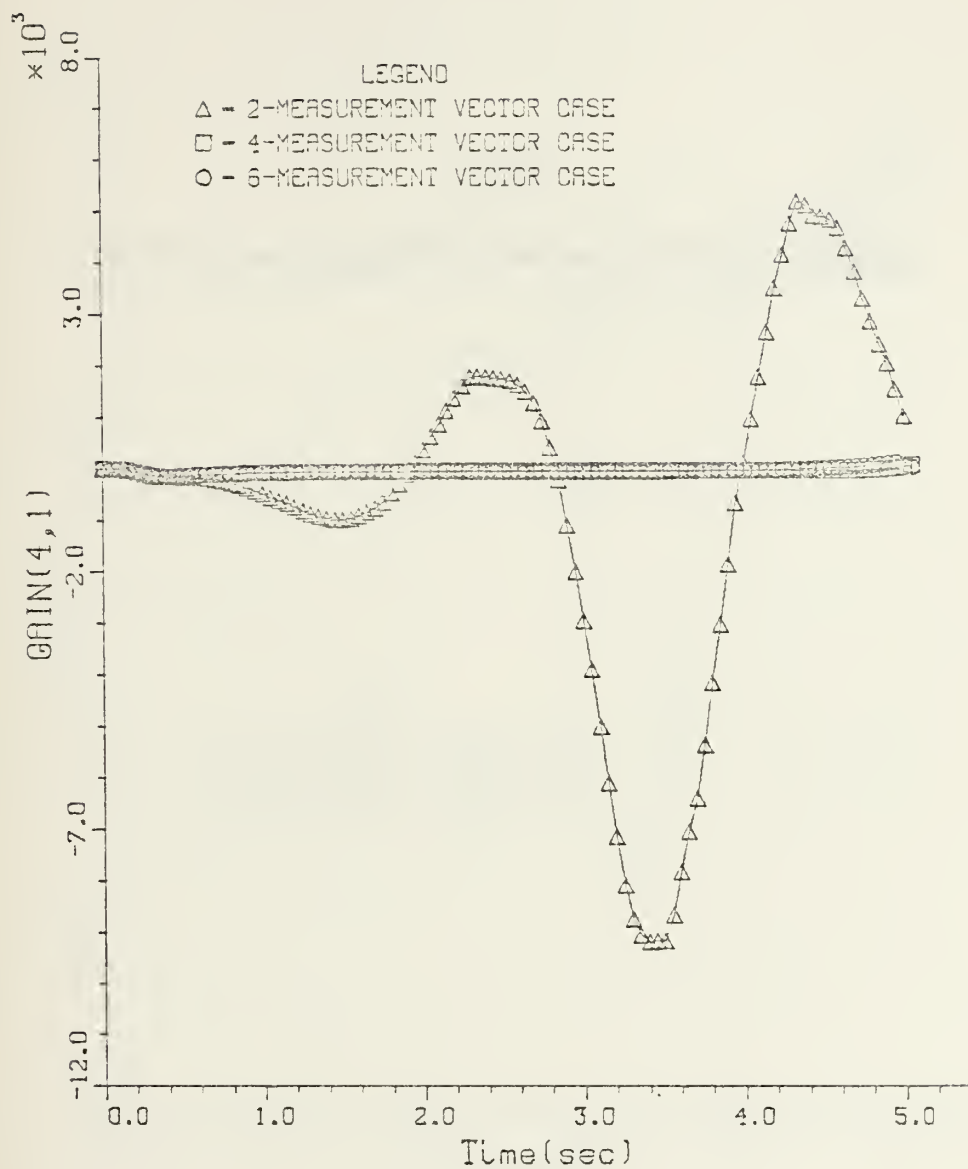


FIGURE 4-16. KALMAN GAIN COMPONENT( $G_{41}$ ) VS TIME



# TAIL-CHASE ENGAGEMENT CASE

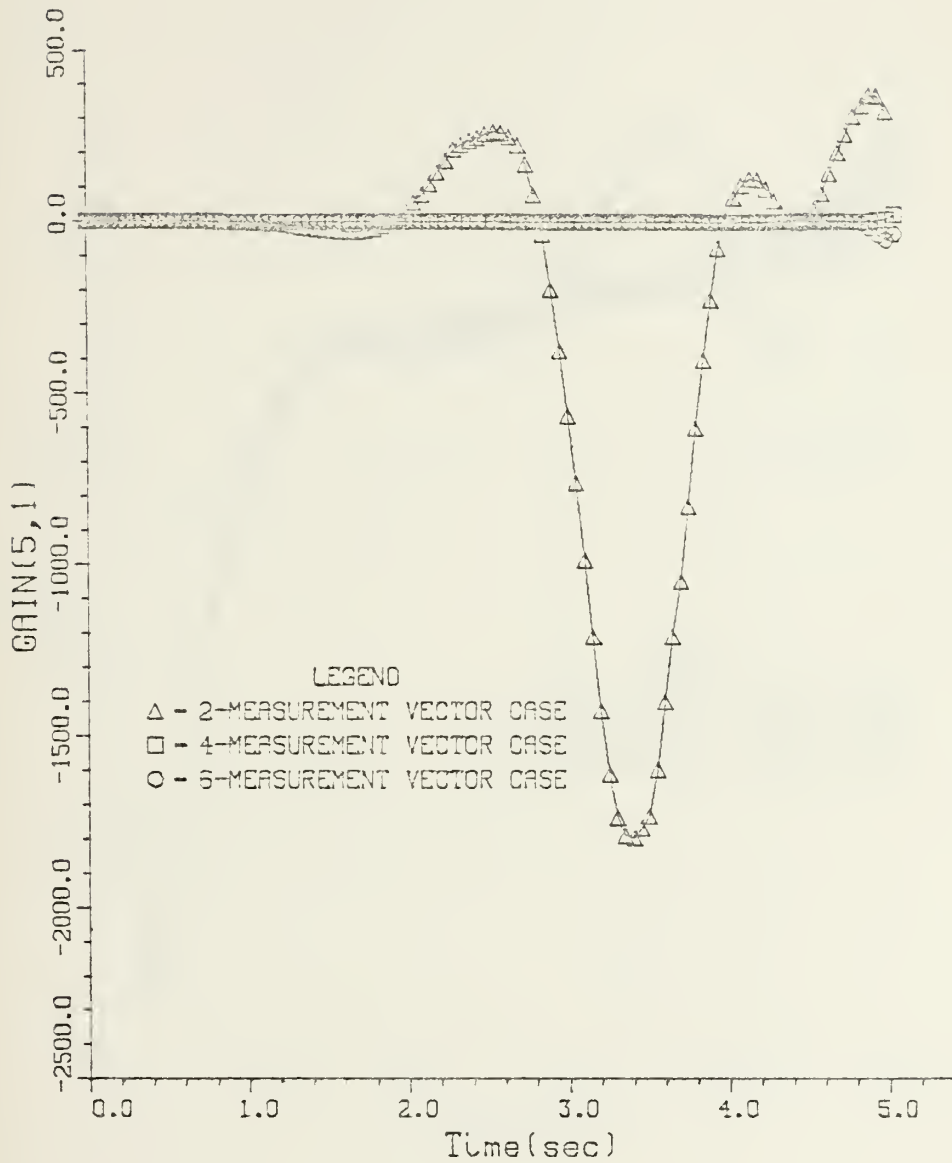


FIGURE 4-17. KALMAN GAIN COMPONENT( $G_{51}$ ) VS TIME



# TAIL-CHASE ENGAGEMENT CASE

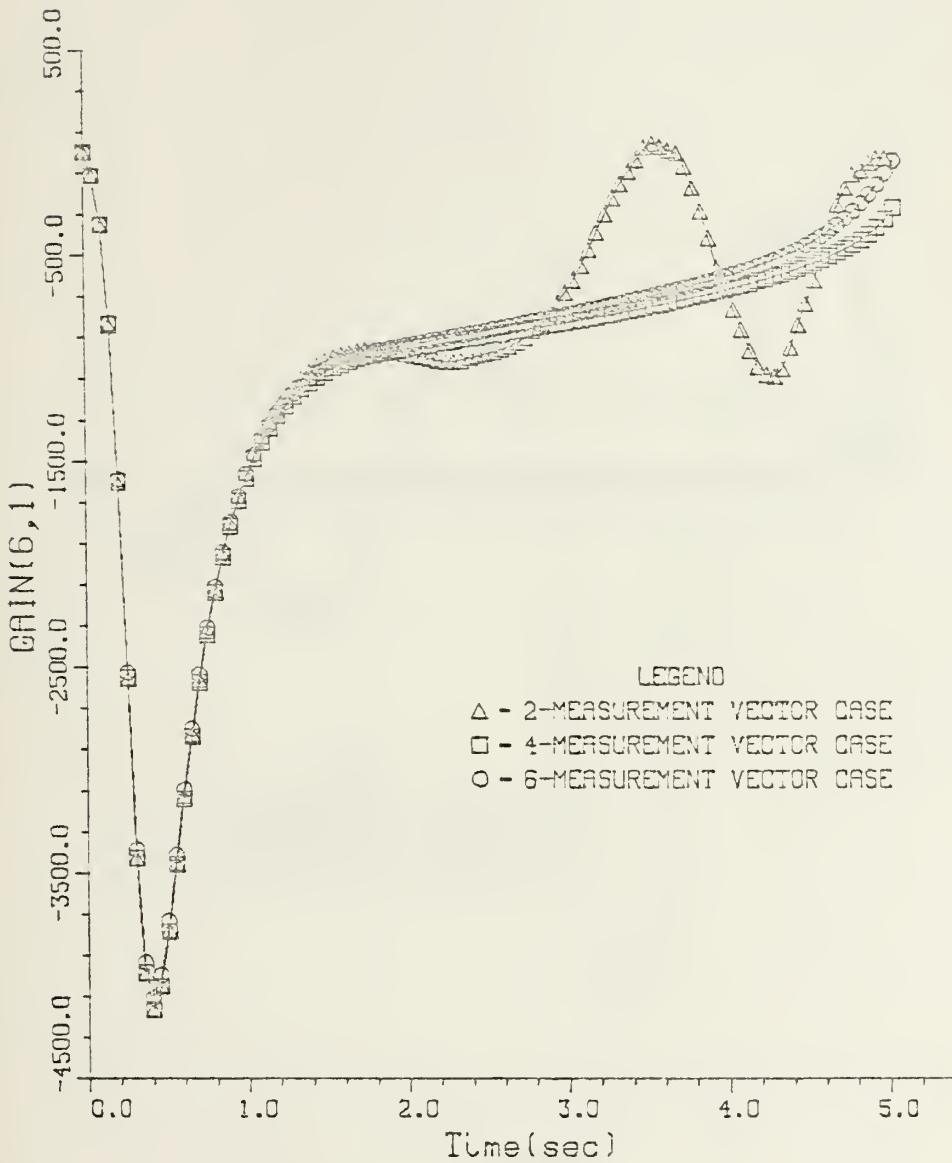


FIGURE 4-18. KALMAN GAIN COMPONENT( $G_{61}$ ) VS TIME



# TAIL-CHASE ENGAGEMENT CASE

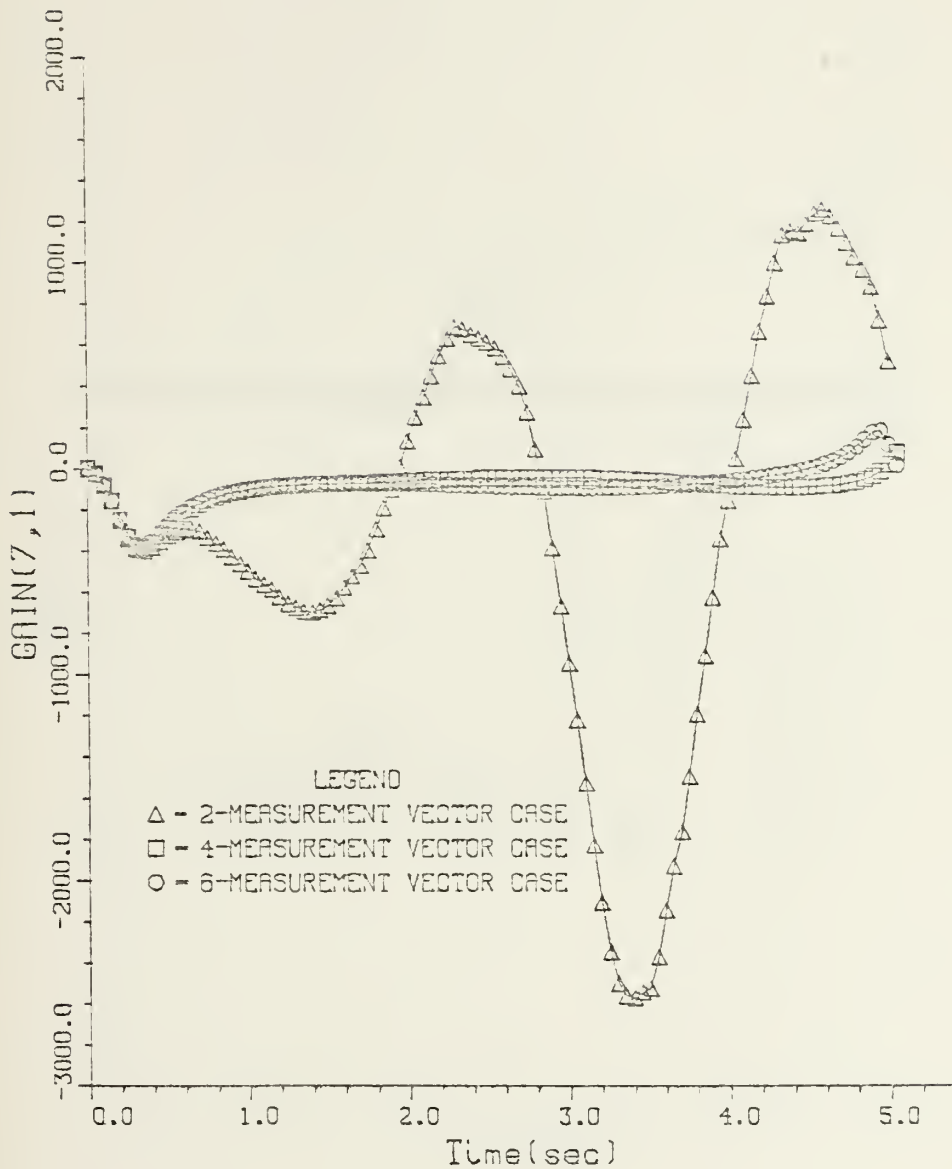


FIGURE 4-19. KALMAN GAIN COMPONENT( $G_{71}$ ) VS TIME





# TAIL-CHASE ENGAGEMENT CASE

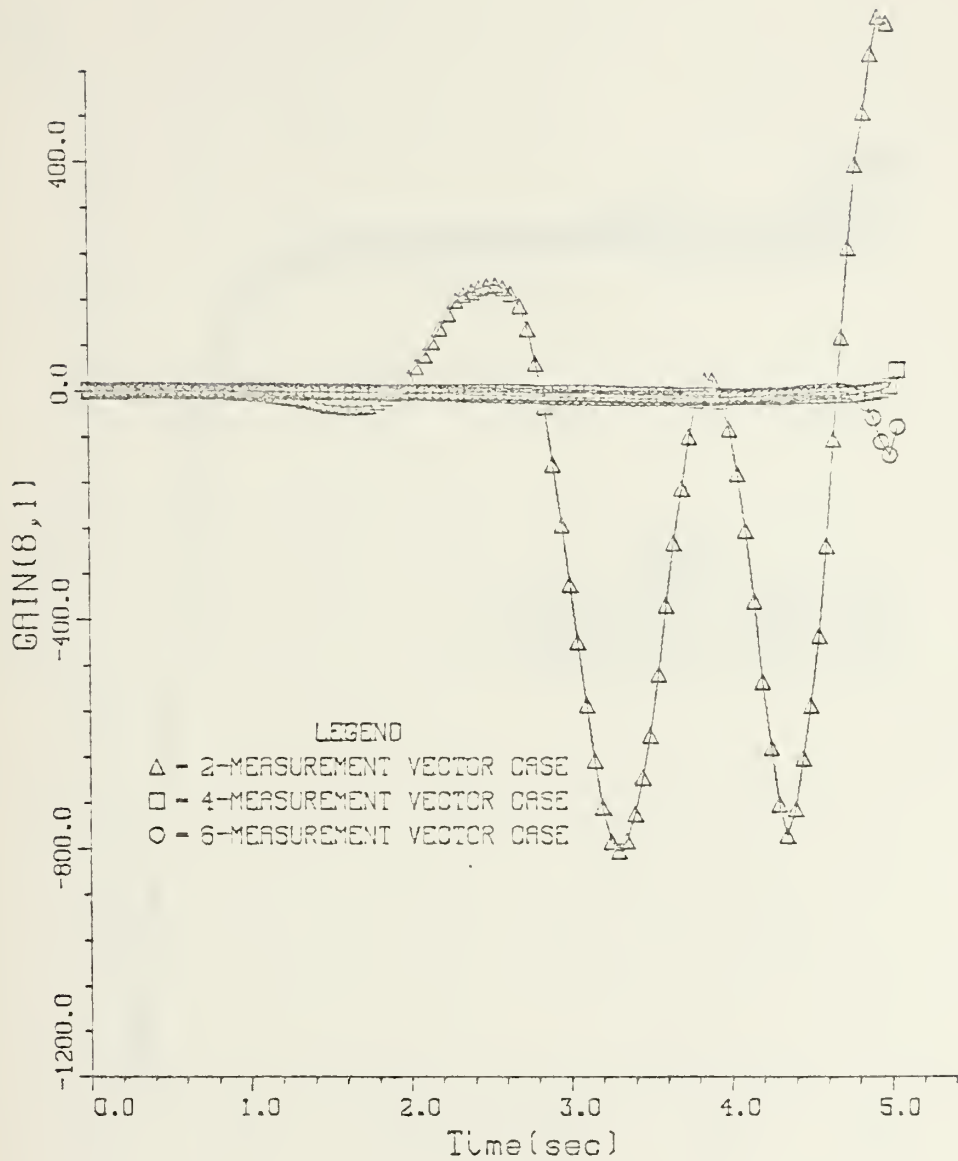


FIGURE 4-20. KALMAN GAIN COMPONENT( $G_{81}$ ) VS TIME



# TAIL-CHASE ENGAGEMENT CASE

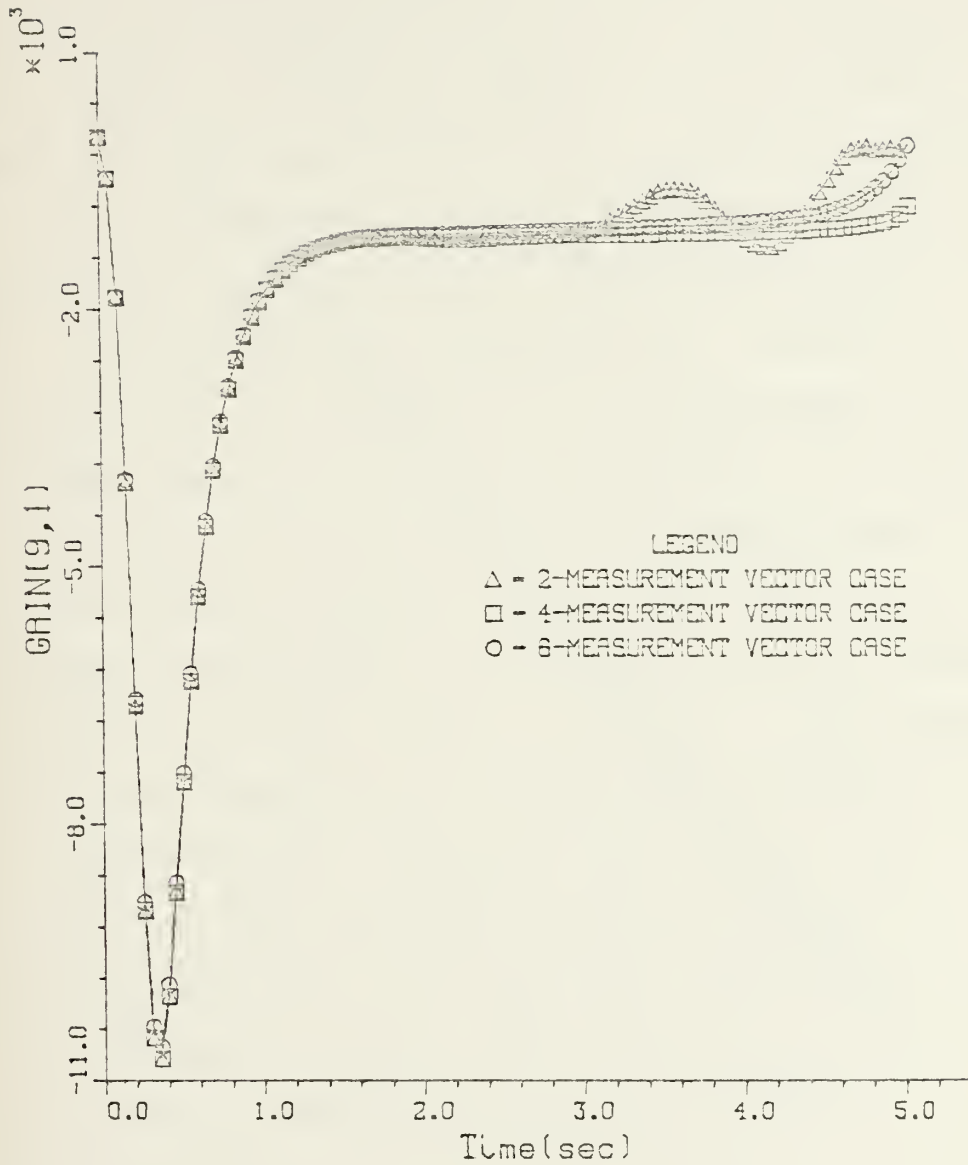


FIGURE 4-21. KALMAN GAIN COMPONENT( $G_{9,1}$ ) VS TIME



the worst miss distance, 15.4m. The control commands in the other cases behave almost like characteristics representing that the control commands are increasing smoothly from the zero to its maximum control command, after two or three seconds then slowly decreasing to converging values. The relatively small variations of the both control commands during a short time interval comparing with the control commands of case 3 result in 9.7, miss distance in case 1 and 8.7m, miss distance in case 2. From above results, the estimator with four-measurement vectors gives the best result, the estimator with six-measurement vectors the worst result and the estimator with two-measurement vectors almost same result as the of four-measurement case comparing with the result of the estimator with six-measurement vectors.

In original measurement equation, for case 1, the missile has two-measurement vectors which give the information about the relative angles,  $\theta_R$  and  $\psi_R$ , was assumed. These two-measurement vectors are non-linear functions of three relative distance components,  $X_1, X_2, X_3$ . For case 2, the missile has four-measurement vectors which give the information about above two angles plus relative range and time rate change of relative range which are also non-linear functions of the components of six state vectors,  $X_1, X_2, X_3, X_4, X_5$  and  $X_6$ . For case 3, eventhough the missile has six-measurement sensors are assumed, the measured



# TAIL-CHASE ENGAGEMENT CASE



FIGURE 4-22. STATE ESTIMATE:  $R_x$  VS TIME





# TAIL-CHASE ENGAGEMENT CASE

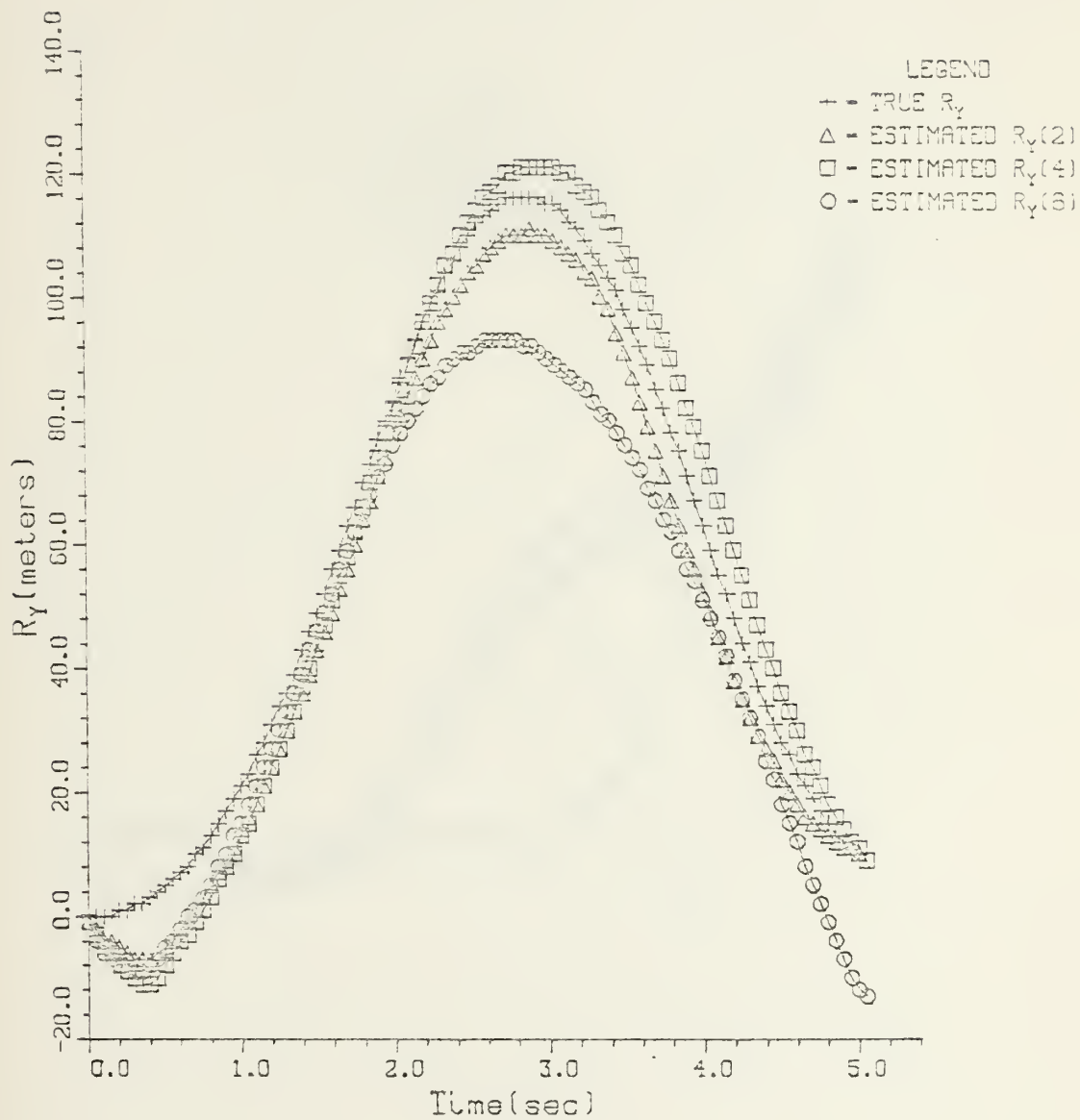


FIGURE 4-23. STATE ESTIMATE:  $R_Y$  VS TIME



# TAIL-CHASE ENGAGEMENT CASE

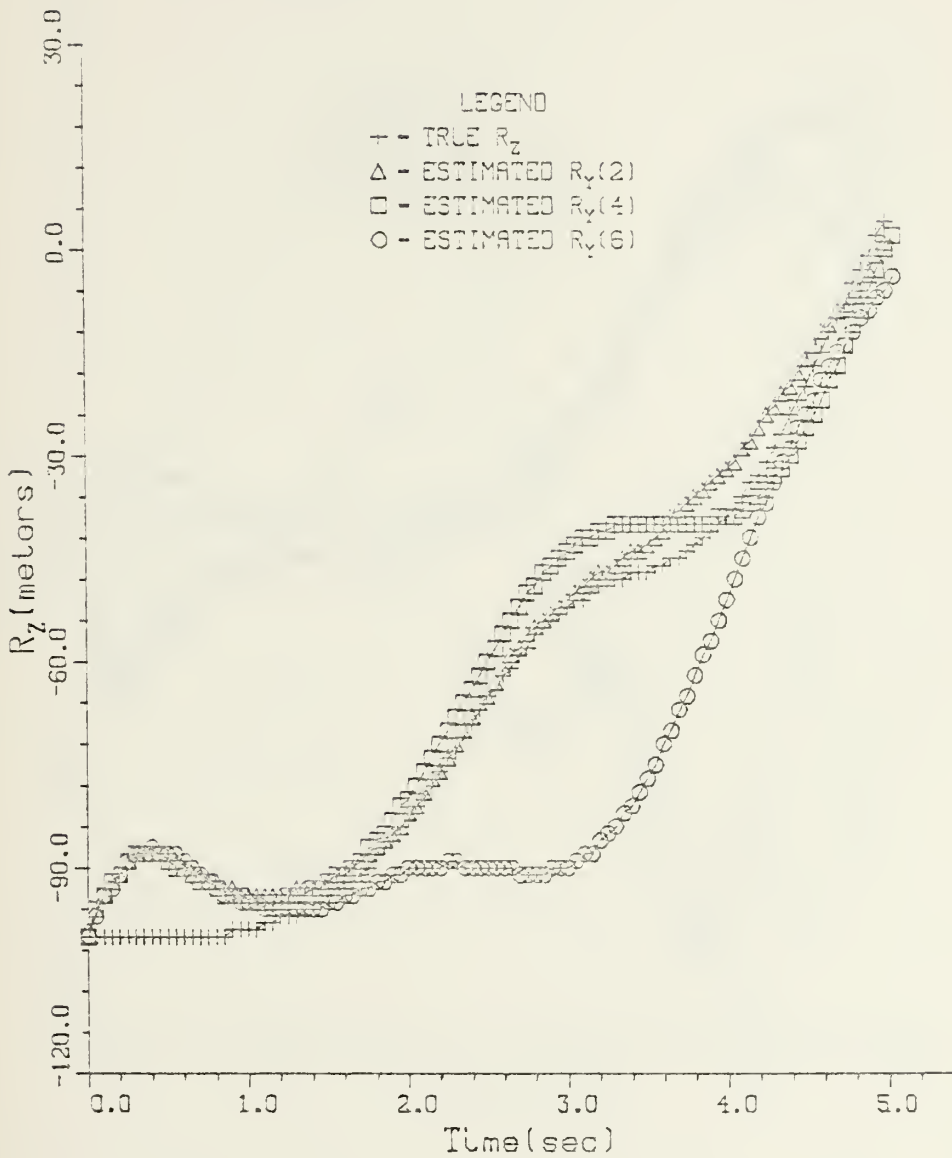


FIGURE 4-24. STATE ESTIMATE:  $R_z$  VS TIME



# TAIL-CHASE ENGAGEMENT CASE

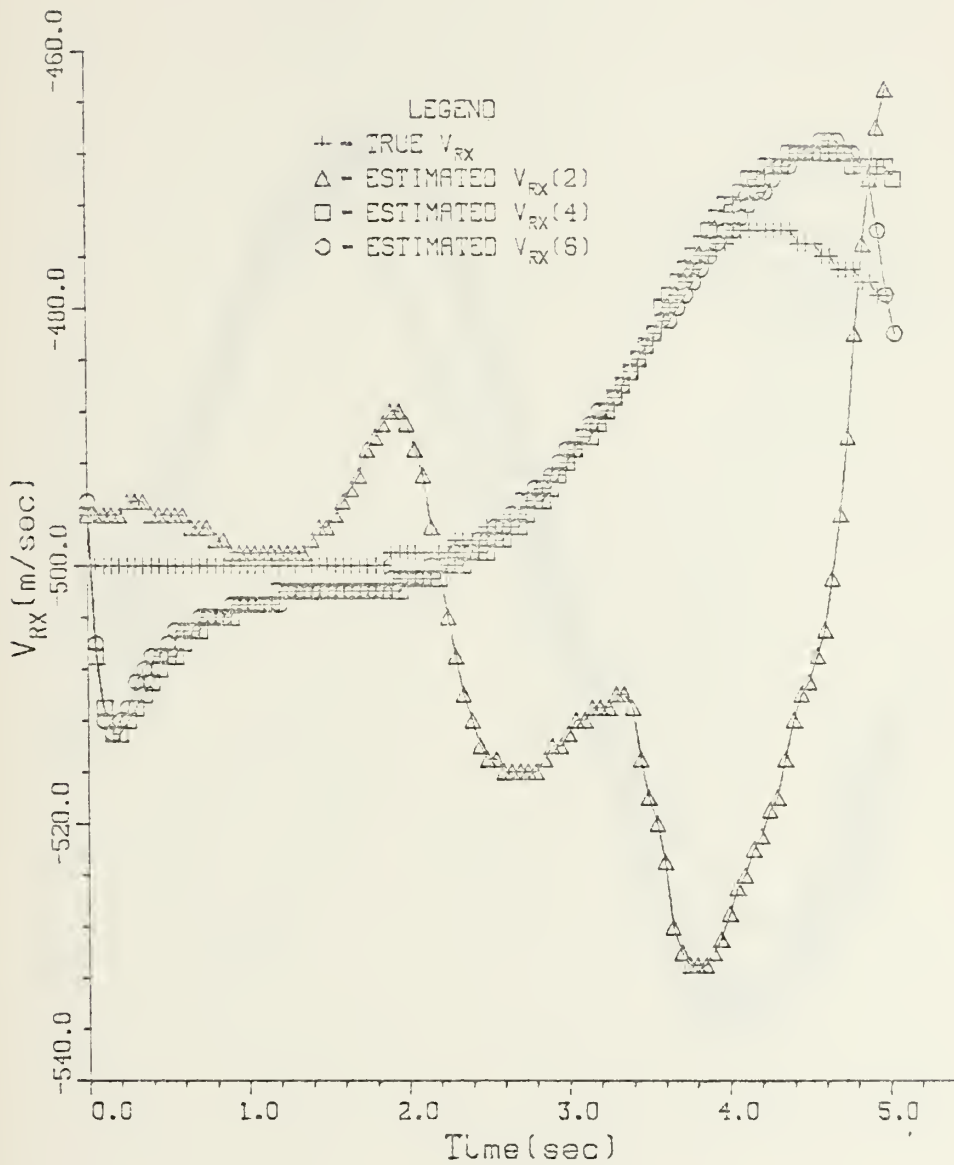


FIGURE 4-25. STATE ESTIMATE:  $V_{RX}$  VS TIME



# TAIL-CHASE ENGAGEMENT CASE

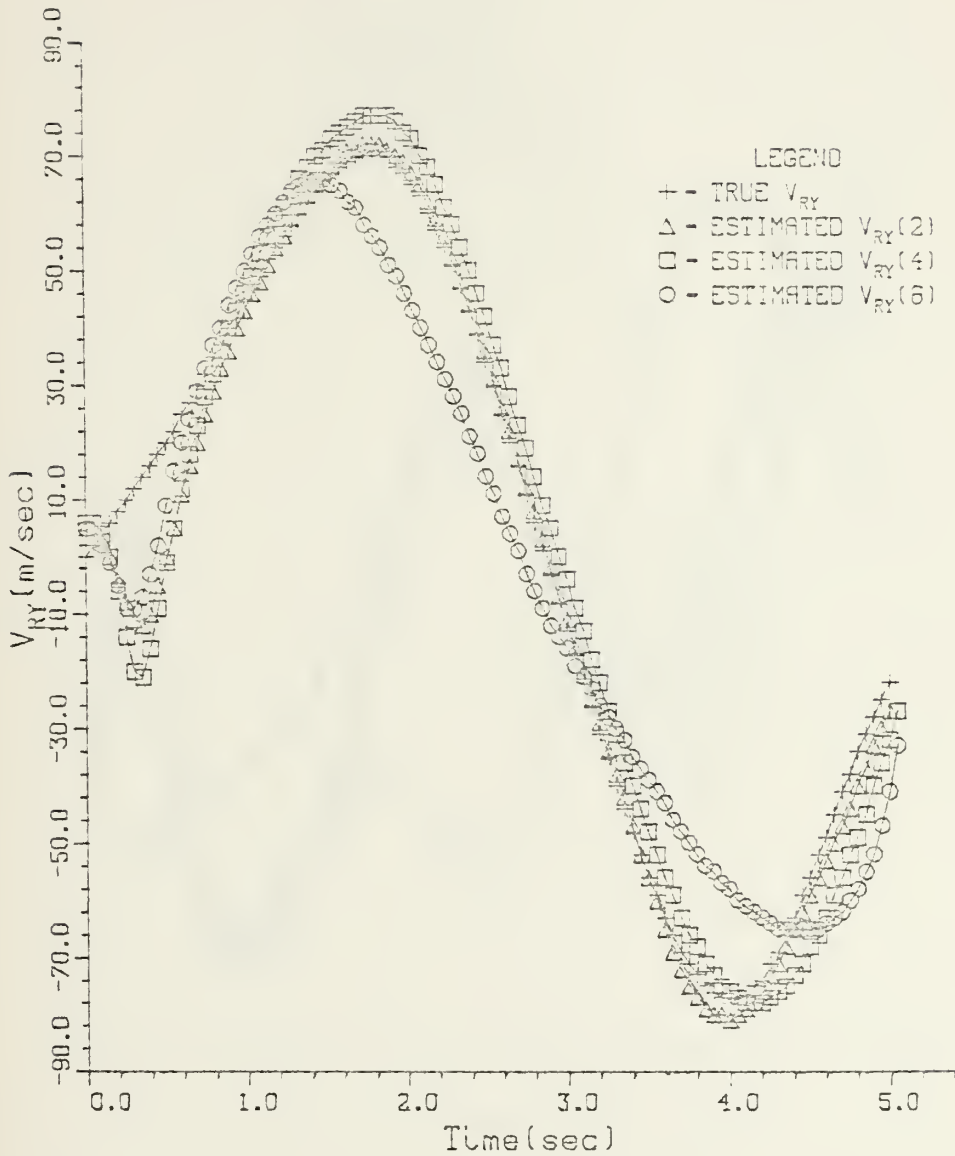


FIGURE 4-26. STATE ESTIMATE:  $V_{RY}$  VS TIME





# TAIL-CHASE ENGAGEMENT CASE

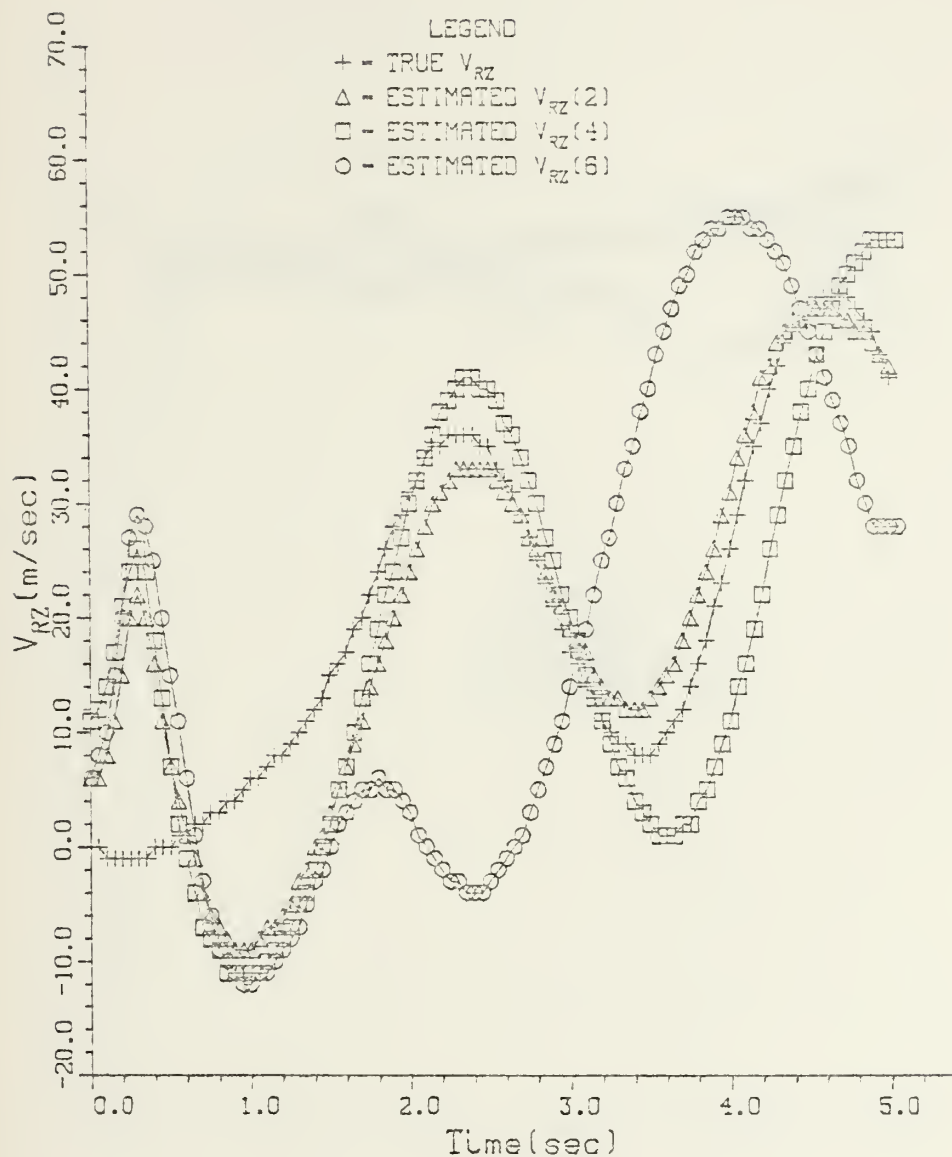


FIGURE 4-27. STATE ESTIMATE:  $V_{RZ}$  VS TIME



# TAIL-CHASE ENGAGEMENT CASE

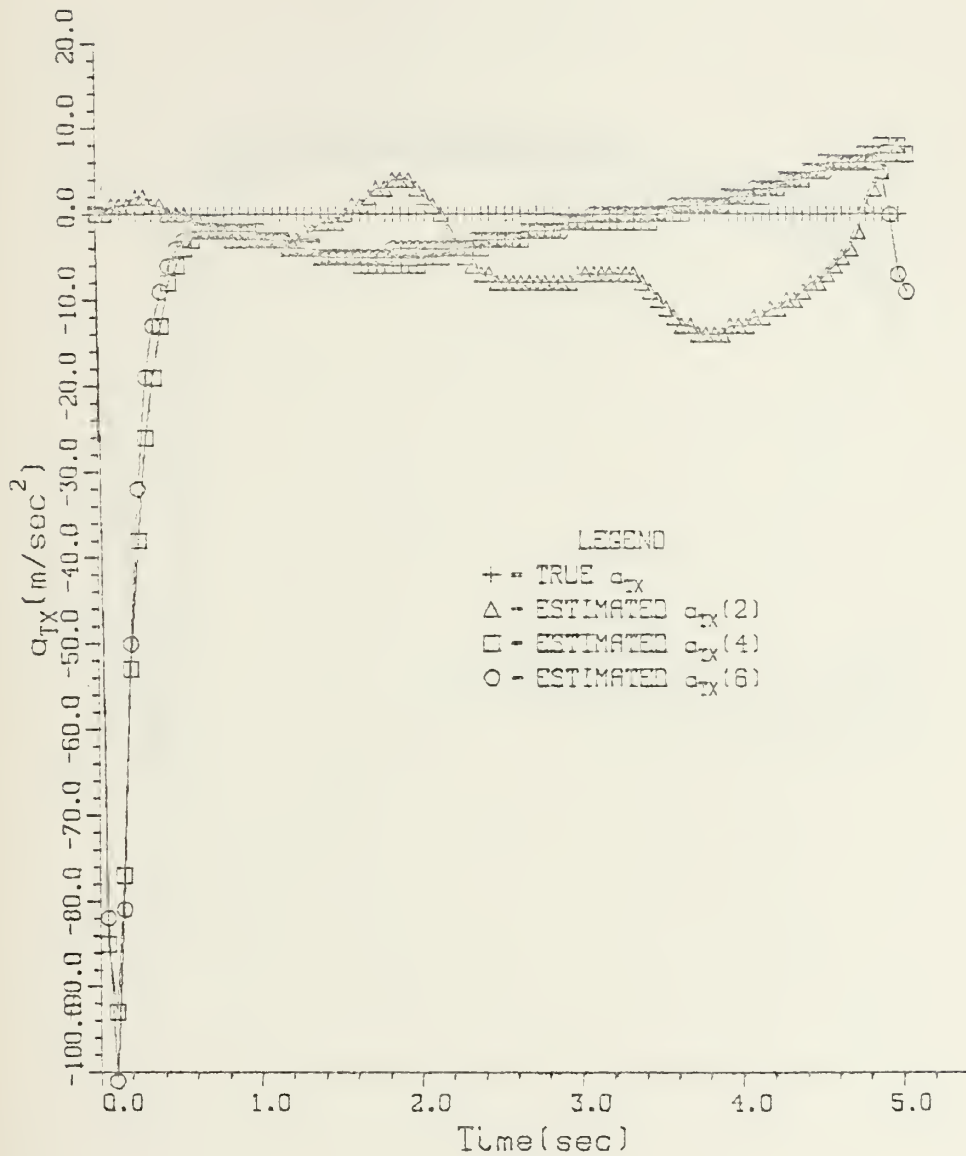


FIGURE 4-28. STATE ESTIMATE:  $a_{TX}$  VS TIME



# TAIL-CHASE ENGAGEMENT CASE

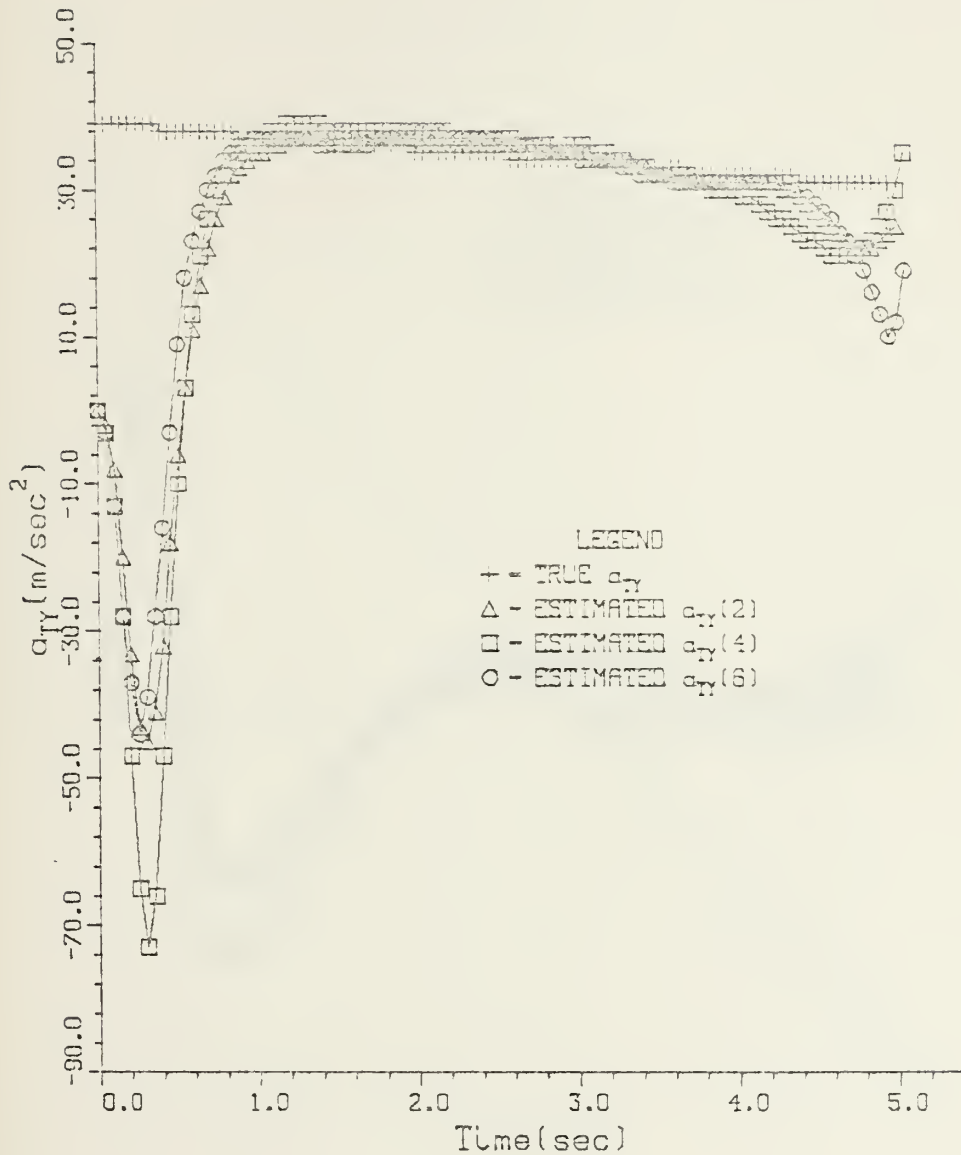


FIGURE 4-29. STATE ESTIMATE:  $a_{TY}$  VS TIME



# TAIL-CHASE ENGAGEMENT CASE

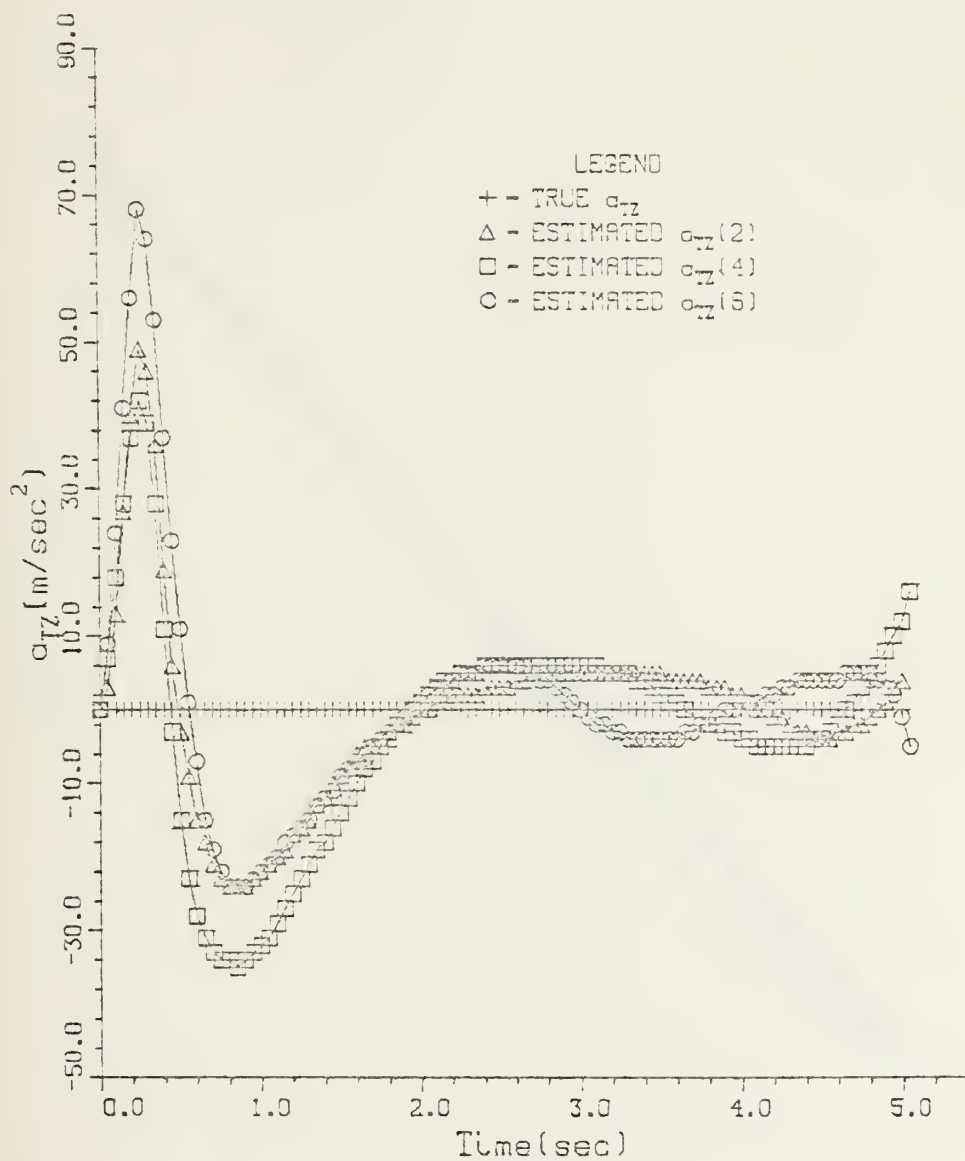


FIGURE 4-30. STATE ESTIMATE:  $a_{TZ}$  VS TIME





## TAIL-CHASE ENGAGEMENT CASE

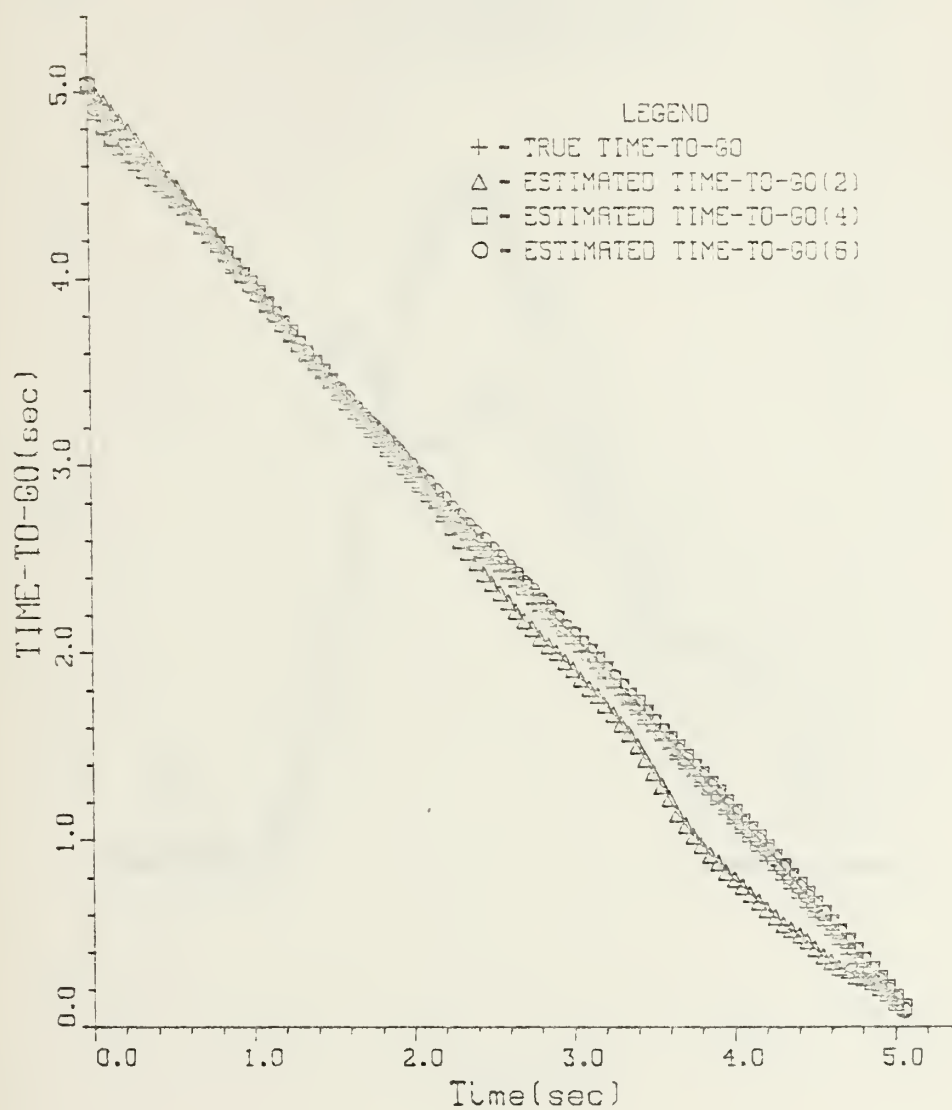


FIGURE 4-31. ESTIMATED TIME-TO-GO VS TIME



# TAIL-CHASE ENGAGEMENT CASE

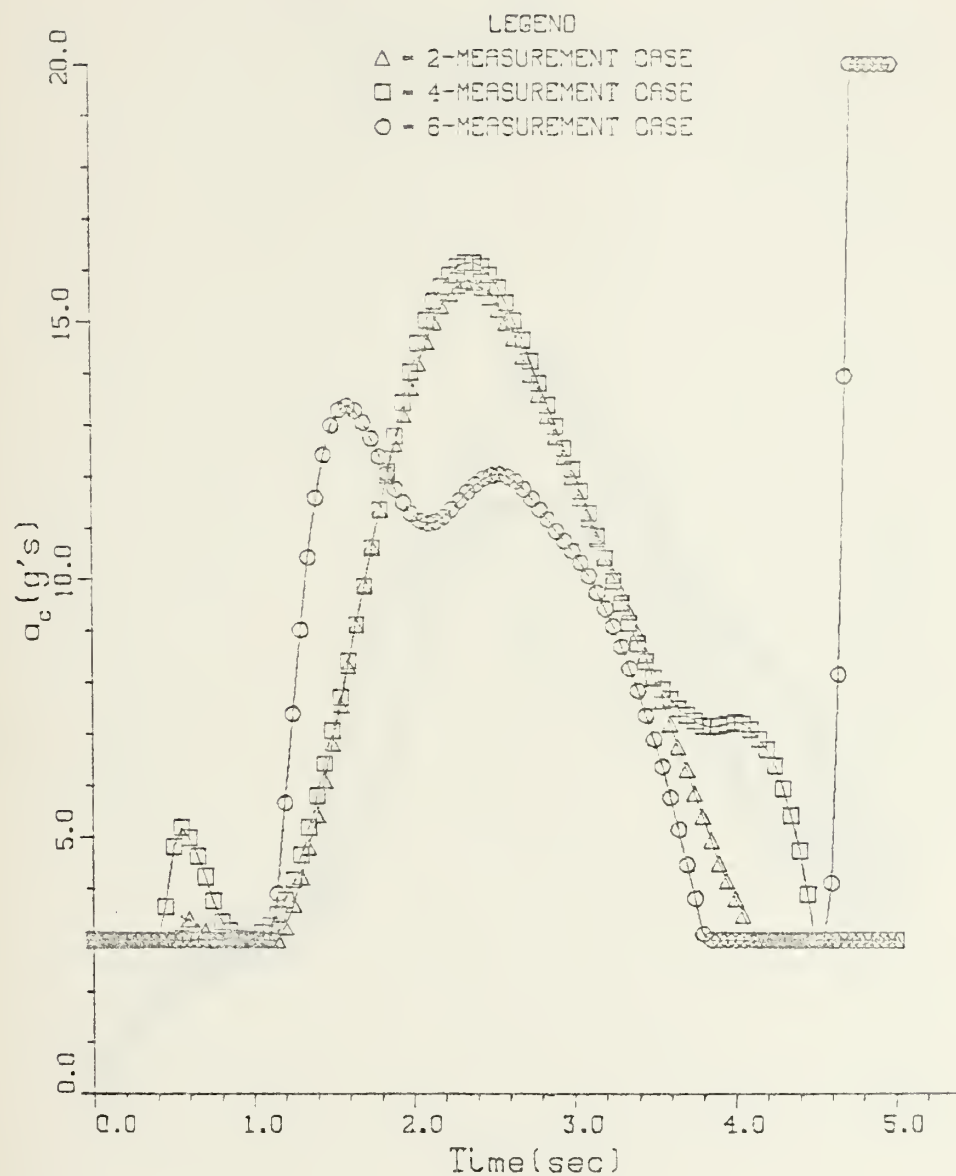


FIGURE 4-32. NORMAL ACCELERATION COMMAND VS TIME



## TAIL-CHASE ENGAGEMENT CASE

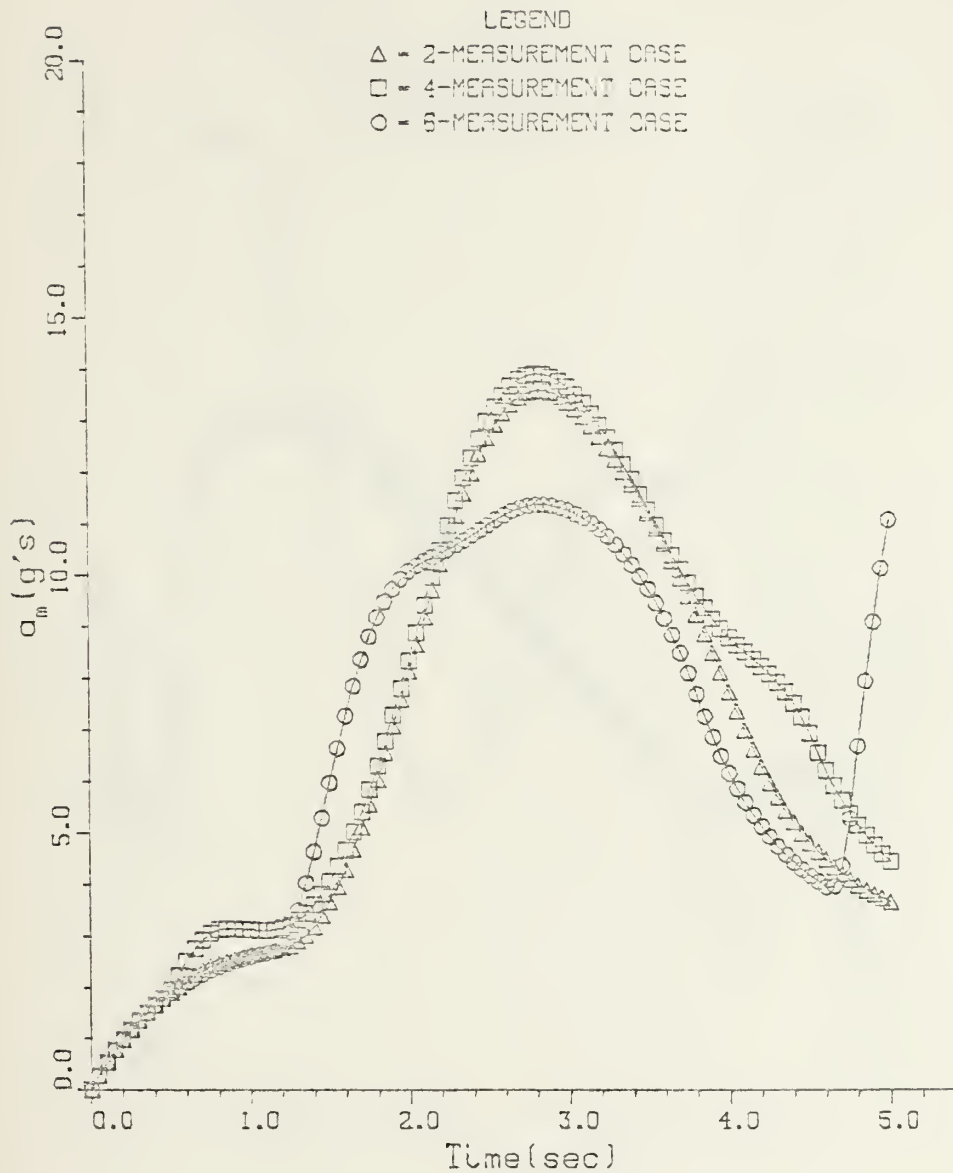


FIGURE 4-33. MISSILE NORMAL LOADING VS TIME



## TAIL-CHASE ENGAGEMENT CASE

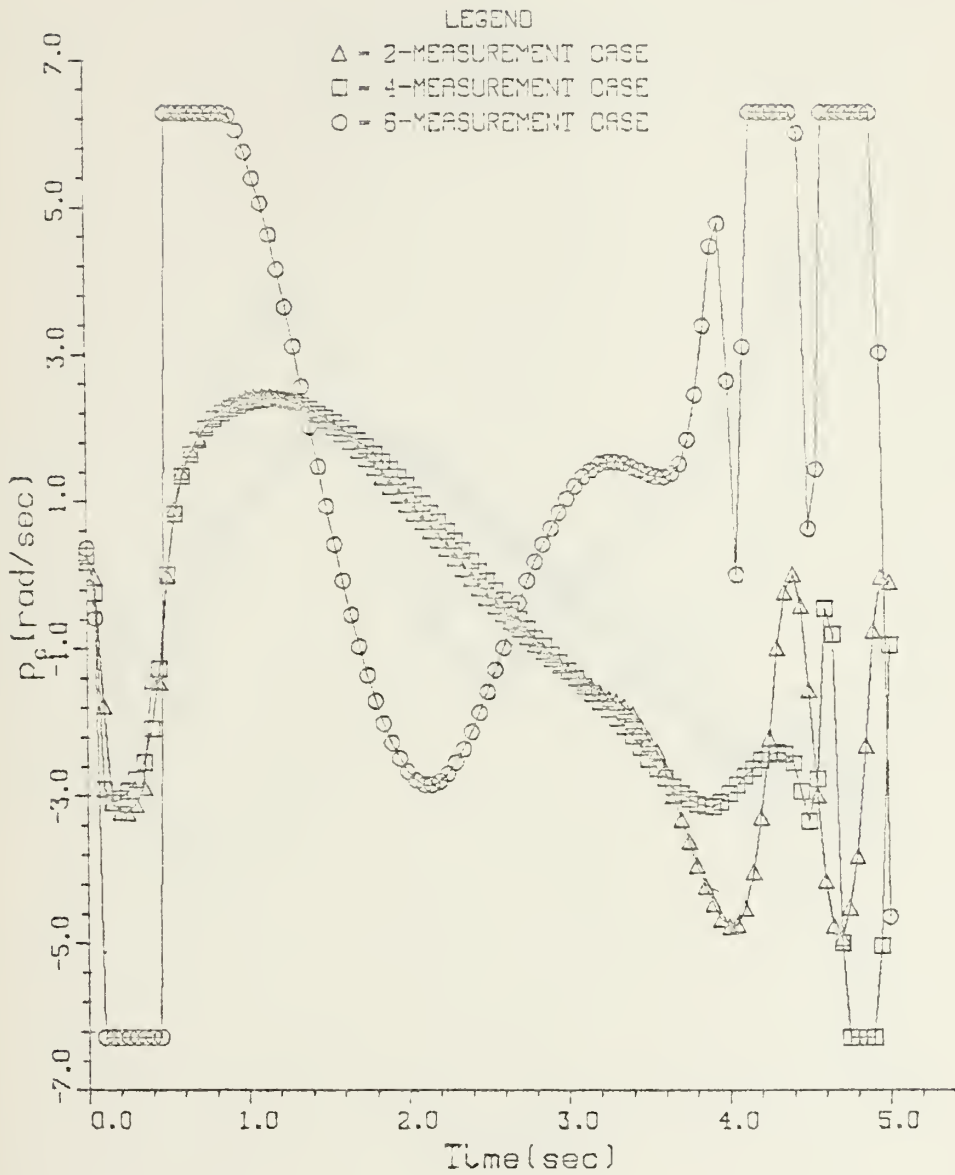


FIGURE 4-34. ROLL RATE COMMAND VS TIME





## TAIL-CHASE ENGAGEMENT CASE

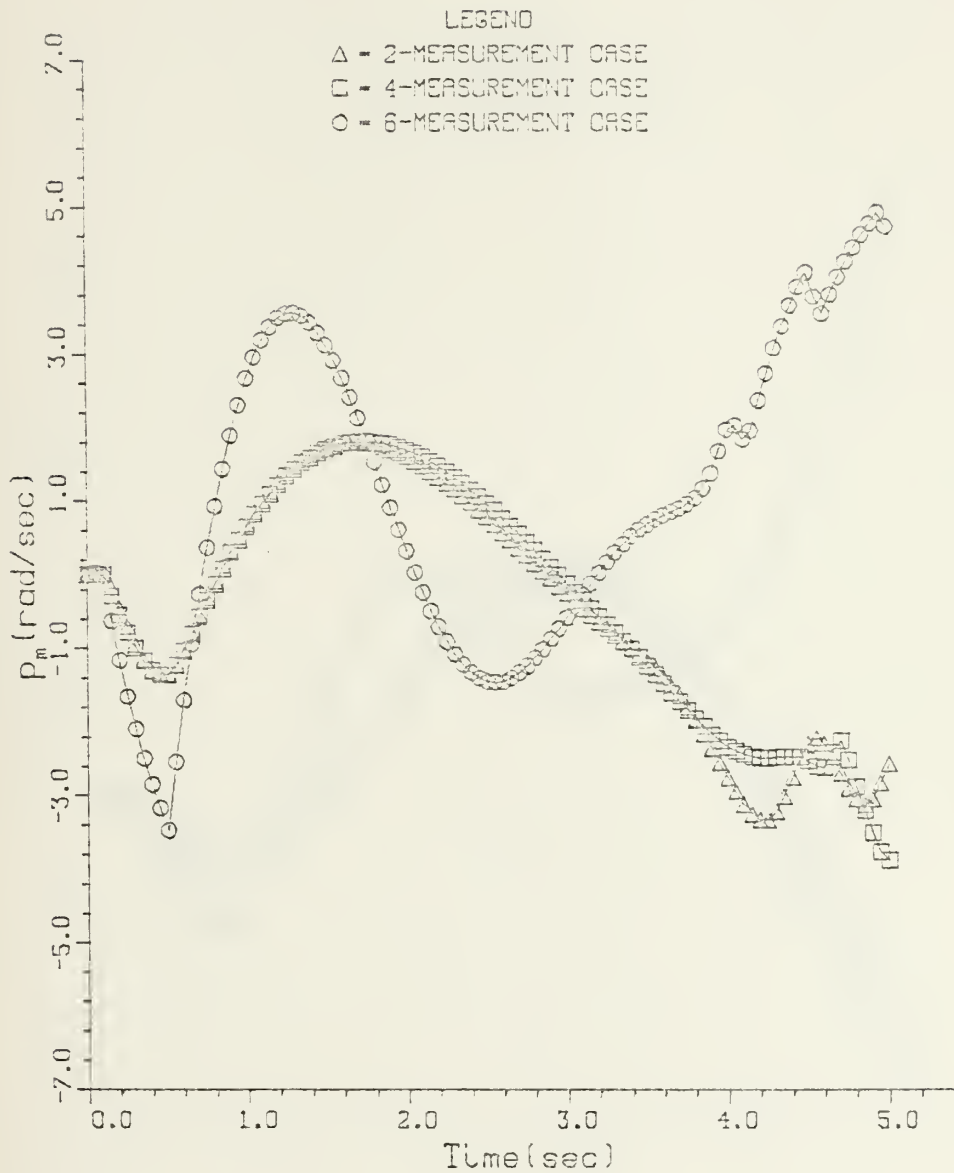


FIGURE 4-35. MISSILE ROLL RATE VS TIME



## TAIL-CHASE ENGAGEMENT CASE

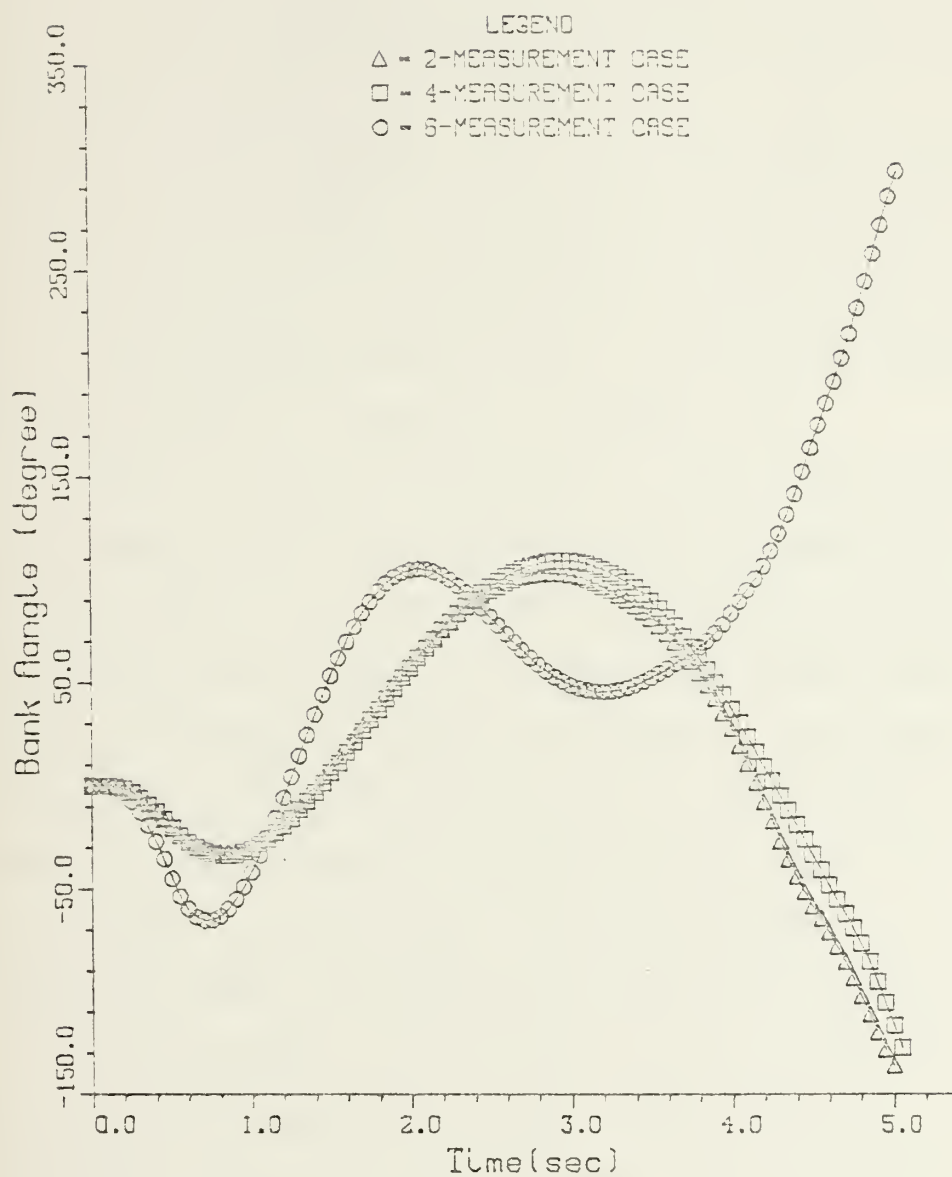


FIGURE 4-36. MISSILE BANK ANGLE VS TIME



vectors using the six-measurement sensors contain only six state vectors which are exactly same kinds and numbers as the measurable state vectors using the four measurement sensors in case 2. As the angle rates,  $\dot{\psi}_R$ ,  $\dot{\phi}_R$ , are included to the estimator as the measurement vectors in case 3, the both angle rates are non-linear functions of only six-state vectors,  $X_1$ ,  $X_2$ ,  $X_3$ ,  $X_4$ ,  $X_5$  and  $X_6$ . The results of the estimator with four-measurement vectors and with six-measurement vectors show the almost same variations of the error covariance and the Kalman gain components of the six measurement case as of the four measurement case as shown in Figures 4.4 through 4.21.

The Kalman filter in this work is a first order filter. Thus the components of the Jacobean matrix contain only the first order term, i.e., all higher order terms are neglected. As the order of the system is increased one would expect a more complex system to response differently. The above reasons affect to the underestimation of the states of six measurement case as shown in Figures 4.22 through 4.30. From the above considerations it can be concluded that as the increased number of measurement vectors is implemented to the extended Kalman filter algorithm, the result of the system may not be enhanced up to the expected degree due to the increased complexity of the system. The system with the



first order filter as a optimal estimator may contribute to make less desirable results due to the effect of neglecting of the higher order terms in the filter algorithm.





## V. PERFORMANCE EVALUATION OF THE CONTROL SYSTEM

This section will discuss the performance of the control system implemented in a bank-to-turn missile for each scenario. The maximum normal acceleration, the maximum roll rate and the time constant are the key parameters which reflect the missile capabilities, the noises to measured vectors are the parameters of the environmental effect, and auxiliary variables of some importance are then total engagement time and missile velocity. The mean miss distance determined from the 50 Monti Carlo runs was used as a performance standard for the estimators of two- (case 1), four- (case 2) and six-measurement vectors (case 3) on each scenario. The simulation results are shown in Figures 5.1 through 5.19. The sensitivities to variations of the parameters will be discussed below. Since the simulation results show essentially the same characteristics for the tail-chase engagement (scenario 1) and for the head-on engagement (scenario 2). The performance on these two scenarios will be discussed together for each parameter. The side-approach engagement (scenario 3) will be discussed separately.

Figures 5.1 and 5.2 show the miss distance variation as a function of missile maximum normal acceleration. For scenario 1, case 1 shows a mean miss distance of 9.8m at



# TAIL-CHASE ENGAGEMENT CASE

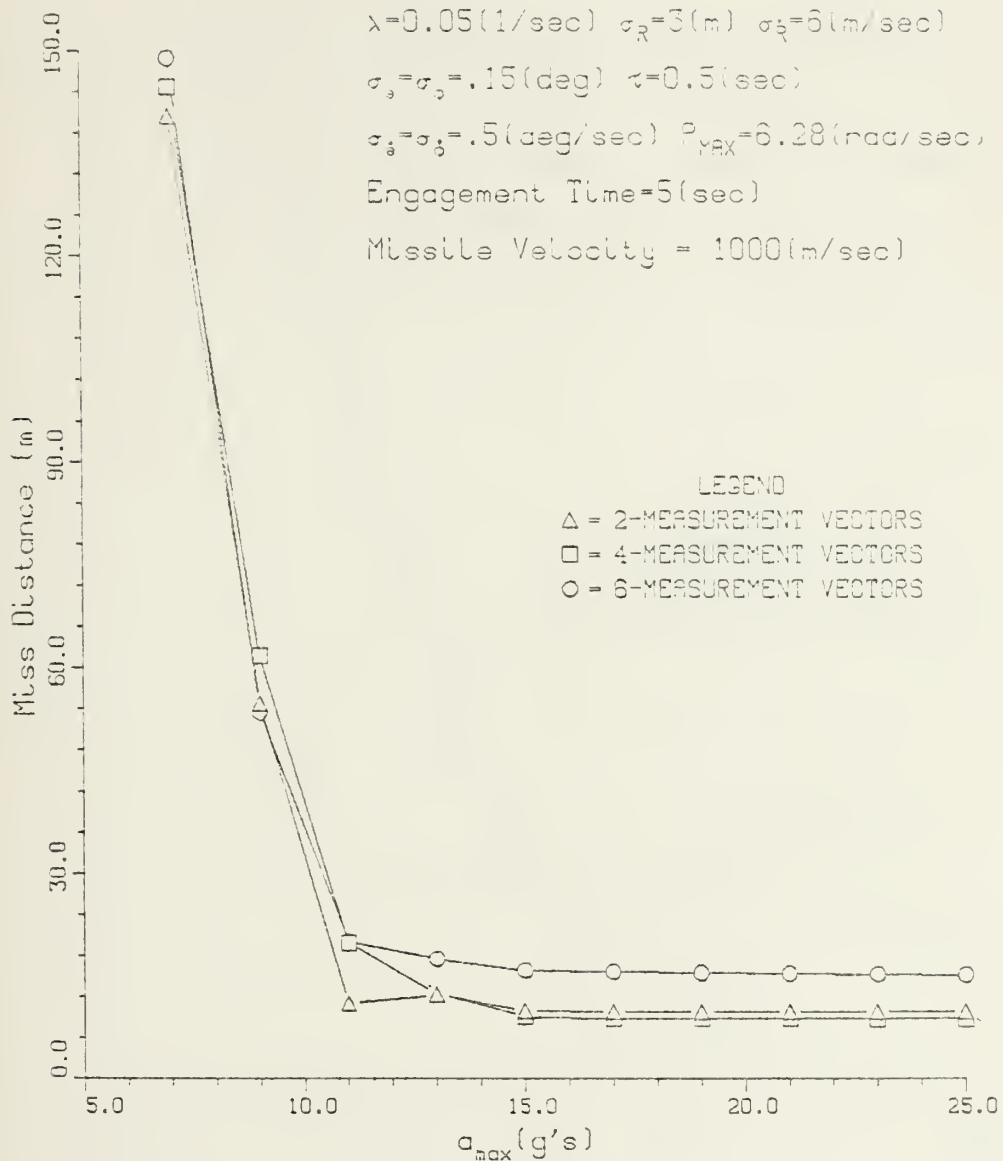


FIGURE 5-1. MISSILE MAXIMUM ACCELERATION VS  
MEAN MISS DISTANCE



# HEAD-ON ENGAGEMENT CASE

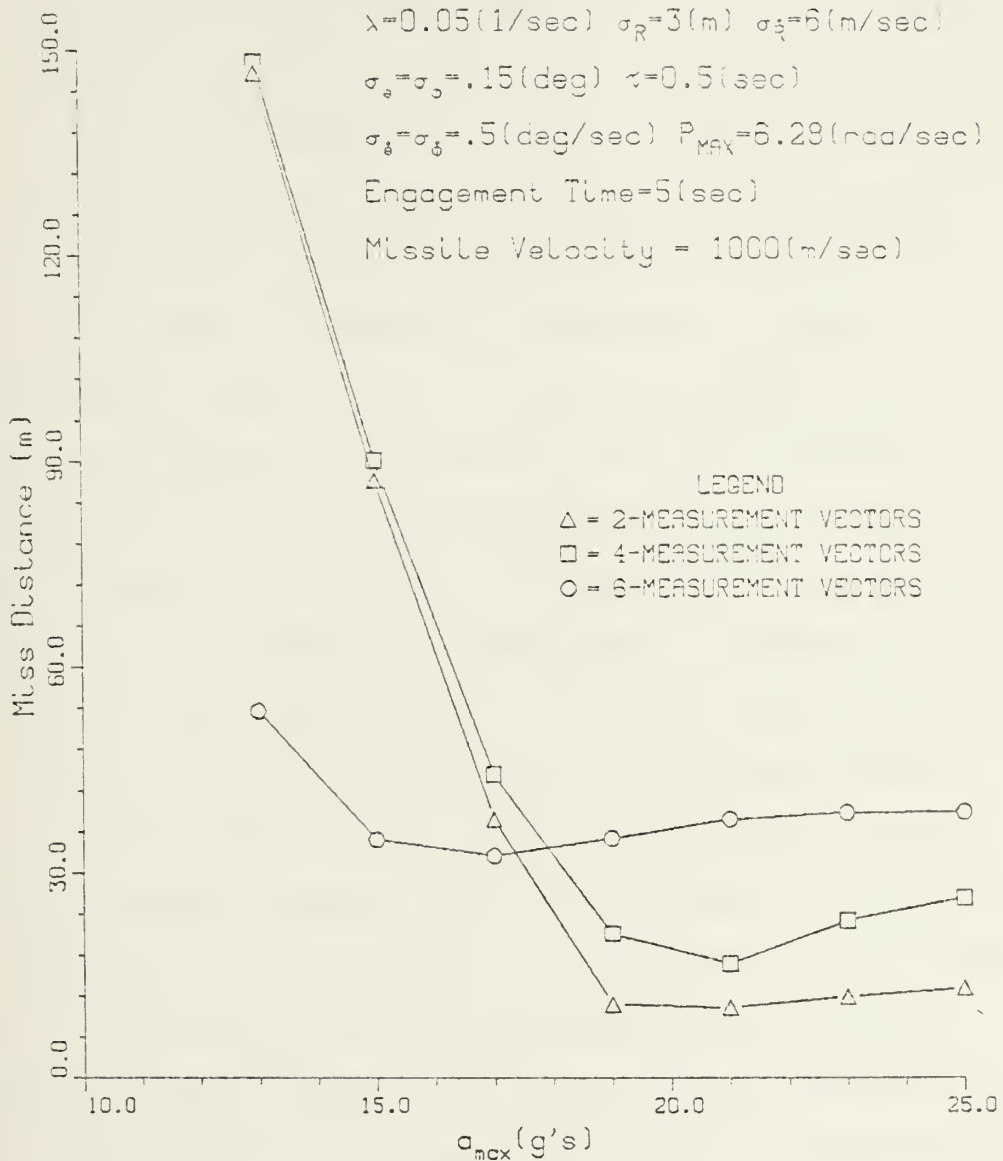


FIGURE 5-2. MISSILE MAXIMUM ACCELERATION VS MEAN MISS DISTANCE



above 15g's, case 2.9m at above 15g's and case 3, 15.4m at above 15g's. Each case also shows that as the maximum limit of the normal acceleration decreases, the mean miss distance in case 1 is less sensitive than in the other two cases. For scenario 2, the result of case 1 shows the minimum mean miss distance is 10m and the result of case 2 is 17m at  $a_{\max} = 21g$ 's respectively, the result of case 3 is 32m at  $a_{\max} = 17g$ 's. The trends of the curves show that the mean miss distances in case 1 and case 2 vary in same manner, which rises sharply as the maximum acceleration decreases. On the other hand, the mean miss distances in case 3, vary smoothly above  $a_{\max} = 13g$ 's. One may conclude from the analysis as follows: for scenario 1, the mean miss distance can be decreased since more information on the state vectors can be obtained from the increased measurement vectors in estimator for low maximum acceleration. In order to get the mean miss distance below 20m for all three cases, one needs  $a_{\max}$  of over 11g's. For scenario 2, as the measurement state vectors are increased in estimator, the mean miss distance does not decrease, possibly due to the effect of neglecting the higher order terms in the extended filter. As the magnitude of the values of the missile and target geometry components becomes larger, the effect of the linearization becomes more pronounced.  $a_{\max} =$  over 19g's is required to





to obtain the mean miss distance below 15m in case 1 and case 2. In case 3, the mean miss distance does not go below 20m.

Figures 5.3 and 5.4 the variations of the mean miss distances as missile maximum roll rate varies. In scenario 1, for case 1 and case 2, a mean miss distance of below 10m can be obtained when  $P_{\max}$  is greater than 3 rad/sec. For case 3, one has a mean miss distance of below 16m with  $P_{\max}$  greater than 6 rad/sec. The trend of the mean miss distances is almost constant over certain range in values of  $P_{\max}$ . The variation of the mean miss distance below this range is a tenth of the magnitude comparing with the variation of the mean miss distances as a function of maximum acceleration. It is concluded that for scenario 1, the mean miss distance in case 1 and case 2 is not effected by the roll rate if the roll rate is above 3 rad/sec. In case 3, higher roll rate limit can reduce the mean miss distance. For scenario 2, the mean miss distances of case 1 and case 2 are like the trends for scenario 1. However, the mean miss distance of case 3 has a minimum of 26m at  $P_{\max} = 4$  rad/sec, then increases up to 36m then decreases slightly. This trend may be due to the effect of the roll rate lag, which is caused by the increased maximum roll rate and by the underestimations of the state variables in case 3. The other characteristics, i.e., the mean miss distance decreases with increased maximum roll rate limit



# TAIL-CHASE ENGAGEMENT CASE

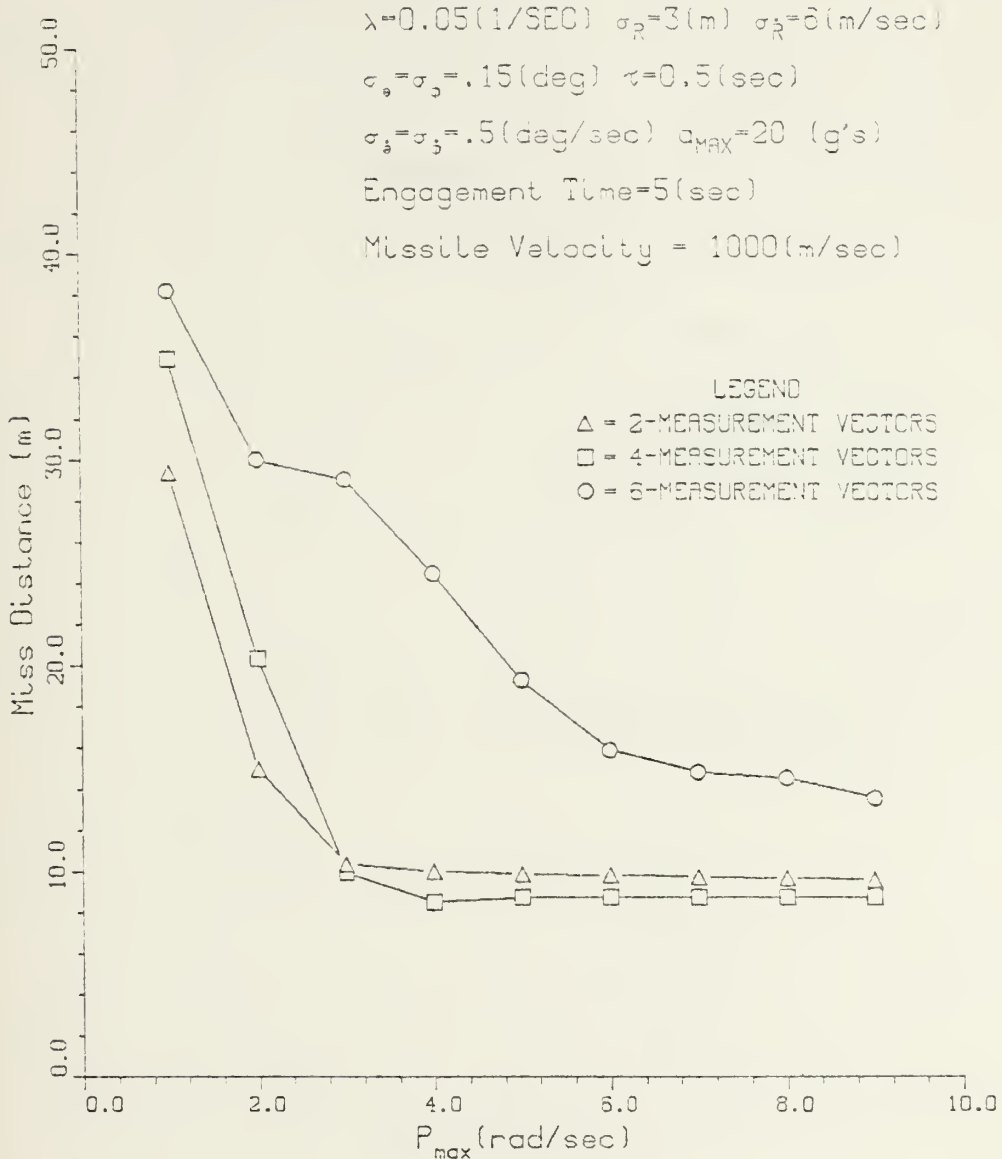


FIGURE 5-3. MISSILE MAXIMUM ROLL RATE VS  
MEAN MISS DISTANCE



# HEAD-ON ENGAGEMENT CASE

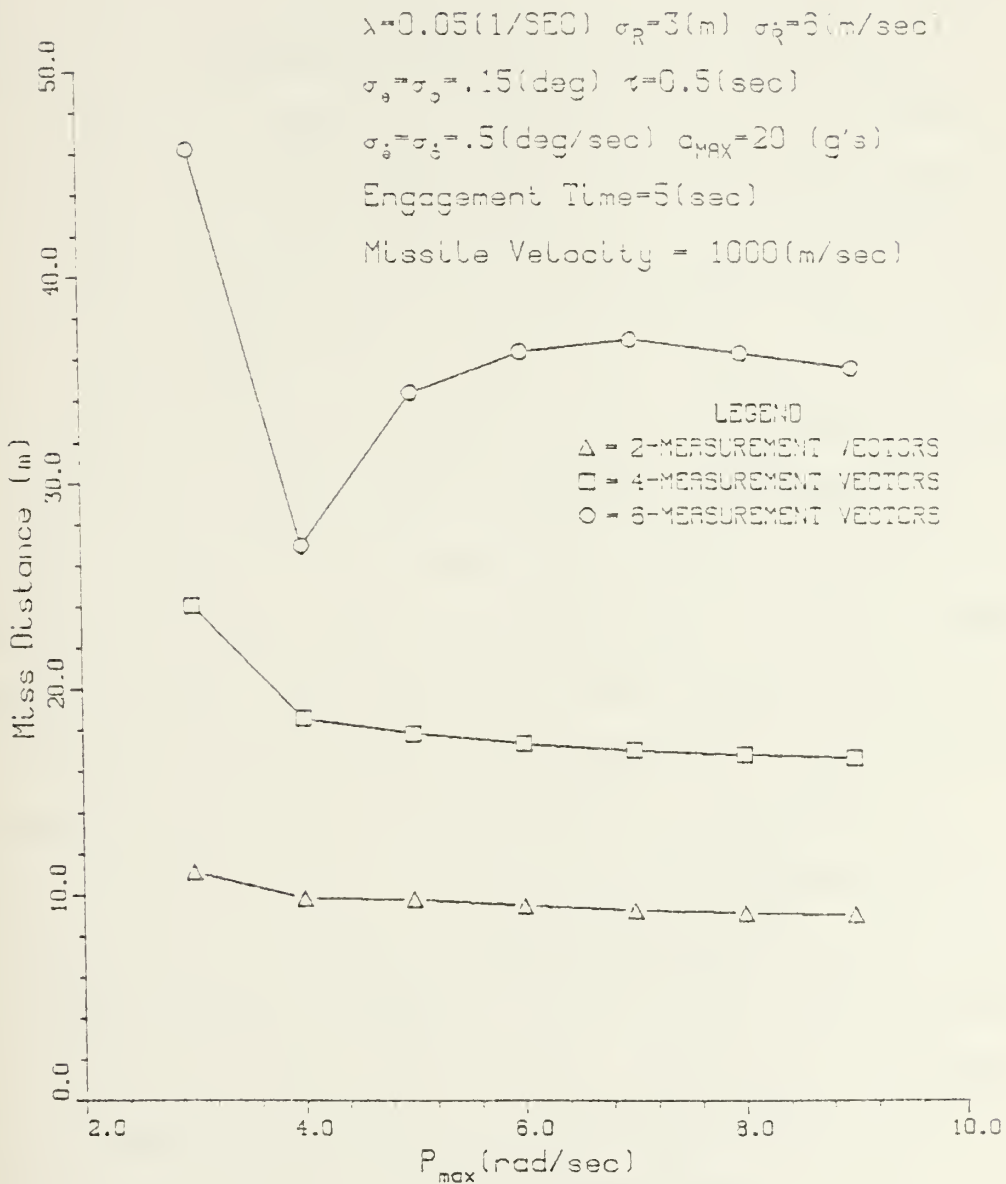


FIGURE 5-4. MISSILE MAXIMUM ROLL RATE VS MEAN MISS DISTANCE



and for scenario 1, case 2 shows less near miss distance than case 1, but for scenario 2, the opposite trend shows, can be explained with the same reasons as those of the first analysis.

The variation of the mean miss distances with the time constant as a parameter is shown in Figures 5.5 and 5.6. For both scenarios, one has a flat plateau for low values of the time constant and a sharp rise with increasing values of the time constant, i.e., for scenario 1, Figure 5.5 shows the curves of the mean miss distances slightly increase up to the time constant of 0.9 second, for scenario 2, the curves up to 0.5 second are plateau, then for both scenarios the curves rise sharply. For scenario 1, the mean miss distance of case 2 is less than that of case 1 up to 0.5 second time lag, but above 0.5 second lag, the results show an opposite trend. Also over this time lag, the curves of case 3 for both scenarios are not sensitive to the variation of parameter up to the time constant of 0.7 second for scenario 1, 0.9 second for scenario 2. The general trend of the curves, i.e., as the time constant becomes longer, the miss distance becomes larger, is due to slow system response. From the figures showing the results, the time lag of less than 0.5 second is necessary to obtain the mean miss distance of the required order of magnitude.

Figures 5.7 and 5.8 show the variations of the mean miss distances as a function of one sigma angle noise. For





# TAIL-CHASE ENGAGEMENT CASE

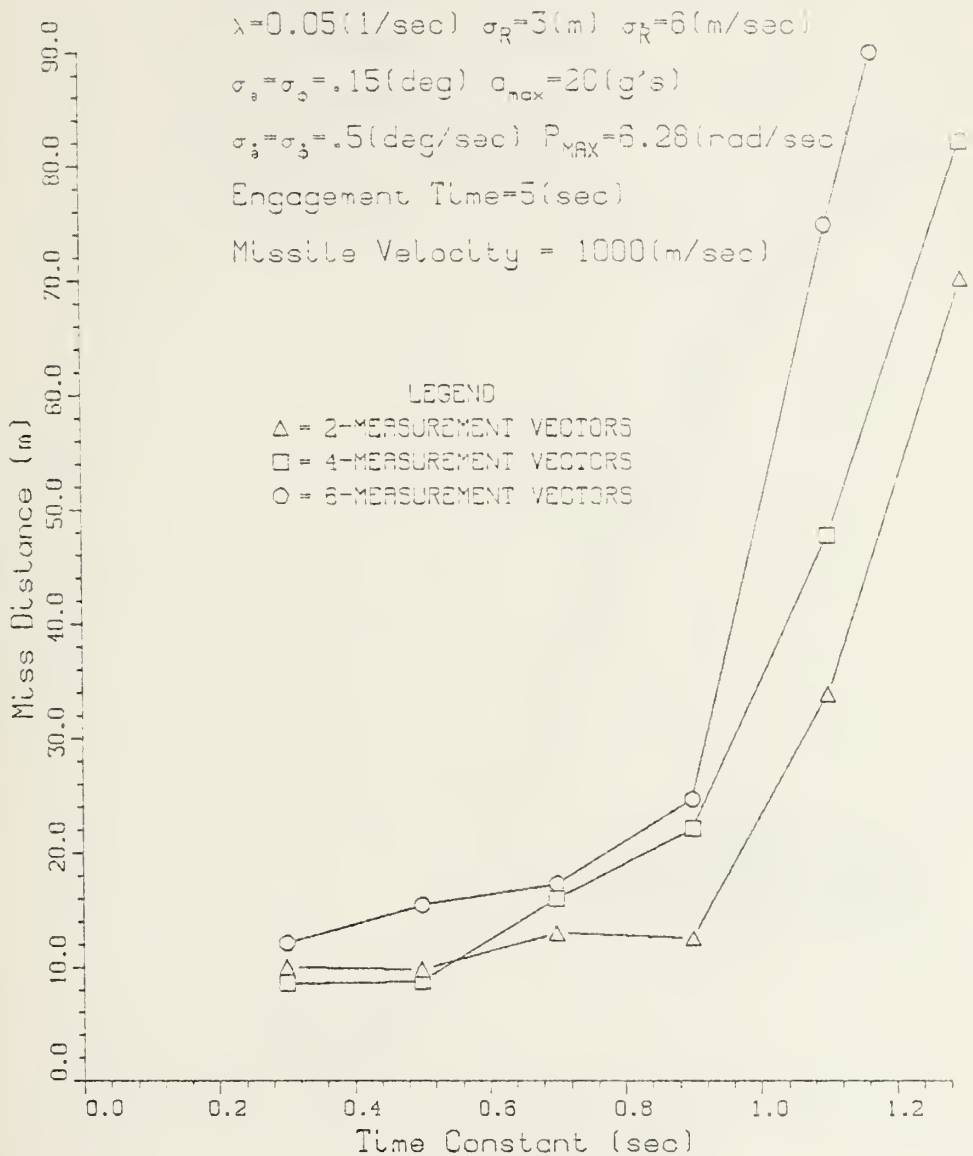


FIGURE 5-5. MISSILE TIME CONSTANT VS MEAN MISS DISTANCE



# HEAD-ON ENGAGEMENT CASE

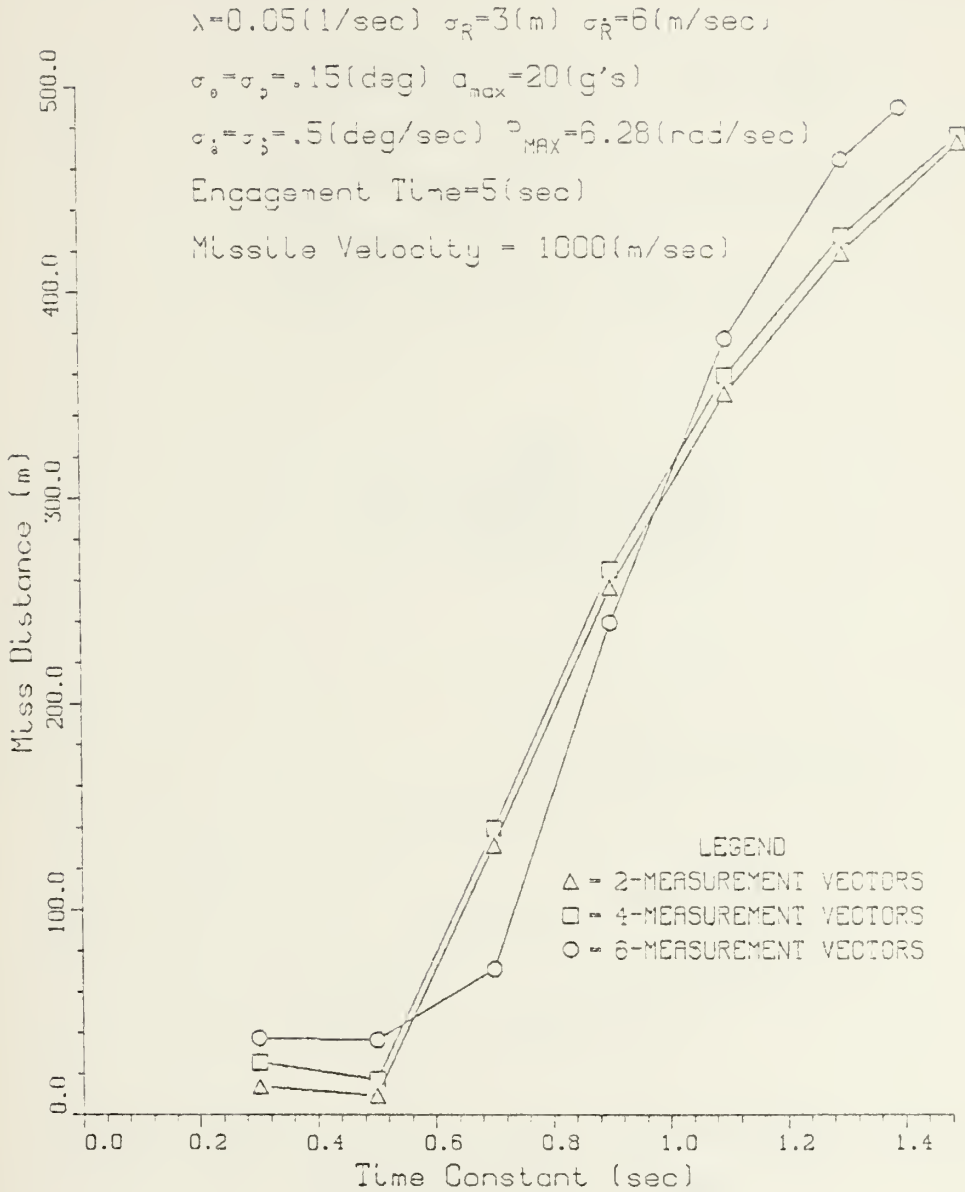


FIGURE 5-6. MISSILE TIME CONSTANT VS  
MEAN MISS DISTANCE



# TAIL-CHASE ENGAGEMENT CASE

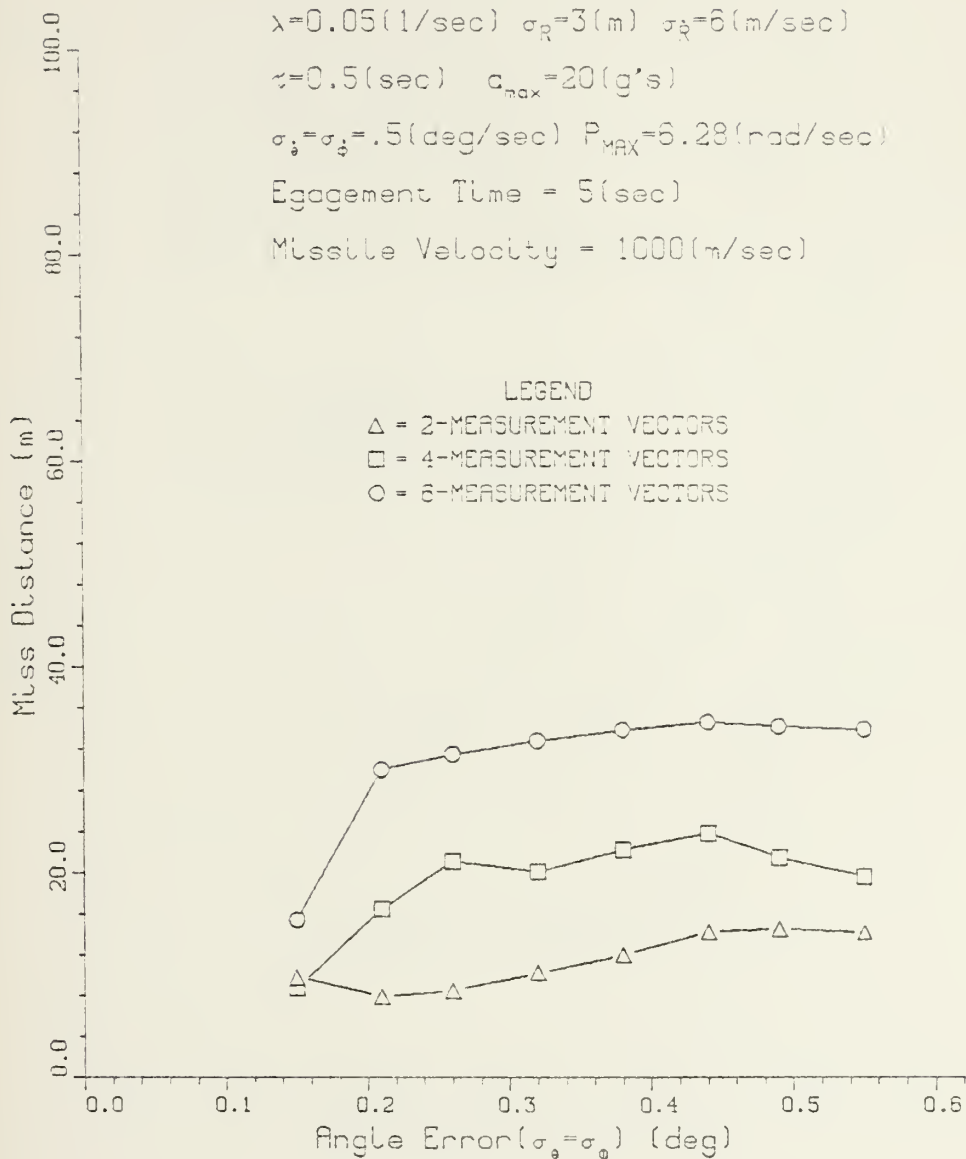


FIGURE 5-7. ONE SIGMA ANGLE ERROR VS MEAN MISS DISTANCE



# HEAD-ON ENGAGEMENT CASE

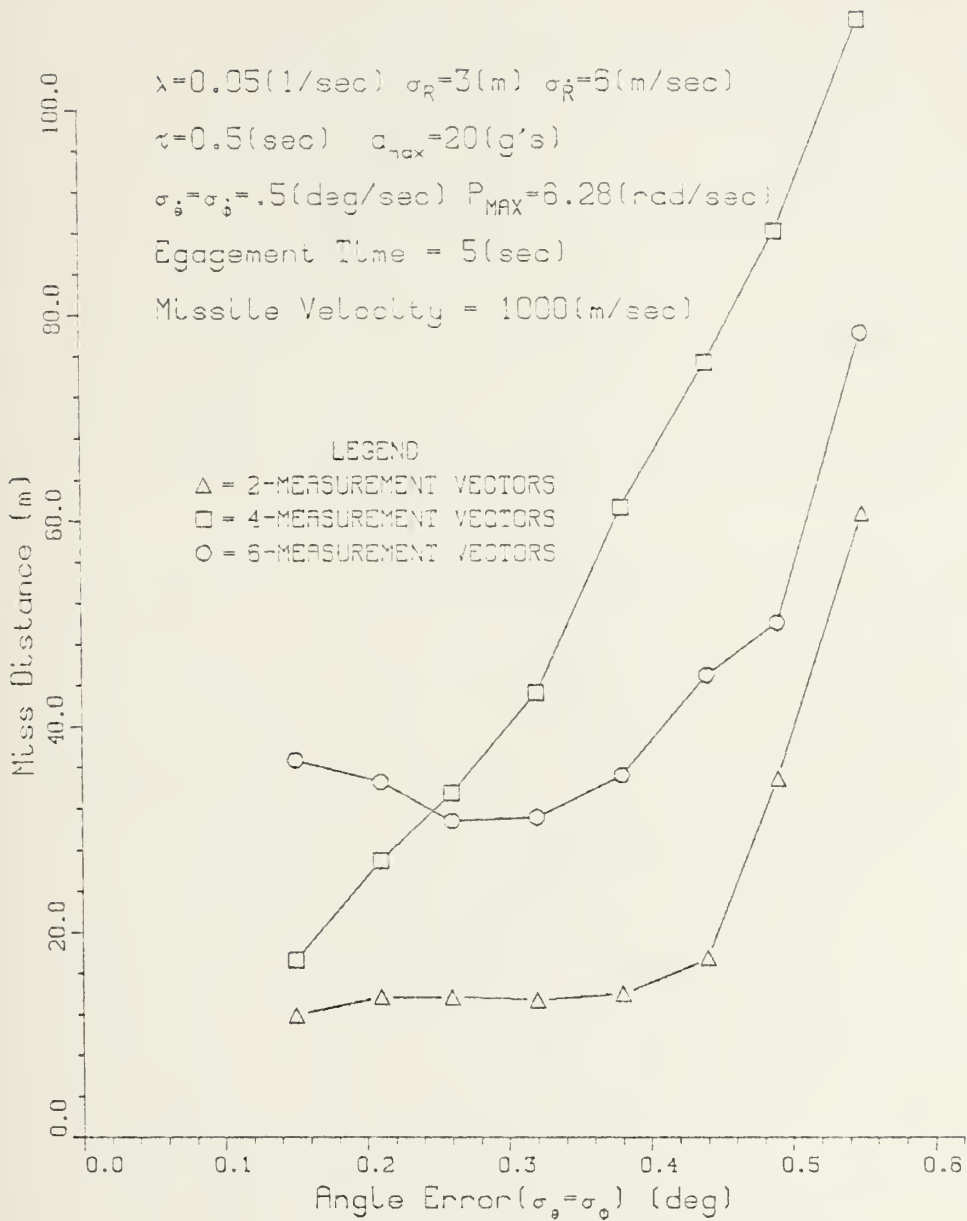


FIGURE 5-8. ONE SIGMA ANGLE ERROR VS MEAN MISS DISTANCE





scenario 1, as shown in Figure 5.7, the maximum miss distance is obtained for the six measurement case with the miss distance being the smallest for the two measurement case. Above about the angle error of 0.3 degree the miss distance is not a strong function of the angle error. For small error values, i.e., less than 0.2 degree, the curves seem to be approaching each other. For the scenario 2, the miss distance is a strong function of the angle error. For the two scenarios (Figure 5.7 and 5.8), the two measurement case has similar results up to an error of 0.4 degree. All cases show a strong rise in the miss distance with increasing error. The four measurement case seems particularly sensitive.

The variation of the miss distances as a function of missile velocity are shown in Figures 5.9 and 5.10. During simulation the initial stand off distance was increased to keep the engagement time the same. One important aspect of Figure 5.9 is that represents an opposite trend of the variations in the mean miss distance to the general trend of the variation in the mean miss distance. Under the missile velocity of 700m/s, the mean miss distance is less than 10m for case 3, from 15m to 12.5m for case 2, from 15.7m to 14.5m for case 1. However, the curves for scenario 2 show the usual trend, i.e., the mean miss distance of case 1 is the smallest and that of case 3 is the largest among the mean miss distances of all three cases at a value of the



# TAIL-CHASE ENGAGEMENT CASE

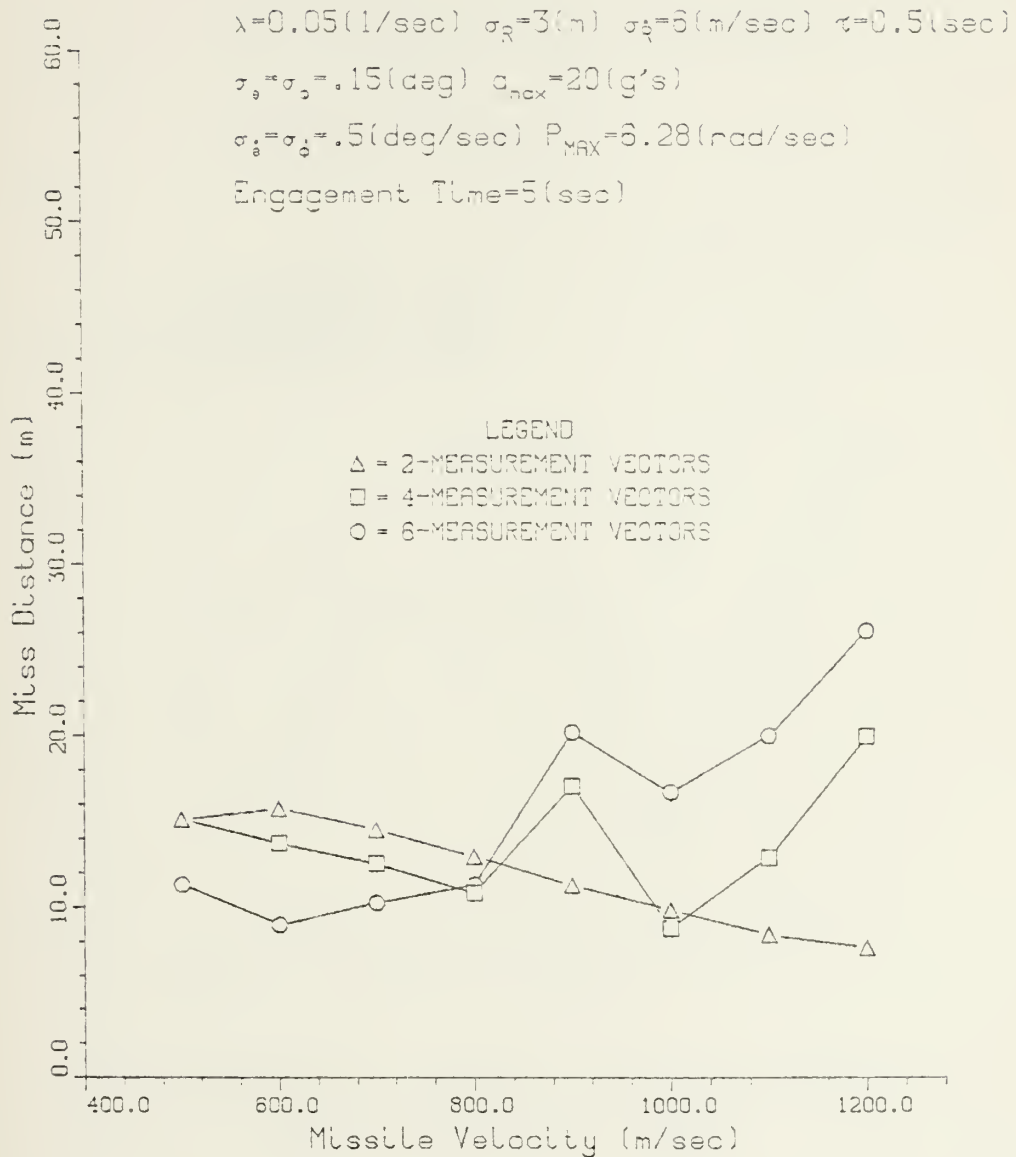


FIGURE 5-9. MISSILE VELOCITY VS  
MEAN MISS DISTANCE



# HEAD-ON ENGAGEMENT CASE

$\lambda=0.05(1/\text{sec})$   $\sigma_R=3(\text{m})$   $\sigma_R=6(\text{m/sec})$   $\tau=0.5(\text{sec})$   
 $\sigma_{\theta}=\sigma_{\dot{\theta}}=.5(\text{deg/sec})$   $P_{\text{MAX}}=6.28(\text{rad/sec})$   
 $\sigma_{\ddot{\theta}}=\sigma_{\dot{\ddot{\theta}}}=.15(\text{deg})$   $a_{\text{max}}=20(\text{g's})$   
 Engagement Time=5(sec)

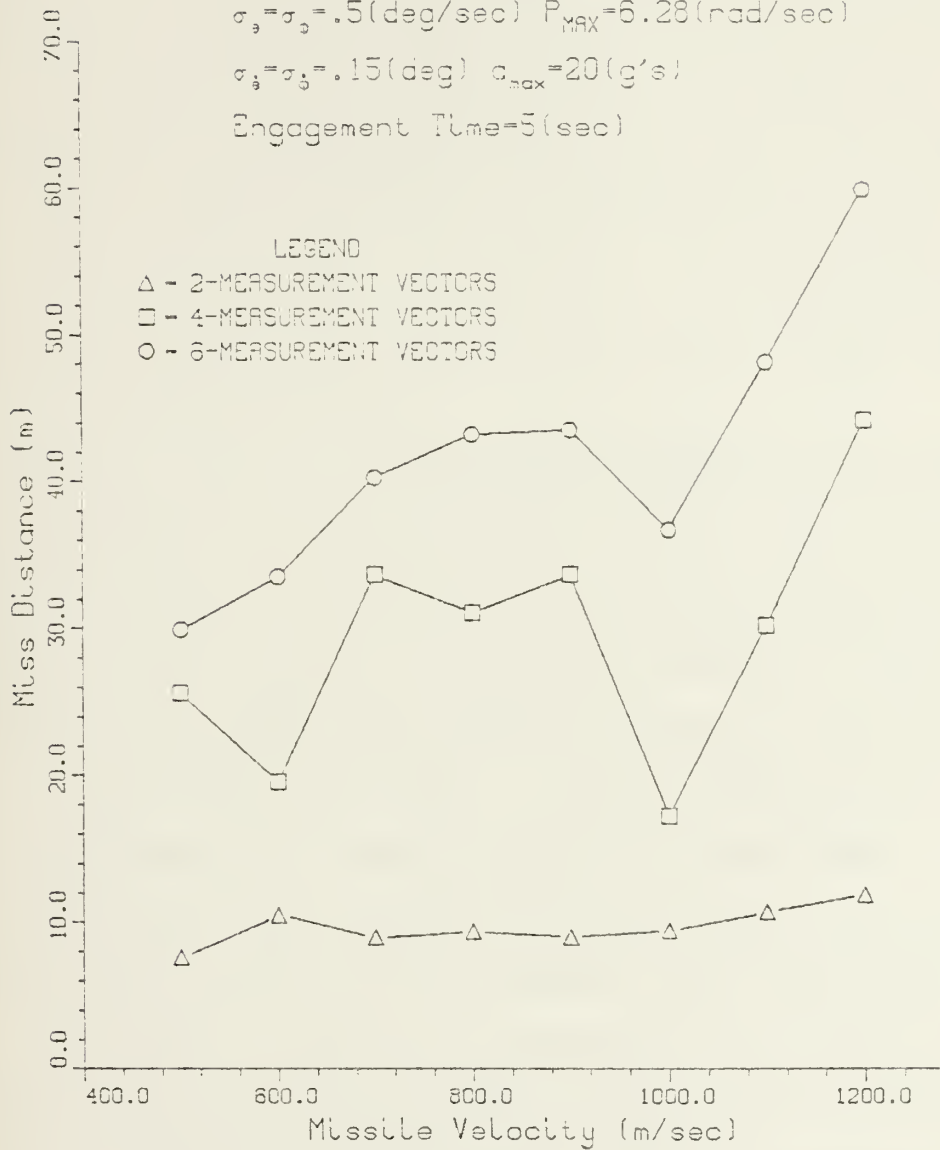


FIGURE 5-10. MISSILE VELOCITY VS  
MEAN MISS DISTANCE



given parameter. For both scenarios, the general trend of the curves slowly increases as the missile velocity increases, except for one curve of case 1. It may be summarized the foregoing considerations as follows: As the values of the missile and target geometry components become smaller, i.e., relatively less effect of neglecting the higher order terms in the first order filter and less contamination of the measured vectors to noises, the mean miss distance can be enhanced with the estimator of the six-measurement vectors. As the estimator algorithm becomes simple, the trend of the mean miss distances is less sensitive to the target geometry.

Figures 5.11 and 5.12 represent the effect on the mean miss distance of the total engagement time. For simulation the initial stand off distance was increased to keep the constant missile velocity. The general behavior of the miss distances of all three cases slowly decrease as the engagement time increases. For case 1, the mean miss distance slowly decreases or is almost constant at below 10m. In the other two cases, there is more variation in the miss distance, but the general trend is still downward with increasing time to go. Note that as time to go increases for a given  $T$ , one has more characteristic time interval available reflected in  $T_{go}/\tau$ . The mean miss distance therefore should be less as the total engagement time increases. This fact is verified from both figures.





# TAIL-CHASE ENGAGEMENT CASE

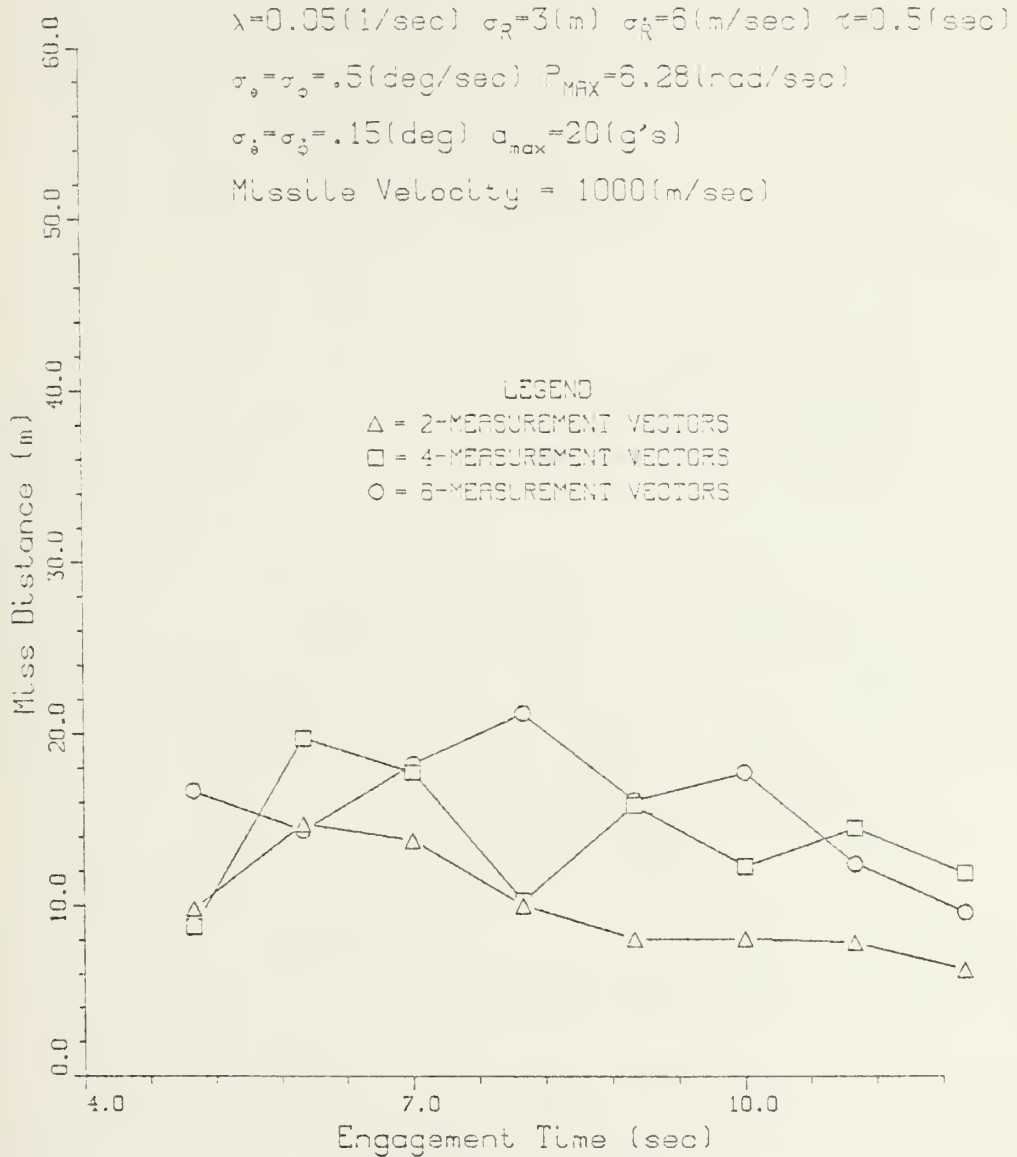


FIGURE 5-11. ENGAGEMENT TIME VS  
MEAN MISS DISTANCE



# HEAD-ON ENGAGEMENT CASE

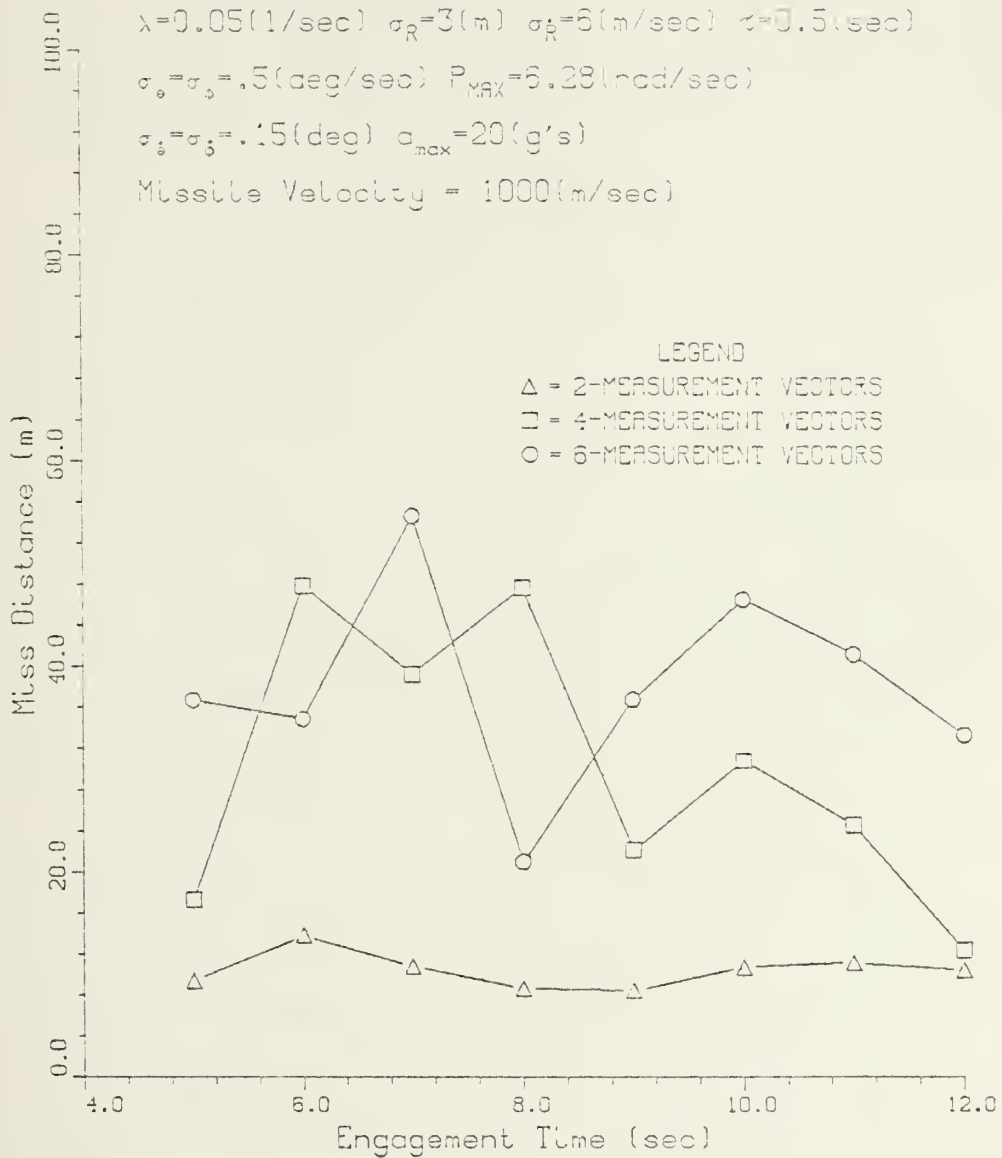


FIGURE 5-12. ENGAGEMENT TIME VS  
MEAN MISS DISTANCE



Figures 5.13 through 5.13 show the variation of the mean miss distances of all three cases for side-approach engagement (scenario 3) as a function of each parameter. The large miss distances resulting from this, scenario 3 motivated its separate consideration. General trends of the curves are similar to the other scenarios but with higher miss distance. This scenario is a strong test of the system. In this scenario, the control laws are subject to the error due to the limitation of the small angle assumption and the higher maximum acceleration capability is required due to the large variation of the PIC-miss in Y- and Z-direction. Thus there are some unexpected trends.

Figure 5.15 shows the variation of the mean miss distances for each case as the  $a_{\max}$  increases. Although the missile velocity is less than that of scenarios 1 and 2, the maximum allowable acceleration is increased. As shown in figure, the mean miss distance for case 1 is 11m, for case 2 is 10m, for case 3 is 15.5m only at  $a_{\max} = 23g$ 's. The figure shows the miss distance variations in this scenario are more sensitive to the  $a_{\max}$  than in the other two scenarios. The mean miss distance of below 40m can be obtained at  $a_{\max} =$  over 19g's, i.e., more  $a_{\max}$  is required than in scenarios 1 and 2. This trend of the mean miss distances can be explained with the larger variation of



the state vector in Y-direction which can cause the large angle ( $\Delta\theta$ ) in control command equations.

As shown in Figure 5.14, the variations of the miss distances of case 1 and 2 as a function of  $p$  are almost constant above  $P_{\max} = 4$  rad/sec. That of case 3, however, continuously decreases up to  $P_{\max} = 6$  rad/sec, then is almost constant. For scenario 3 one needs a maximum roll rate of about 5 or 6 rad/sec to have an effective BTM missile, which is higher than in scenarios 1 and 2.

Figure 5.15 shows the variations of the mean miss distances as a function of time constant. Up to the time constant of 0.7 second, the mean miss distance is less than 20m. For all three cases, comparing with the results for scenarios 1 and 2, the figure shows the curves of the mean miss distances are less sensitive in this scenario. The target acceleration vector lies in same direction as the missile velocity as shown in Figure 3.4. Because the components of the relative velocity are major components in computing the control commands, the more correct control commands may be computed due to the small uncertainty in  $M_{by}$  and  $M_{bz}$  components. This results in smooth variation of the mean miss distance curve. The trend of the miss distances as the one sigma angle error increases, shows some different characteristics from the trend for scenarios 1 and 2 in Figure 5.16. The mean miss distances for all cases increase continuously as the noise input increases up to the





# SIDE-APPROACH ENGAGEMENT CASE

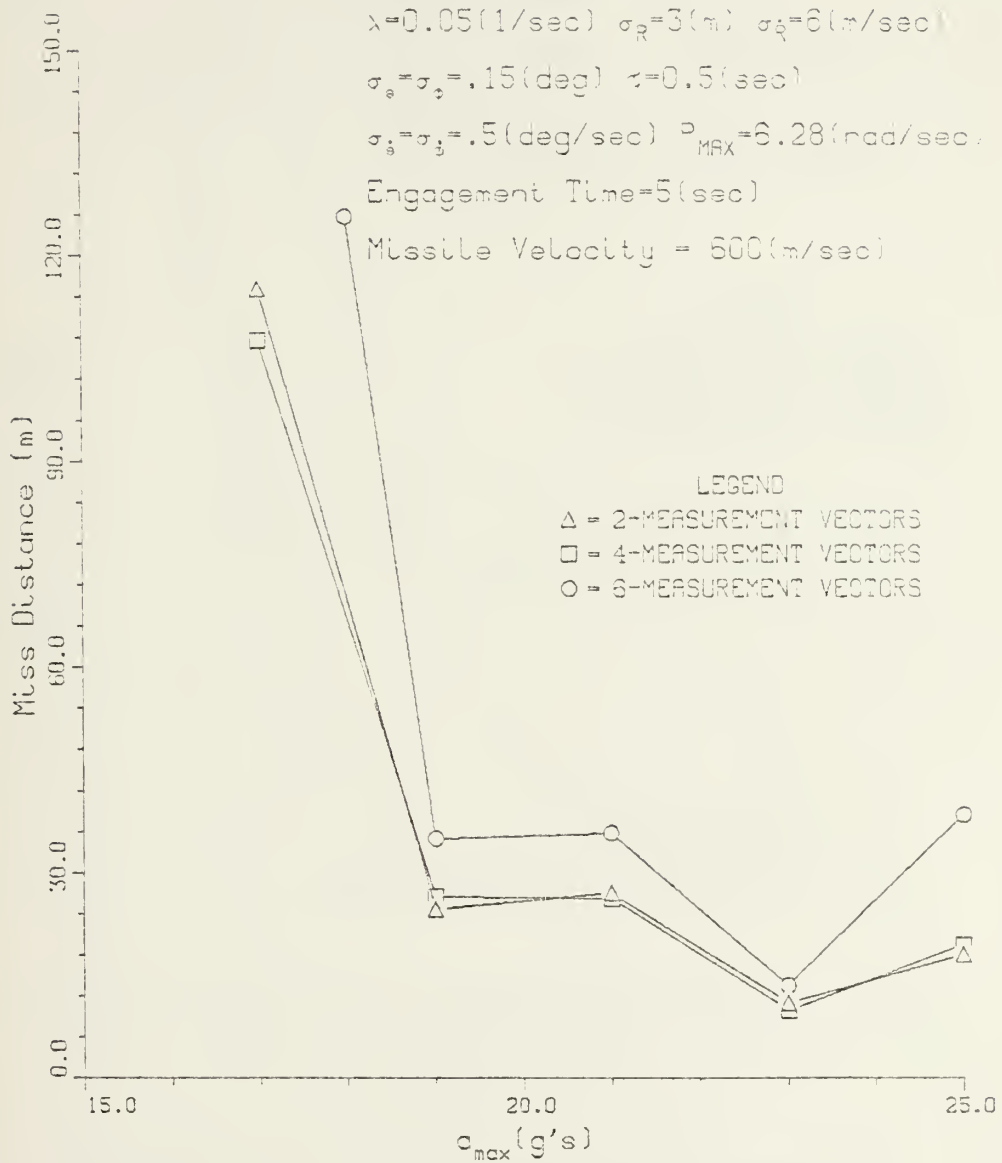


FIGURE 5-13. MISSILE MAXIMUM ACCELERATION VS MEAN MISS DISTANCE



# SIDE-APPROACH ENGAGEMENT CASE

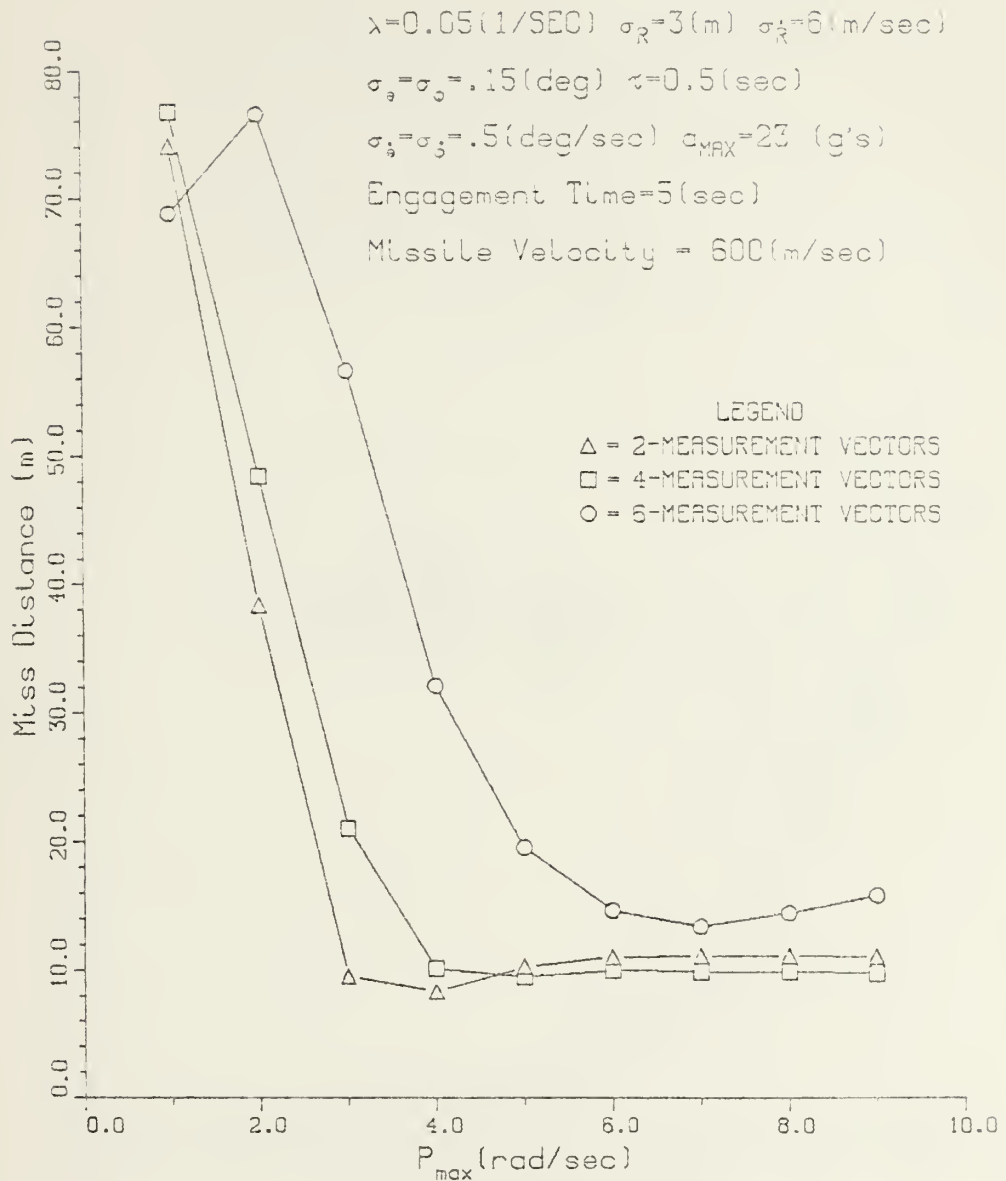


FIGURE 5-14. MISSILE MAXIMUM ROLL RATE VS  
MEAN MISS DISTANCE



# SIDE-APPROACH ENGAGEMENT CASE

$\lambda=0.05(1/\text{sec})$   $\sigma_R=3(\text{m})$   $\sigma_{\dot{R}}=6(\text{m/sec})$

$\sigma_{\theta}=\sigma_{\dot{\theta}}=.15(\text{deg})$   $a_{\text{max}}=23(\text{g's})$

$\sigma_{\dot{\theta}}=\sigma_{\ddot{\theta}}=.5(\text{deg/sec})$   $P_{\text{MAX}}=6.28(\text{rad/sec})$

Engagement Time=5(sec)

Missile Velocity = 600(m/sec)

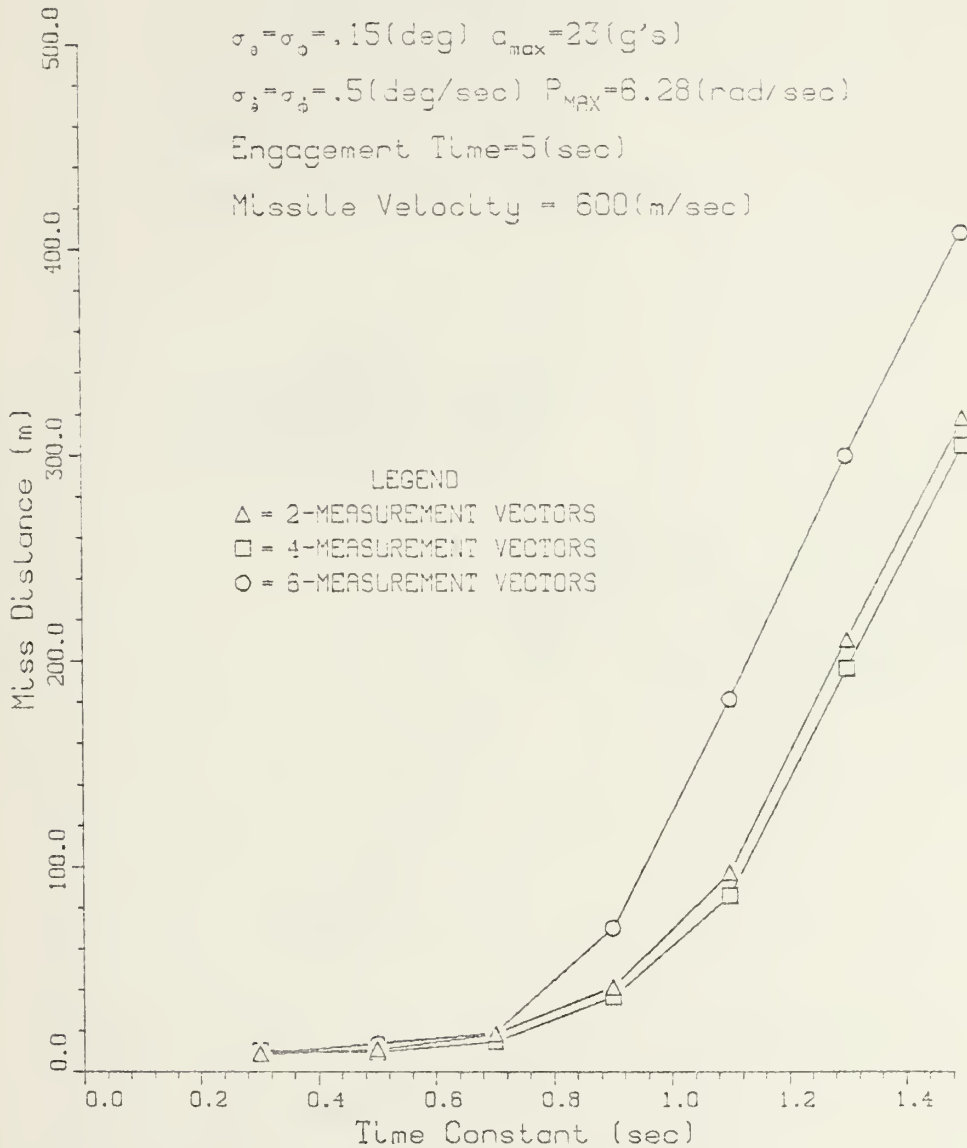


FIGURE 5-15. MISSILE TIME CONSTANT VS MEAN MISS DISTANCE



# SIDE-APPROACH ENGAGEMENT CASE

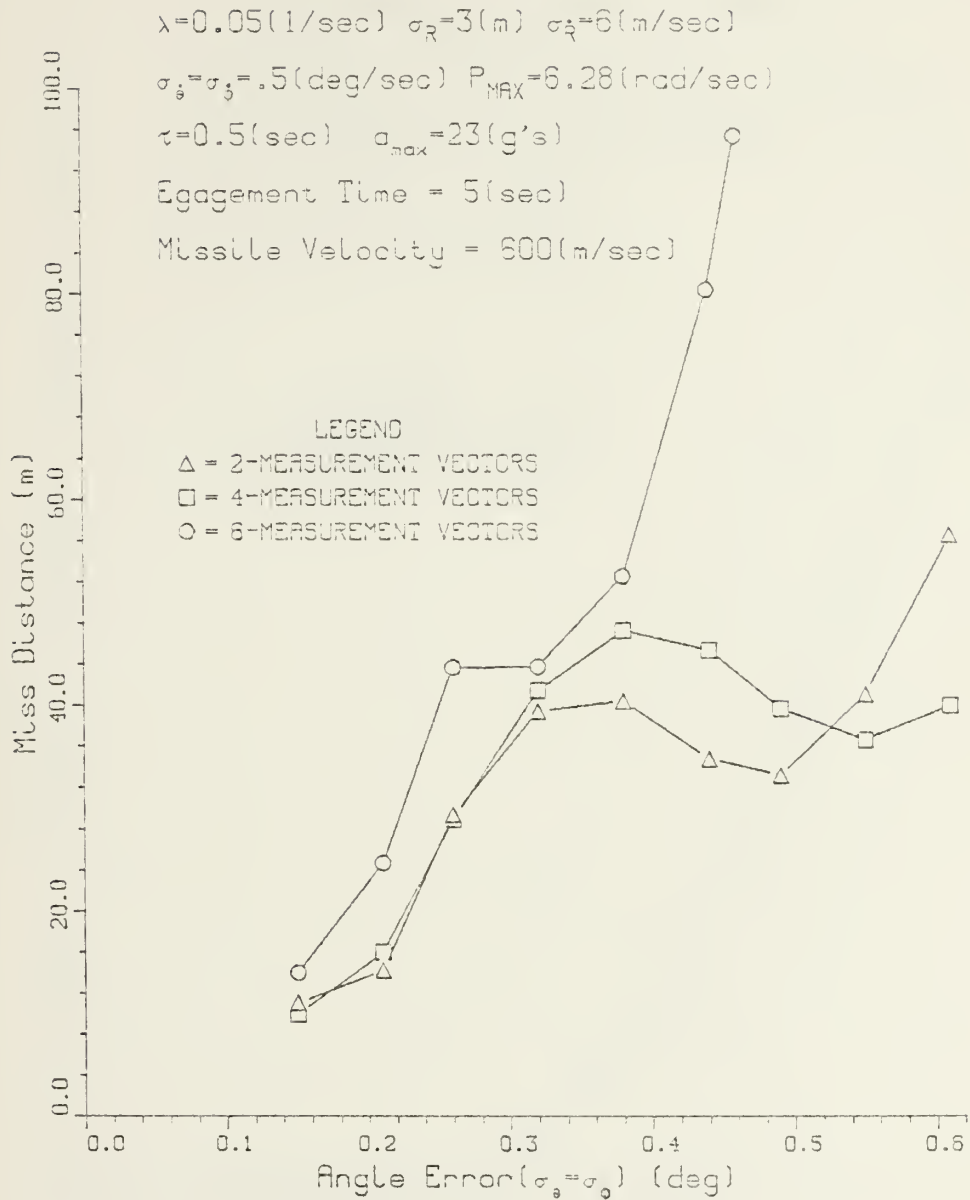


FIGURE 5-16. ONE SIGMA ANGLE ERROR VS MEAN MISS DISTANCE





# SIDE-APPROACH ENGAGEMENT CASE

$\lambda=0.05(1/\text{sec})$   $\sigma_R=3(\text{m})$   $\sigma_R=6(\text{m/sec})$   $\tau=0.5(\text{sec})$

$\sigma_{\theta}=\sigma_{\dot{\theta}}=.5(\text{deg/sec})$   $P_{\text{MAX}}=5.28(\text{rad/sec})$

$\sigma_{\dot{\theta}}=\sigma_{\ddot{\theta}}=.15(\text{deg})$   $a_{\text{max}}=23(\text{g's})$

Engagement Time=5(sec)

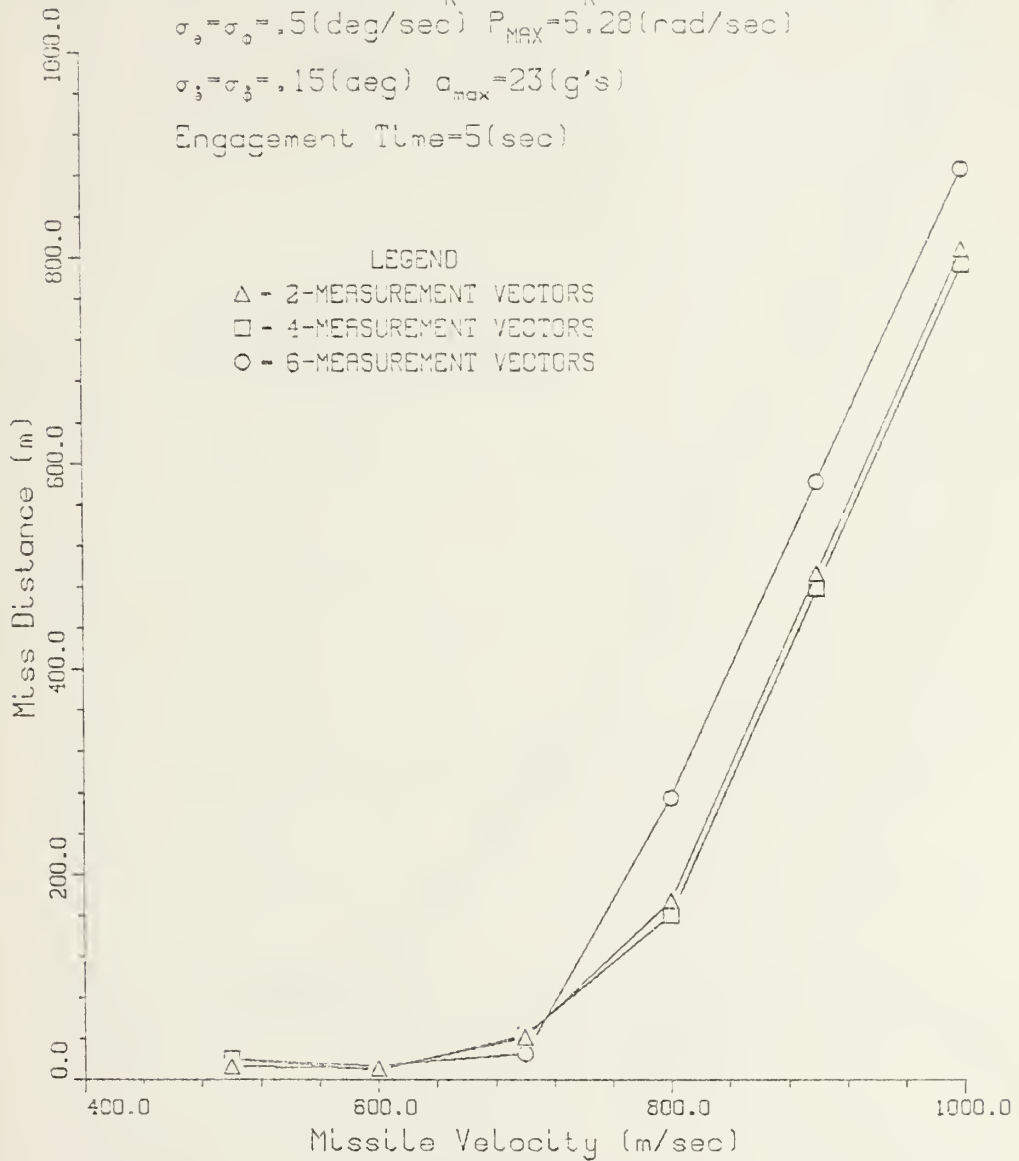


FIGURE 5-17. MISSILE VELOCITY VS  
MEAN MISS DISTANCE



# SIDE-APPROACH ENGAGEMENT CASE

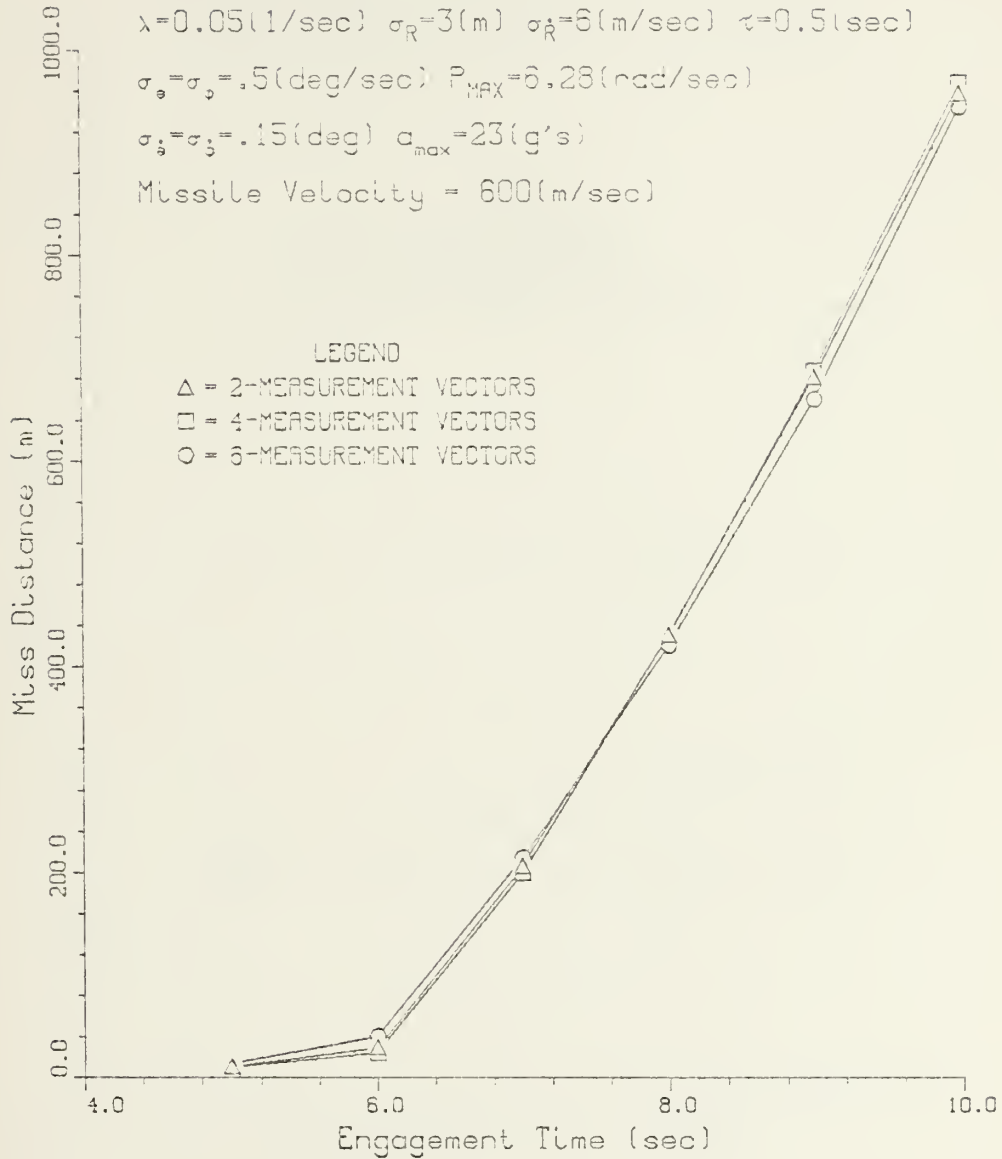


FIGURE 5-18. ENGAGEMENT TIME VS  
MEAN MISS DISTANCE



$\lambda=0.05(1/\text{sec})$   $\sigma_R=3(\text{m})$   $\sigma_{\dot{R}}=6(\text{m/sec})$   $\tau=0.5(\text{sec})$

$\sigma_y=\sigma_z=.5(\text{deg/sec})$   $P_{\text{MAX}}=6.28(\text{rad/sec})$

$\sigma_{\dot{y}}=\sigma_{\dot{z}}=.15(\text{deg})$  Engagement Time=5(sec)

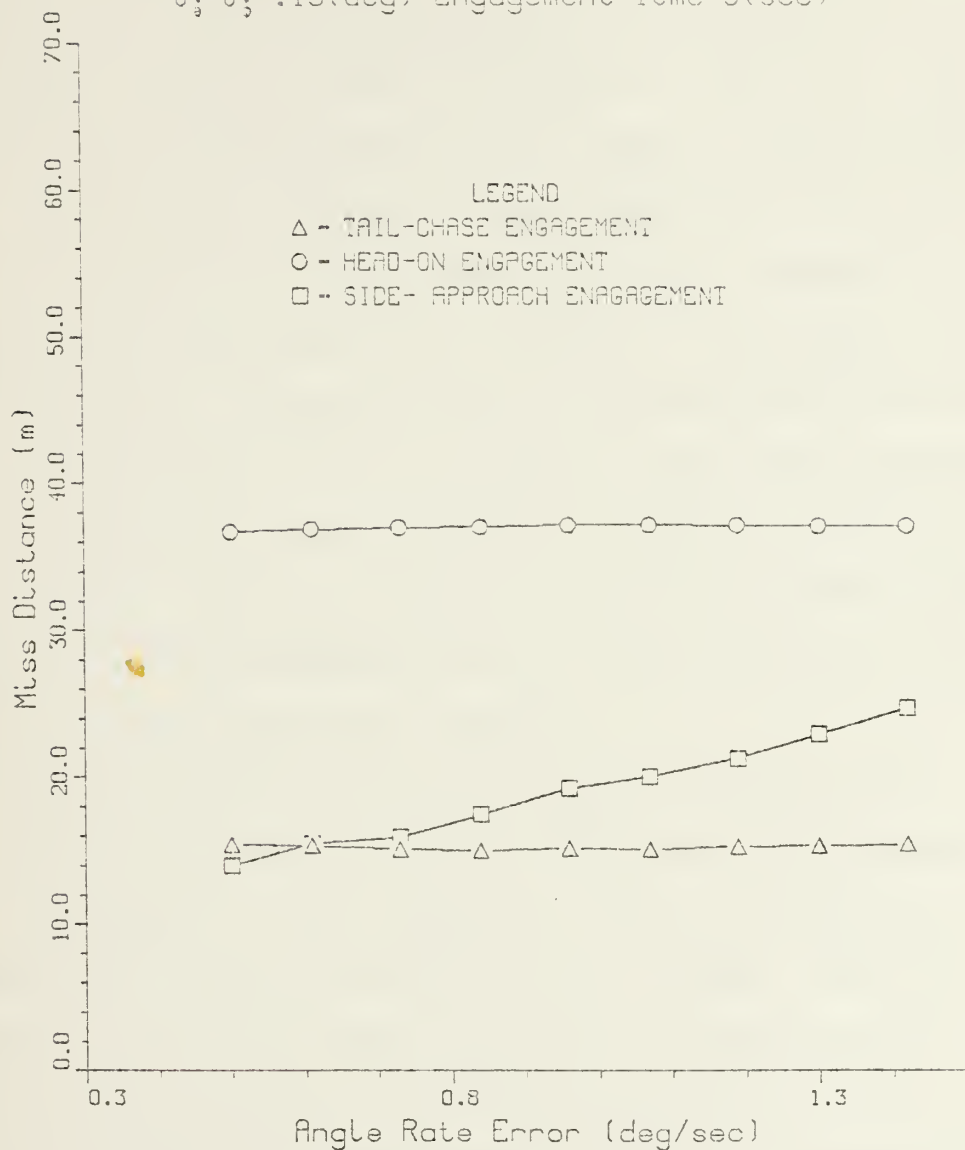


FIGURE 5-19. ONE SIGMA ANGLE RATE ERROR VS MEAN MISS DISTANCE



one sigma error of about 0.4 degree. Above the one sigma error of 0.48 degree, case 1 decreases then rises sharply, case 2 continues decreasing slowly, case 3 increases continuously. The variations of the mean miss distances in scenario 1 are almost plateau and in scenario 2 are almost constant up to the one sigma angle error of about 0.4 degree then rises sharply as shown in Figures 5.7 and 5.8. This reason can be deduced from the fact that as the one sigma angle error becomes large, the same magnitude of the two state vectors in different direction, i.e., relative distance in X-direction and relative in Y-direction, having the same order of magnitude may be contaminated to the noise, on the other hand, the other scenarios, only the components in the X-direction being relatively large are contaminated to the noise. From this fact, it can be concluded that the missile in a side-engagement case is more sensitive to the angle error than the other scenario.

Figure 5.17 shows the variations of the mean miss distances as the missile velocity increases as a parameter (i.e., holding the total engagement time of 5 seconds and changing the relative position of the target). Up to the missile velocity of 700m/s the curves of the mean miss distances are plateau, after that velocity the curves rise sharply. Figure 5.8 shows the variations of the mean miss





distances as a function of the total engagement time (i.e., holding the constant velocities of the missile and the target and changing the relative position of the target in scenario).

Figure 3.18 shows the mean miss distances rise sharply over the engagement time of 6 seconds. This is somewhat unexpected and may be an artifact of the implementation procedure. In other scenarios the mean miss distance as a function of the missile velocity increases slightly as the missile velocity increases and that as a function of the total engagement time decreases slowly with increased engagement time. From above analysis one has a conclusion that the computed control commands should converge in the final time as the computed commands of the two- four- measurement case shown in Figure 3.32 and Figure 3.34 to obtain the low mean miss distance. However, it can be expected in this scenario that the computed control commands do not converge possibly due to the violation of the small angle assumption in deriving the equations of the control commands (i.e., in this scenario the  $M_{bz}$  component is large in Equation (3.7), that causes the large mean miss distances). However, in the case of relatively small magnitude of the missile and target geometry components, the error caused by the violation of small angle assumption is relatively small comparing with the errors caused by the contaminated of the measured vectors to noises,



limitations of the control inputs, and the estimation of the state vectors using first-order filter. This fact is verified with the results that the mean miss distance is 11m for case 1, 10m for case 2, 14m for case 3 at the missile velocity of 600m/s and the engagement time of 5 seconds, as shown in Figures 5.17 and 5.18.

The final Figure 5.19 shows the variations of the mean miss distances for case 3 of all three scenarios as a function of the one sigma angle rate error. The result represents that the variations of the mean miss distances due to increased input values of one sigma angle rate error are almost constant for scenarios 1 and 2. For scenario 3, the mean miss distance varies at constant rate of inclination. This slope of the curve is relatively small comparing with the slopes of the mean miss distance curves as the other parameters change. From this analysis, it may be concluded that the exposure of the measured vectors to the angle rate error noise is negligible in the case of present study.



## VI. CONCLUSIONS

A simple but effective biased guidance law and three extended Kalman filter equations have been derived from the optimal control theory for a bank-to-turn missile with zero-lag and with 0.5 second time lag autopilots for pitch acceleration and roll state.

The equations of motion are linearized around the present orientation of the missile with the assumption of small future roll angles. During computer simulation, the optimal control laws and estimators were tested separately invoking the separation theorem. In the simulation of the system three optimal estimators were used, i.e., estimator with two measurement vectors, with four-measurement vectors and with six-measurement vectors. The system has been evaluated for three scenarios, tail chase engagement, head on engagement and side approach engagement.

From the analyses of the simulation results in Chapters 3, 4 and 5, it can be concluded as follows: The control law was successfully simulated for a hypothetical bank-to-turn missile with pitch acceleration and roll rate autopilot within the imposed limits on three scenarios. Miss distances with zero-lag were negligible for all three scenarios (below 0.5m). For the time lag case one had miss distance of 5.9m for scenario 1, 0.8m for scenario 2 and 32.9m, with



0.5 second lag and with  $a_{\max} = 20g$ 's. By imposing a higher maximum  $g$  of 23 on the scenario 3, the miss distance was reduced to below 5m miss distance. One would expect a high  $g$  requirement for a side engagement situation as in the case of scenario 3. It is evident that the missile's tracking ability against the target is very sensitive to the missile and target geometry, the missile's maneuvering capability is also a very important factor. Optimal control laws applied to the side approach engagement place a severe strain on the system from the viewpoint of the small angle approximation. Increasing the number of measurements did not result in increased performance in the sense of smaller miss distances for the missile except in isolated cases. This may be due to the increased complexity of the system as the number of measurements was augmented. Further, in this study only first order extended filters were implemented. It is possible that better performance could be obtained at the expense of increased computational load, by using a second order extended Kalman filter.





## APPENDIX A: PROGRAM LISTING

This appendix provides listing of the computer program used in the present study. Only one program for the six measurement case is provided. Except for a few differences in the subroutine filter the programs for the two other cases are identical to the program included here.







```

A(1,1)=3.45
B(1,1)=5.2
C(1,1)=1.
D(1,1)=675

```

```

C
C *****
C
C INITIALIZE A,C,B MATRICES
C
C DO 110 I=1,3
C DO 110 J=1,3
C   DEL(I,J)=0.
C   IF(I.EQ.J) DEL(I,J)=1.
C   C(1,J)=DEL(I,J)
C 110 CONTINUE
C
C DO 120 I=1,2
C DO 120 J=1,2
C   B(I,J)=0.
C 120 CONTINUE
C
C B(1,1)=5.2
C B(1,2)=5.2
C B(2,1)=5.2
C B(2,2)=5.2
C
C A(1,4)=0.1
C A(2,5)=0.1
C A(3,6)=0.1
C
C CALL FUNC( SAT,CT,DT,F1,F2,F3,X11,Q12,Q13,Q22,Q23,Q33)
C
C A(1,7)=5.1
C A(2,7)=5.2
C A(3,7)=5.3
C
C Q(1,1)=0.1
C Q(1,4)=0.1
C Q(1,7)=0.1
C Q(4,1)=0.1
C Q(4,4)=0.1
C Q(4,7)=0.1
C Q(7,1)=0.1
C Q(7,4)=0.1
C Q(7,7)=0.1
C
C A(2,8)=5.1
C A(3,8)=5.2
C A(6,8)=5.3
C
C Q(2,2)=0.1
C Q(2,5)=0.1
C Q(2,8)=0.1
C Q(5,2)=0.1
C Q(5,5)=0.1
C Q(5,8)=0.1
C Q(8,2)=0.1
C Q(8,5)=0.1
C Q(8,8)=0.1
C
C A(3,9)=5.1
C A(6,9)=5.2
C A(9,9)=5.3
C
C Q(3,3)=0.1
C Q(3,6)=0.1
C Q(3,9)=0.1
C Q(6,3)=0.1
C Q(6,6)=0.1
C Q(6,9)=0.1
C Q(9,3)=0.1
C Q(9,6)=0.1
C Q(9,9)=0.1

```



```

      Q(9,6)=Q223
      Q(9,7)=Q224
C
      WRITE(6,5)
      WRITE(6,6)
      DO 135 I=1,9
      WRITE(6,7) Q(I,1),Q(I,2),Q(I,3),Q(I,4),Q(I,5),Q(I,6),Q(I,7)
      * Q(I,8),Q(I,9)
134 CONTINUE
5
6
7
8
      PRINT(1,1)
      PRINT(1,2,'ORIGINAL Q MATRIX'//)
      PRINT(1,3)
      PRINT(1,4,'MATRIX WITH PSEUDO NOISE, QPSU=',QPSU//)
C
C
      ADD PSEUDO NOISE TO Q MATRIX
C
      F11=(QPSU**2)*(DIT**4)/4.
      F12=(QPSU**2)*(DIT**3)/2.
      F22=(QPSU**2)*(DIT**2)
C
      Q(1,1)=Q(1,1)+F11
      Q(2,2)=Q(2,2)+F11
      Q(3,3)=Q(3,3)+F11
C
      Q(4,4)=Q(4,4)+F22
      Q(5,5)=Q(5,5)+F22
      Q(6,6)=Q(6,6)+F22
C
      Q(1,4)=Q(1,4)+F12
      Q(2,5)=Q(2,5)+F12
      Q(3,6)=Q(3,6)+F12
C
      Q(4,1)=Q(4,1)+F12
      Q(5,2)=Q(5,2)+F12
      Q(6,3)=Q(6,3)+F12
C
      WRITE(6,8),QPSU
      DO 135 I=1,9
      WRITE(6,7) Q(I,1),Q(I,2),Q(I,3),Q(I,4),Q(I,5),Q(I,6),Q(I,7)
      * Q(I,8),Q(I,9)
135 CONTINUE
C
      DO 150 I=1,9
      DO 140 J=1,9
      AT(I,J)=A(J,I)
140 CONTINUE
150 CONTINUE
C
      WRITE(6,5)
C
      START CASE LOOP
C
      DO 950 III=1,NCASE
C
      INITIALIZE
C
      N=C
      K=KPRINT-1
      L=LPRINT-1
      ISTCP=0
      DT=DTT
C
      IF(NCASE.EQ.1) GO TO 160
      KPRINT=100000
      LPRINT=100000
      ISTCT=0
      K=C
      L=0
160 CONTINUE
C
      Y(1)=0.
      Y(2)=THETA
      Y(3)=DTHETA
      Y(4)=VELOCITY
      Y(5)=XMO
      Y(6)=YMO

```





[illegible]

























```

C
SUBROUTINE GUID3(X,TGO,AC,BC,CT)
DIMENSION BE(3),CE(3)
COMMON/THREE/ A21,A22,A23,A31,A32,A33,B1,B2

C
G=9.8
RX=X(1)
RY=X(2)
RZ=X(3)
VEX=X(4)
VRY=X(5)
VRZ=X(6)
ATA=X(7)
ATX=X(8)
ATZ=X(9)
TGO=(VEX*VEX+VRY*VRY+VRZ*VRZ)/(VEX**2+VRY**2+VRZ**2)
TGO=4*(GCT+TGO-1)+EXE(-CT*TGO)/(CT**2)
BE(1)=RX+VEX*BE(1)+VRY*BE(2)+VRY*BE(3)+VRY*BE(4)+VRY*BE(5)+VRY*BE(6)+VRY*BE(7)+VRY*BE(8)+VRY*BE(9)
BE(2)=RY+VEX*BE(1)+VRY*BE(2)+VRY*BE(3)+VRY*BE(4)+VRY*BE(5)+VRY*BE(6)+VRY*BE(7)+VRY*BE(8)+VRY*BE(9)
BE(3)=RZ+VEX*BE(1)+VRY*BE(2)+VRY*BE(3)+VRY*BE(4)+VRY*BE(5)+VRY*BE(6)+VRY*BE(7)+VRY*BE(8)+VRY*BE(9)
BE(4)=A21*BE(1)+A22*BE(2)+A23*BE(3)+A31*BE(4)+A32*BE(5)+A33*BE(6)
BE(5)=A21*BE(1)+A22*BE(2)+A23*BE(3)+A31*BE(4)+A32*BE(5)+A33*BE(6)
BE(6)=A21*BE(1)+A22*BE(2)+A23*BE(3)+A31*BE(4)+A32*BE(5)+A33*BE(6)
BE(7)=A21*BE(1)+A22*BE(2)+A23*BE(3)+A31*BE(4)+A32*BE(5)+A33*BE(6)
BE(8)=A21*BE(1)+A22*BE(2)+A23*BE(3)+A31*BE(4)+A32*BE(5)+A33*BE(6)
BE(9)=A21*BE(1)+A22*BE(2)+A23*BE(3)+A31*BE(4)+A32*BE(5)+A33*BE(6)
AC=0.
BC=0.
COMMON/THREE/ A21,A22,A23,A31,A32,A33,B1,B2
C
50
COMMON/THREE/ A21,A22,A23,A31,A32,A33,B1,B2
100
COMMON/THREE/ A21,A22,A23,A31,A32,A33,B1,B2
RETURN
END

```



```

C
SUBROUTINE INTEG (DEIN,3)
IMPLICIT REAL*8 (A-H,O-Z)
DIMENSION DEIN (16), DEOUT (16), DE1 (16), DE2 (16), DE3 (16)
COMMON /AC/ AC,PC,ATX0,ATY0,ATZ0,CTX,CTY,CZ,DT,TS,TOT,TACC
G=5.3
NGRAM=16
THT0=DEIN (2)
PSI0=DEIN (3)
VC=DEIN (4)
XC=DEIN (5)
YC=DEIN (6)
ZC=DEIN (7)
VXC=V0*DCCS (THT0)*DCCS (PSI0)
VYC=V0*DCCS (THT0)*DSIN (PSI0)
VZC=-V0*DSIN (THT0)

C
C
C NUMERICAL INTEGRATION (4TH-ORDER RUNGE-KUTTA)
C
DC 75 N1=1,4
T=DEIN (1)
TH1=DEIN (2)
PS1=DEIN (3)
V=DEIN (4)
PH1=DEIN (14)
AM=AC
PM=PC
IF (T.GT.0.) PH=DEIN (15)
IF (T.GT.0.) PM=DEIN (16)
DEOUT (1)=1.
DEOUT (2)=(AM*DEIN (14)-3*DCCS (THT))/7
DEOUT (3)=(AM*DSIN (TH1))/(7*DCCS (THT))
DEOUT (4)=-G*DCCS (TH1)
DEOUT (5)=7*DCCS (TH1)*DCCS (PS1)
DEOUT (6)=7*DCCS (TH1)*DSIN (PS1)
DEOUT (7)=-7*DSIN (THT)
DEOUT (8)=ATX0*DSIN (THT)*(-CTX+3)
DEOUT (9)=ATY0*DSIN (THT)*(-CTY+3)
DEOUT (10)=ATZ0*DSIN (THT)*(-CZ+3)
DEOUT (11)=DEIN (5)
DEOUT (12)=DEIN (6)
DEOUT (13)=DEIN (7)
DEOUT (14)=PM
DEOUT (15)=0.
DEOUT (16)=0.
IF (T.GT.0.) DEOUT (15)=(PC+PM)/735E14
IF (T.GT.0.) DEOUT (16)=(AC+AM)/TACC
DC 75 N1=1,NGRAM
IF (N1.EQ.2) GC TC 60
IF (N1.EQ.3) GC TC 65
IF (N1.EQ.4) GC TC 70
DE1 (1)=DEIN (1)
DE2 (1)=DEOUT (1)*DT
DE3 (1)=DE1 (1)*.5
GC TO 75
55 USE1=DEOUT (1)*2.*DT
DE2 (1)=DE2 (1)+USE1
USE1=DE1 (1)*.25
GC TO 75
60 USE1=DEOUT (1)*2.*DT
DE2 (1)=DE2 (1)+USE1
USE1=DE1 (1)*.5
GC TO 75
65 USE1=DEOUT (1)*DT
DE2 (1)=DE2 (1)+USE1
USE1=DE1 (1)*.5
GC TO 75
70 USE1=DEOUT (1)*DT
DE2 (1)=DE2 (1)+USE1
75 DEIN (1)=DE1 (1)+USE1
C
IF (TSPIN.LE.0.) DEIN (15)=EC
IF (TACC.LE.0.) DEIN (16)=AC
C
C
THT=DEIN (2)
PS1=DEIN (3)
V=DEIN (4)
VX=V*DCCS (THT)*DCCS (PS1)
VY=V*DCCS (THT)*DSIN (PS1)
VZ=-V*DSIN (THT)

```





C

```

(1) = (1)
(2) = (2)
(3) = (3)
(4) = (4)
(5) = (5)
(6) = (6)
(7) = (7)
(8) = (8)
(9) = (9)
(10) = (10)
(11) = (11)
(12) = (12)
(13) = (13)
(14) = (14)
(15) = (15)
(16) = (16)
(17) = (17)
(18) = (18)
(19) = (19)
(20) = (20)
(21) = (21)
(22) = (22)
(23) = (23)
(24) = (24)
(25) = (25)
(26) = (26)
(27) = (27)
(28) = (28)
(29) = (29)
(30) = (30)
(31) = (31)
(32) = (32)
(33) = (33)
(34) = (34)
(35) = (35)
(36) = (36)
(37) = (37)
(38) = (38)
(39) = (39)
(40) = (40)
(41) = (41)
(42) = (42)
(43) = (43)
(44) = (44)
(45) = (45)
(46) = (46)
(47) = (47)
(48) = (48)
(49) = (49)
(50) = (50)
(51) = (51)
(52) = (52)
(53) = (53)
(54) = (54)
(55) = (55)
(56) = (56)
(57) = (57)
(58) = (58)
(59) = (59)
(60) = (60)
(61) = (61)
(62) = (62)
(63) = (63)
(64) = (64)
(65) = (65)
(66) = (66)
(67) = (67)
(68) = (68)
(69) = (69)
(70) = (70)
(71) = (71)
(72) = (72)
(73) = (73)
(74) = (74)
(75) = (75)
(76) = (76)
(77) = (77)
(78) = (78)
(79) = (79)
(80) = (80)
(81) = (81)
(82) = (82)
(83) = (83)
(84) = (84)
(85) = (85)
(86) = (86)
(87) = (87)
(88) = (88)
(89) = (89)
(90) = (90)
(91) = (91)
(92) = (92)
(93) = (93)
(94) = (94)
(95) = (95)
(96) = (96)
(97) = (97)
(98) = (98)
(99) = (99)
(100) = (100)

```







```

      H(5,3)=X3/D
      H(6,1)=(D*D*(X1-D2*X1))/(D*D*D)
      H(6,2)=(D*D*(S-D2*X2))/(D*D*D)
      H(6,3)=(D*D*(Y6-D2*Y5))/(D*D*D)
      H(6,4)=X1/D
      H(6,5)=X2/D
      H(6,6)=X3/D
C
      DO 350 I=1,3
      DO 350 J=1,3
      HT(I,J)=H(I,J,I)
300  CONTINUE
350  CONTINUE
C
      COMPUTE KALMAN GAIN MATRIX
C
      CALL VMULFF(PF,H1,9,9,6,9,9,PHI,9,I4)
C
      CALL VMULFF(H,ZHT,6,9,6,6,9,HHT,6,I5)
C
      DO 450 I=1,6
      DO 450 J=1,6
      Y(I,J)=HHT(I,J)+F(I,J)
400  CONTINUE
450  CONTINUE
C
      INVERT Y MATRIX
C
      CALL LINVIF(Y,6,6,YINV,6,WORK,IER)
C
      CALL VMULFF(PHI,YINV,6,6,6,9,6,G,9,I6)
C
      UPDATE STATE VECTORS
C
      HH(1)=-DATAN2(Y3,S1)
      HH(2)={(X1*X1*X3*X4)+(X2*X2*X3*X5)+(D1*D1*X3*X6)}/(D*D*D1)
      HH(3)=DATAN2(X2,X1)
      HH(4)={(-X1*X2*(4)+(X1=X2*X5)}/(D*D1*D1)
      HH(5)=D
      HH(6)=D2/D
C
      DO 500 I=1,6
      DZ(I)=Z(I)-HH(I)
500  CONTINUE
C
      CALL VMULFF(G,DZ,9,6,1,9,6,DX,9,I7)
C
      DO 550 I=1,9
      X(I)=XX(I)+DX(I)
550  CONTINUE
C
      UPDATE COVARIANCE
C
      CALL VMULFF(G,H,9,6,9,9,6,GH,9,I8)
C
      DO 650 I=1,9
      DO 650 J=1,9
      F(I,J)=DEI(I,J)-GH(I,J)
600  CONTINUE
650  CONTINUE
C
      CALL VMULFF(F,PF,9,9,9,9,9,P,9,I9)
C
      RETURN
      END

```



```

C
C
SUBROUTINE FUNC (S1T, C, DT, F1, F2, F3, Q11, V12, Q13, Q21, Q22, Q33)
IMPLICIT REAL*8 (A-H, C-Z)
C
V=SAT**2
A=C*DT
F1=DEXP (-A)
F2=DEXP (-2.*A)
C
V11=V/(C**4)
V12=V/(C**3)
V13=V/(C**2)
V22=V/(C**2)
V23=V/C
V33=V
C
Q11=V11*(1.-F2+F2.*F2+(2./3.)*(A**3)-2.*A*A-.5.*A*F1)
Q12=V12*(F2+1.-F2.*F2+2.*A*F1-2.*A*A*A)
Q13=V13*(1.-F2-F2.*A*F1)
Q22=V22*(1.-F2+1.-F2.*F2+2.*A)
Q23=V23*(F2+1.-F2.*F1)
Q33=V33*(1.-F2)
C
F1=(A-1.+F1)/(C**2)
F2=(1.-F1)/C
F3=F1
C
RETURN
END

```





```

C      SUBROUTINE STAT (X,N,AVG,RES)
      IMPLICIT REAL*8 (A-H,O-Z)
      DIMENSION X(50)
      AN=N
      SUM=0.
      DO 100 I=1,N
      SUM=SUM+X(I)
100    CONTINUE
      AVG=SUM/AN
      SUM2=0.
      DO 200 I=1,N
      SUM2=SUM2+(X(I)-AVG)**2
200    CONTINUE
      RES=DSQRT(SUM2/AN)
      RETURN
      END
/*
//GO.RYSIN DD *
/*

```



## LIST OF REFERENCES

1. Meriam, J. L., Dynamics, Wiley, 1971.
2. Etkin, B., Dynamics of Atmospheric Flight, Wiley, 1972.
3. Garnell, P. and East, D. J., Guided Weapon Control Systems, Pergamon Press, 1977.
4. Ogata, K., Modern Control Engineering, Prentice-Hall, Inc., 1970.
5. Bryson, A. E. and Ho, Y. C., Applied Optimal Control Systems, Wiley-Interscience, 1972.
6. Gelb, A., Applied Optimal Estimation, MIT Press, 1974.
7. Jazwinski, A.H., Stochastic Processes and Filtering Theory, Academic Press, 1970.
8. Stallard, D. V., An Approach to Optimal Guidance for a Bank-to-Turn Missile Guidance Systems, Afatl-Tr-7929, February 1979.
9. Naval Surface Weapon Center Technical Report Tr-3445, Development of an Adaptive Kalman Target Tracking Filter and Predictor for Fire Control Applications, Clark, B. L., March 1977.
10. Singer, R. A., "Estimating Optimal Tracking Filter Performance for Manned Maneuvering Targets," IEEE Transactions on Aerospace and Electronic Systems, Vol. Aes-6, no. 4, July 1970.
11. Mcgehee, R. M., "Bank-To-Turn Auto-Pilot Technology," National Aerospace and Electronics Conference, Vol. 2, 1978, pp. 688-696.
12. Mcchee, R. M., "Bank-To-Turn Technology," AIAA Guidance and Control Conference, August 6-8, 1979, pp. 413-422.
13. Howard, D., Predicting Target-Caused Errors in Radar Measurements, Naval Research Laboratory, Eascon, 1976.
14. Ohlmeyer, E. J., Application of Optimal Estimation on Control Concepts to a Bank-To-Turn Missile, Naval Post-graduate School, Master Thesis, October 1982.



# INITIAL DISTRIBUTION LIST

Number of copies

1. Defense Technical Information Center 2  
Cameron Station  
Alexandria, Virginia 22314
2. Library, Code 0142 2  
Naval Postgraduate School  
Monterey, California 93943
3. Department Chairman, Code 67 1  
Department of Aeronautics  
Naval Postgraduate School  
Monterey, California 93943
4. Professor D. J. Collins, Code 67Co 2  
Department of Aeronautics  
Naval Postgraduate School  
Monterey, California 93943
5. Professor H. A. Titus, Code 62Ts 2  
Naval Postgraduate School  
Monterey, California 93943
6. Shin, Hyunchul 3  
224-17(20Tong 6 BAN)  
Chun-ho-1 dong, Kang-dong ku  
Seoul, Korea
7. An, Byunggul 1  
SMC #2816  
Naval Postgraduate School  
Monterey, California 93943
8. Lee, Cheongkoo 1  
SMC #2781  
Naval Postgraduate School  
Monterey, California 93943
9. Chang, Jinhwa 1  
SMC #2391  
Naval Postgraduate School  
Monterey, California 93943.













207604

Thesis

S4737 Shin

c.1

Application of modern  
guidance control theory  
to a back-to-turn mis-  
sile.

ALG 14 85  
25 SEP 85

33139  
33249

207604

Thesis

S4737 Shin

c.1

Application of modern  
guidance control theory  
to a back-to-turn mis-  
sile.



thesS4737

Application of modern guidance control t



3 2768 001 95325 0

DUDLEY KNOX LIBRARY